Theses and Dissertations

Spring 2016

Inhibition of neutrophil serine proteases by N-arylacyl O-sulfonated aminoglycosides: new therapeutic approach to treat inflammatory lung diseases

Ioana Craciun
University of Iowa

INHIBITION OF NEUTROPHIL SERINE PROTEASES BY *N*-ARYLACYL *O*-SULFONATED AMINOGLYCOSIDES: NEW THERAPEUTIC APPROACH TO TREAT INFLAMMATORY LUNG DISEASES

by

Ioana Craciun

A thesis submitted in partial fulfillment
of the requirements for the Doctor of Philosophy
degree in Pharmacy in the
Graduate College of
The University of Iowa

May 2016

Thesis Supervisor: Professor Robert J. Kerns

Graduate College
The University of Iowa
Iowa City, Iowa

CERTIFICATE OF APPROVAL

_____

PH.D. THESIS

_____

This is to certify that the Ph.D. thesis of

Ioana Craciun

has been approved by the Examining Committee for
the thesis requirement for the Doctor of Philosophy degree
in Pharmacy at the May 2016 graduation.

Thesis Committee: _____
                     Robert J. Kerns, Thesis Supervisor

                     _____
                     Jonathan A. Doorn

                     _____
                     Michael W. Duffel

                     _____
                     David L. Roman

                     _____
                     Daniel M. Quinn

To Didina Bărbulescu – "Dacă trebuie, cu plăcere"

ACKNOWLEDGEMENTS

I would like to thank my advisor Dr. Robert Kerns for his guidance over the years, encouragement and mentorship. I will be forever grateful. I would also like to thank my committee members Dr. Jonathan Doorn, Dr. Michael Duffel, Dr. Dave Roman and Dr. Daniel Quinn for their time, training and assistance. I thank Dr. Rice for recruiting me into the division and starting my career.

The work presented here would not have been possible without the support of many collaborators. I would like to especially thank Dr. Roman and all the members of his group as well as Andrea Dodd and Peter Thorne for not only opening their labs to me and training me in their areas of expertise, but also helping me develop scientific experiments that made my work more rounded.

I want to extend my thanks to the Kerns' lab members and all my fellow students in the division for their unwavering friendship and support. I appreciate each and everyone's encouragement during the lows of graduate school as well as companionship in celebrating the highs.

Finally, I would like to thank my family for all their sacrifices in laying the foundation so that I can succeed.

ABSTRACT

Neutrophil serine proteases (NSPs) play an important role in the innate immune system. However, when the balance between NSPs and their endogenous protease inhibitors (PIs) is disrupted, they also play a critical role in the pathogenesis of inflammatory lung disease. Excessive release of NSPs such as human neutrophil elastase (HNE), proteinase 3 (Pr3) and cathepsin G (CatG), leads to destruction of the lung matrix and continued propagation of acute inflammation. Under normal conditions, endogenous PIs counteract these effects by inactivating NSPs. In inflammatory lung diseases, including chronic obstructive pulmonary disease, cystic fibrosis, emphysema, and acute lung injury, there are insufficient levels of endogenous PIs to mitigate damage. Therapeutic strategies are needed to modulate excessive NSP proteolytic activity in conditions of inflammatory lung disease, in order to restore the NSP-endogenous PI balance and decrease the inflammatory response.

The Kerns laboratory previously demonstrated that heparin derivatives substituted with structurally unique aromatic residues bind with high affinity and selectivity to select glycosaminoglycan-binding proteins, and more recently, using the neomycin, kanamycin and apramycin aminoglycosides as chemical scaffolds, a panel of *N*-arylacyl *O*-sulfonated aminoglycosides was prepared as novel structural mimics of heparin. The hypothesis guiding the study presented here is that structurally unique *N*-arylacyl *O*-sulfonated aminoglycoside derivatives will selectively bind and modulate the function of NSPs both *in vitro* and *in vivo*, thus representing novel lead structures for future development of a new class of therapeutic agents capable of modulating excessive NSP activity in the lung.

To this end, the first objective was to screen the recently synthesized panel of *N*-arylacyl *O*-sulfonated aminoglycosides for their ability to inhibit each of the NSPs. The inhibitory profile of each *N*-arylacyl *O*-sulfonated aminoglycoside with respect to HNE,

CatG and Pr3 was characterized to determine if one *N*-arylacyl *O*-sulfonated aminoglycoside could inhibit multiple NSPs. Furthermore, the mechanism of protease inhibition of two lead *N*-arylacyl *O*-sulfonated aminoglycosides, identified in the initial screen, was elucidated using CatG as the representative NSP.

The *N*-arylacyl *O*-sulfonated aminoglycosides were also evaluated for their ability to inhibit the proteolytic activity of the three NSPs in a cell based assay that evaluates the ability of test compounds to inhibit NSP-mediated detachment of A549 lung epithelial cells from the surface of a 96-well plate. After concluding the *in vitro* analysis of the panel of *N*-arylacyl *O*-sulfonated aminoglycosides, one lead compound that inhibited all three of the NSPs was further evaluated *in vivo* to determine if this class of compounds exhibits any overt toxicity, and if so, at what concentrations, and secondly, if our lead compound is able to decrease LPS-induced acute inflammation in the lung.

The results of these studies validate the approach of using *N*-arylacyl *O*-sulfonated aminoglycosides to target the three NSPs as a new therapeutic method for the treatment of inflammatory lung diseases.

PUBLIC ABSTRACT

Neutrophil serine proteases (NSPs) play an important role in the innate immune system and protect against invading pathogens. However, in inflammatory lung diseases such as chronic obstructive pulmonary disease, acute lung injury and cystic fibrosis there is an imbalance between the amount of NSPs secreted and endogenous protease inhibitors (PIs) that inhibit the NSPs. Excessive release of NSPs such as human neutrophil elastase (HNE), proteinase 3 (Pr3) and cathepsin G (CatG), leads to destruction of the lung matrix and continued propagation of acute inflammation. A therapeutic strategy that can be employed for the treatment of inflammatory lung diseases is to target and inhibit the three NSPs. By inhibiting the proteolytic activity of the NSPs the balance between endogenous PIs and NSPs is restored resulting in a decrease in the inflammatory response. The work presented here encompasses the evaluation of a new class of compounds, *N*-arylacyl *O*-sulfonated aminoglycosides, as novel lead structures capable of decreasing excessive NSP activity in the lung.

TABLE OF CONTENTS

LIST OF TABLES

LIST OF FIGURES

LIST OF SCHEMES

LIST OF ABBREVIATIONS

ACE: angiotensin-converting enzyme

ACN: acetonitrile

a1PI: alpha-1 protease inhibitor

BAL: bronchoalveolar lavage

CatG: cathepsin G

COPD: chronic obstructive pulmonary disease

DCM: dichloromethane

DMF: *N, N*-dimethylformamide

ESI-MS: electrospray ionization mass spectrometry

FBS: fetal bovine serum

GAG: glycosaminoglycans

HNE: human neutrophil elastase

HRMS: high resolution mass spectrometry

IC_{50}: half maximal inhibitory concentrations

IL: interleukin

IREH: Institute of Rural and Environmental Health

LPS: lipopolysaccharide

LRMS: low resolution mass spectrometry

MMP: matrix metalloproteinase

Naph: naphthylacetyl

NFκB : nuclear factor kappa B

NSP: neutrophil serine protease

PBS: phosphate buffered saline

PDB: Protein Data Bank

PI: protease inhibitor

PhP: phenylpropionyl

PhcP: phenylcyclopropionyl

PMN: Polymorphonuclear neutrophils

Pr3: proteinase 3

RPIP: reversed-phase ion pairing

SLPI: secretory leukocyte protease inhibitor

TEA: triethylamine

TFA: trifluoroacetic acid

CHAPTER 1: INTRODUCTION

1.1 Inflammatory lung diseases

In chronic inflammatory lung diseases such as chronic obstructive pulmonary disease (COPD), cystic fibrosis, bronchiectasis, and acute lung injury, inflammation becomes excessive and there is an abnormal increase of inflammatory cells present in the airways, especially polymorphonuclear neutrophils (PMNs).[1] PMNs are essential for protection against invading pathogens and are the primary mediators of inflammatory response.[2] During inflammation PMNs migrate from the blood to the injured tissue, where neutrophil serine proteases (NSPs) are released by the PMNs. PMNs contain three different NSPs in their primary granules, human neutrophil elastase (HNE), cathepsin G (CatG) and proteinase 3 (Pr3), and release of these NSPs by the PMNs plays a critical role in the innate immune system by protecting the lung against invading pathogens.[3, 4] However, if unregulated their action can be detrimental and result in degradation of the host tissue.[5, 6] In addition, NSPs also propagate the inflammatory response by activating pro-inflammatory factors which, in turn, recruit additional PMNs to the site of inflammation, thus amplifying the inflammatory response. Endogenous protease inhibitors (PIs) inactivate NSPs to regulate NSP activity and to protect the host from the potentially damaging effects of excessive NSP release. In inflammatory lung diseases there is an imbalance between NSP secretion and levels of endogenous PIs available to modulate NSP activity (Figure 1.1).[7] This imbalance between proteases and PIs leads to excessive inflammation and contributes to the pathogenesis of chronic inflammatory lung disease.[8]

The protease-protease inhibitor theory emerged when studies first showed that patients with a hereditary alpha-1 antitrypsin (an endogenous PI) deficiency were genetically predisposed to develop pulmonary emphysema.[9] This hereditary deficiency results in disruption of the balance between proteases and endogenous PIs, manifested via

an increase in the concentration of NSPs. When the concentration of secreted NSPs

exceeds that of endogenous PIs, destruction of the extracellular matrix and structural

proteins, along with excessive inflammation is observed. NSPs have the ability to

propagate the immune response during inflammation via multiple pathways.
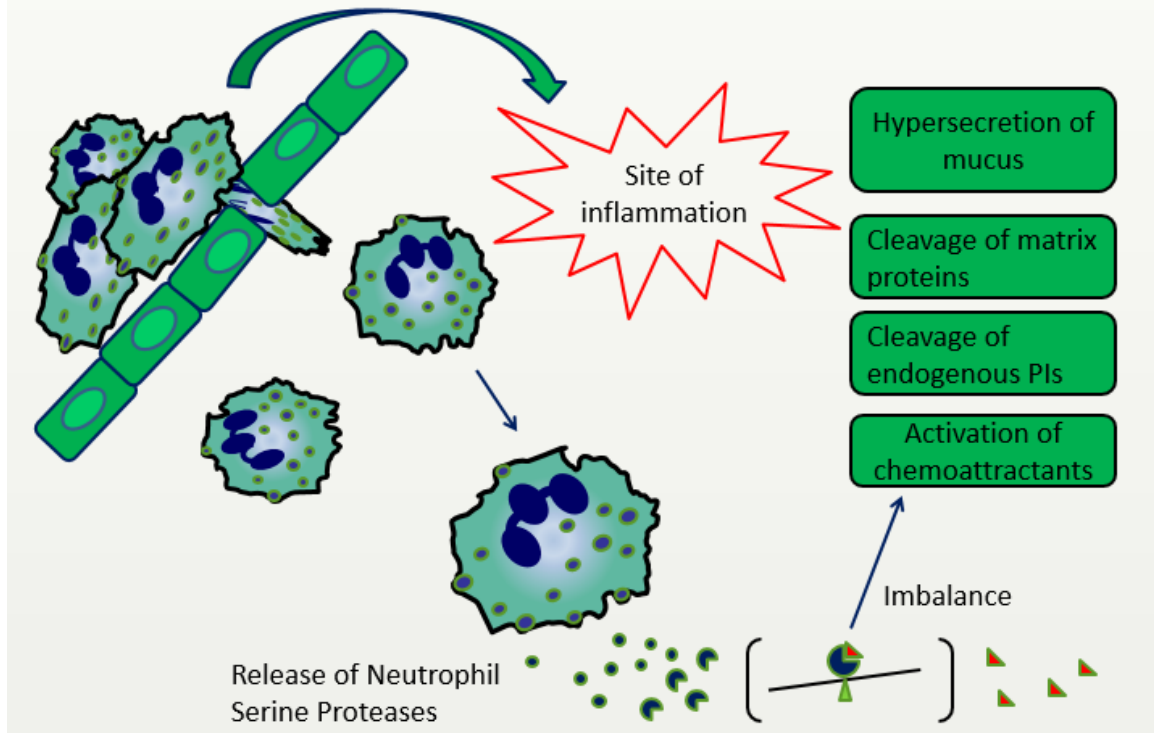
Figure 1.1. Role of NSPs in inflammation. In chronic inflammatory lung diseases
activated PMNs migrate to the site of inflammation where they release three
neutrophil serine proteases: HNE, CatG and Pr3. This can result in an
imbalance between the amounts of NSPs secreted and endogenous PIs.
Excessive NSP activity destroys the lung matrix, further inactivates
endogenous PIs and propagates the inflammatory response through activation
of chemoattractants.
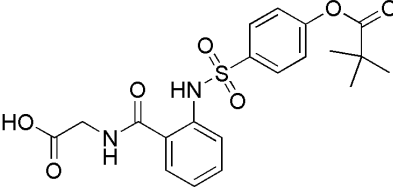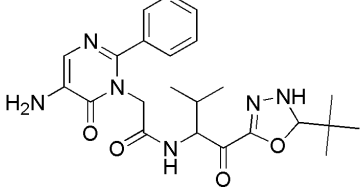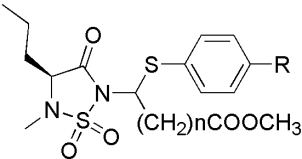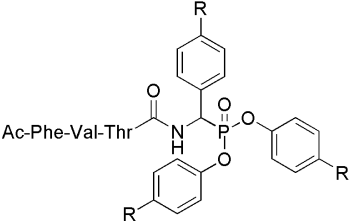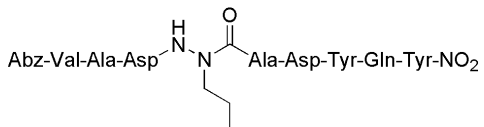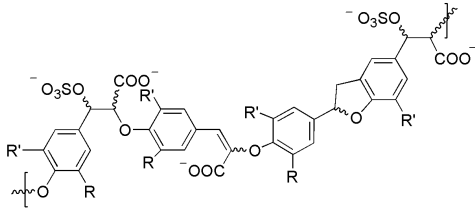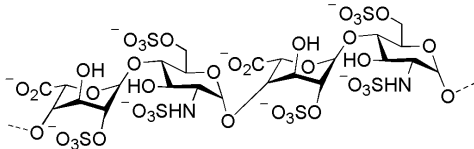
For example, Pr3 proteolytically activates interleukin-32 (IL-32) which, in turn,

triggers the release of potent neutrophil chemoattractants such as IL-8.[10] NSPs also

induce hypersecretion of mucus and cleave cell surface adhesion proteins such as

intercellular adhesion molecule 1 and epithelial (E)-cadherin, thus terminating cell-cell or cell-extracellular matrix interactions resulting in airflow obstruction, degradation of the lung matrix, and perpetuation of the inflammatory response.[6] These pathways are summarized in Figure 1.1. Based on these findings, a great deal of effort has been invested in the development of NSP inhibitors to restore the protease-protease inhibitor balance, decrease the damage due to excessive NSP activity, and decrease the inflammatory response.

<div align="center">1.2 NSP inhibitors</div>

HNE is the most aggressive NSP and has been studied extensively as a drug target for the treatment of COPD and other inflammatory lung diseases. Similarly to other serine proteases, HNE has a catalytic triad containing the residues Ser^{195}, His^{57} and Asp^{102}.[11] The design of HNE inhibitors has focused on four major classes of inhibitors: acylating inhibitors, transition state analogs, mechanism-based or suicide inhibitors and natural endogenous PIs. [8, 12, 13, 14] Sulfated polymers as well as various glycosaminoglycans (GAGs) were also studied for their ability to inhibit NSPs, and will be discussed later in this section. Representative members of each class of HNE inhibitors are shown in Table 1.1. Acylating inhibitors rely on the formation of an acyl-HNE complex at the Ser^{195} residue in the active site.[13] Multiple transition state analogs were designed to interact with both the His^{57} through hydrogen bonding and with Ser^{195} covalently.[15] Most of the promising lead compounds were discontinued due to their off-target effects. Mechanism-based inhibitors are more selective and generally act by covalently binding to both Ser^{195} and His^{57}, thus irreversibly inactivating the enzyme.[14, 16, 17, 18, 19] All of these inhibitors have low nanomolar potency towards HNE, however a majority of these drugs were discontinued due to their off-target effects, other than the acylating inhibitor Sivelestat (Ono Pharmaceuticals) which is approved in Japan for the treatment of acute respiratory failure.

Table 1.1: Representative examples of NSP inhibitors

Inhibitor Type	Structure	References
HNE inhibitors		
Acylating inhibitors ONO5046 (Sivelestat)		13, 20
Transition state inhibitors ONO6818		13, 15, 21
Mechanism-based inhibitors 1,2,5-thiadiazolidin-3-one 1,1-dioxide scafolds		16, 17, 19
CatG Inhibitors		22, 23
Irreversible inhibitors diphenyl (α-aminoa1kyl) phosphonate		
Pr3 Inhibitors		
Reversible inhibitors Azapeptides		24, 25
Sulfated polymers		26, 27, 28
Sulfated dehydropolymer caffeic acids		
Heparin		29, 30, 31, 32

Specific inhibitors of CatG and Pr3 have also been reported. Irreversible phosphonate inhibitors of CatG, due to their toxicity, have been explored mostly as molecular probes to elucidate the role of CatG in inflammatory diseases (Table 1.1).[22, 23] Increased release of Pr3 has been associated with Wegener's disease, a form of vasculitis.[33, 34] Because Pr3 and HNE are homologous proteases that share 56% sequence identity, a majority of the HNE inhibitors tend to also inhibit Pr3.[24] Specific azapeptide inhibitors of Pr3 have been synthesized as tools to further explore the role of Pr3 in inflammation and not necessarily for therapeutic uses since HNE inhibitors target Pr3 as well (Table 1.1).[25]

The use of natural endogenous PIs as exogenously administered NSP inhibitors has been studied extensively.[35, 36] In particular, alpha-1 PI (a1PI) augmentation therapy has been explored for inhibiting HNE in order to restore the protease-protease inhibitor balance.[37, 38] This approach resulted in limited success due to the fact that a1PI is prone to degradation by various enzymes present in the human body and large quantities are needed to observe a therapeutic effect. Using endogenous or recombinant NSPs to restore the protease-protease inhibitor balance has well established downfalls: 1) NSPs can adhere to the extracellular matrix and are deposited in close proximity to their substrates, thus allowing proteolysis to occur even in the presence of PIs; 2) NSPs can escape inhibition by adhering to the negatively charged proteoglycans; 3) they are not cost efficient.[39, 40]

Due to the fact that multiple selective inhibitors with low nanomolar $IC_{50}s$ for each protease showed no therapeutic benefit in patients suffering from chronic inflammatory lung diseases, the focus switched from solely inhibiting one protease, to inhibiting all three NSPs simultaneously in order to more effectively treat these types of diseases.[41]

One route to target all three NSPs is through developing mutants of endogenous PIs. One such inhibitor is trappin-2 A62L, a trappin-2 variant in which the Ala residue is

replaced by Leu.[42] Trappin-2 is a 12 kDa precursor of elafin, an endogenous PI selective for HNE and Pr3.[43, 43b, 44] Both trappin-2 and elafin have the same potency towards their target proteases and are sometimes both mistakenly referred to as elafin, thus causing some confusion.[45] Trappin-2 A62L has been shown to effectively inhibit HNE, Pr3 and CatG.[46] However, as with the endogenous PIs, these engineered protease inhibitors can still be degraded or inactivated by other proteases both upon administration and at the site of inflammation.

Another type of endogenous NSP inhibitor is heparan sulfate, which is secreted under normal inflammatory response to aid in maintaining the protease-protease inhibitor balance.[30] Heparan sulfate is a cell surface GAG, comprised of repeating disaccharide units with regions of high anionic content, which selectively and/or nonselectively binds to many proteins. During inflammation, heparan sulfate is cleaved from the cell surface by HNE resulting in a feedback mechanism that may limit elastase activity.[30] Heparin, a highly sulfated GAG that is structurally similar to heparan sulfate, as well as various heparin derivatives have been explored for their therapeutic potential as inhaled therapeutics for the treatment of chronic inflammatory lung diseases.[30, 31, 32, 47, 48, 49, 50,] Heparin is a potent inhibitor of HNE, and moderately inhibits Pr3 and CatG. However, heparin as well as low-molecular-weight heparins inhibit the proteolytic activity of NSPs in a hyperbolic manner (Figure 1.2), therefore dosing above or below the optimal inhibitory concentrations results in activation or retention of NSP activity.[29, 51] The precise mechanism for this hyperbolic inhibition is not fully understood. Another fundamental problem with using heparin as a potential treatment for inflammatory lung diseases is that polysulfated polysaccharides nonselectively bind many GAG-binding proteins resulting in undesirable off-target effects. For example, it is known that heparin not only binds and inhibits NSPs, it also binds the endogenous protease inhibitors a1PI, Secretory Leukocyte Protease Inhibitor (SLPI) and elafin.[30, 52, 53, 54]
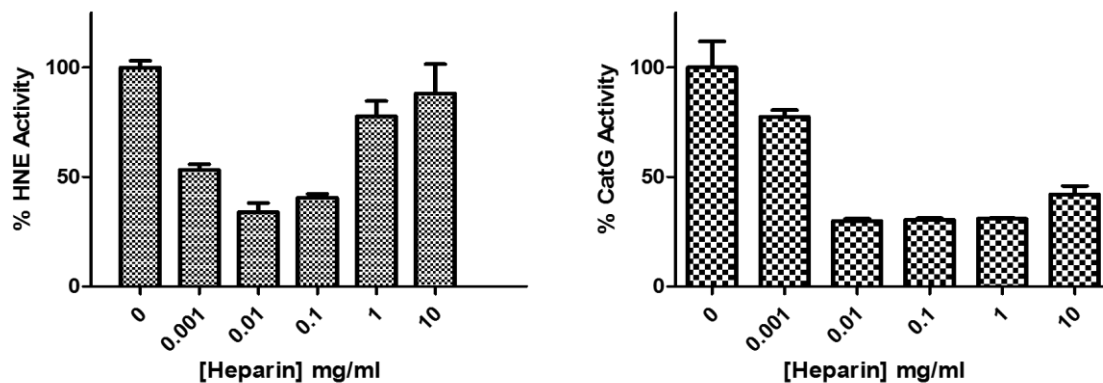
Figure 1.2: Hyperbolic inhibition of HNE and CatG by Heparin. HNE (left) and CatG (right) were each incubated with increasing concentration of Heparin (0 to 10 mg/mL) in Tris-Buffer (pH 7.4) according to published procedures.[29] Heparin inhibits both HNE and CatG at low concentrations however as the concentration of heparin is increased there is a regain in function of both proteases. This effect is more pronounced with HNE where the enzyme fully regains its activity at the highest concentration tested. Experimental methods are presented in Chapter 3.

Other types of sulfated polymers and GAGs have also been explored as potential therapeutics for treating inflammatory lung diseases.[55, 56, 57, 58] Desai and coworkers have been studying sulfated low molecular weight lignins for serine protease inhibition and other activities.[26, 27, 28] These compounds are inhibitors of HNE, but do not inhibit CatG or Pr3. However, they do act on multiple pathways of the inflammatory system by repression of nuclear factor kappa B (NFκB) and inhibiting the release of IL-8.[28]

1.3 *N*-arylacyl *O*-sulfonated aminoglycosides as heparin

mimics

It was previously demonstrated that the high degree of nonspecific protein binding seen with heparin can be mitigated by synthesizing heparin derivatives substituted with aromatic residues in place of the *N*-sulfo or carboxylate groups.[59, 60, 61] Incorporating non-anionic aryl moieties into heparin replaces nonspecific charge-charge binding contacts between heparin and target protein with more sterically hindered, due to

their larger size, and selective cation-π binding interactions.[59, 60, 61] The chemically modified heparin derivatives selectively bind certain heparin-binding proteins and also, due to the reduced charge-charge interactions, have lower nonspecific binding. More recently, using the neomycin, kanamycin and apramycin aminoglycosides as chemical scaffolds a panel of *N*-arylacyl *O*-sulfonated aminoglycosides (Figure 1.3) was prepared as novel structural mimics of heparin. However, unlike heparin they are smaller, lower charged, tri- and tetra- saccharides that are more selective in binding individual heparin-binding proteins and would overcome many of the problems seen with heparin as a possible modulator of inflammatory lung diseases.[62, 63] Each aminoglycoside core was *N*-substituted with a benzoyl, phenylacetyl or carbobenzyloxy functional group and per-*O*-sulfonated to obtain a panel of nine compounds.

Using a filtration binding assay developed in the Kerns laboratory, each member of this panel of *N*-arylacyl *O*-sulfonated aminoglycosides was screened for their ability to bind nine select heparin-binding proteins as well as compete with heparin for binding. It was shown in this previous study that *N*-arylacyl *O*-sulfonated aminoglycosides bind with various affinities to heparin-binding proteins, thus identifying our panel of *N*-arylacyl *O*-sulfonated aminoglycosides as the smallest known heparin mimics that not only maintain heparin like activity but also show selectivity. It is believed that these relatively smaller heparin-like derivatives could overcome the off-target effects seen with heparin thus inhibiting only the NSPs and not the endogenous PIs. Furthermore, due to their reduced size and charge, they might interact with the NSPs via a different mechanism thus the hyperbolic inhibition observed with heparin for inhibiting each NSPs may not ensue in the case of the *N*-arylacyl *O*-sulfonated aminoglycosides. For these reasons, the *N*-arylacyl *O*-sulfonated aminoglycosides were explored as a potentially improved new class of molecules with possible relevant applications in inflammatory lung diseases.
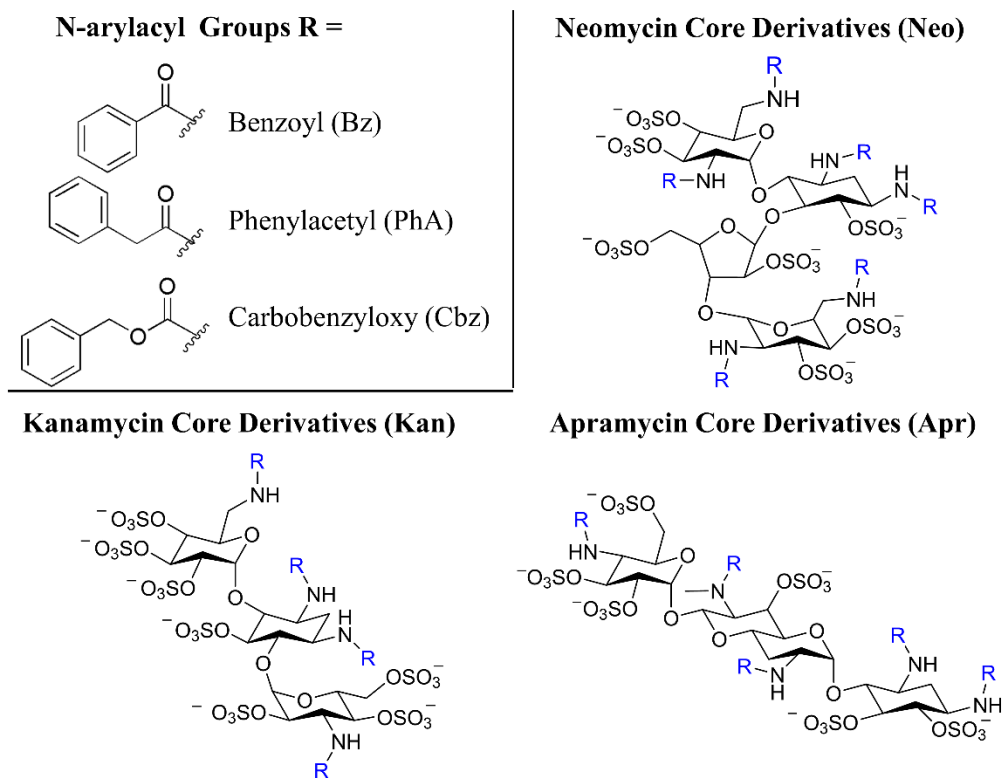
Figure 1.3. Structures and Degree of Sulfation (DS) of *N*-arylacyl *O*-sulfonated aminoglycosides. The three aminoglycoside neomycin, kanamycin and apramycin are N-substituted with three different arylacyl groups and per-*O*-sulfonated, affording the panel of nine derivatives: *N*-carbobenzyloxy *O*-sulfonated neomycin (**NeoCbz**, DS = 7), *N*-phenylacetyl *O*-sulfonated neomycin (**NeoPhA**, DS = 6.8), *N*-benzoyl *O*-sulfonated neomycin (**NeoBz**, DS = 7), *N*-carbobenzyloxy *O*-sulfonated kanamycin (**KanCbz**, DS = 6), *N*-phenylacetyl *O*-sulfonated kanamycin (**KanPhA**, DS = 5.8), *N*-benzoyl *O*-sulfonated kanamycin (**KanBz**, DS = 5.1), *N*-carbobenzyloxy *O*-sulfonated apramycin (**AprCbz**, DS = 6), *N*-phenylacetyl *O*-sulfonated apramycin (**AprPhA**, DS = 6), *N*-benzoyl *O*-sulfonated apramycin (**AprBz**, DS = 6).[64]

CHAPTER 2: STATEMENT OF PURPOSE

NSPs are key mediators of the inflammatory response and are essential in protecting against invading pathogens. In chronic inflammatory lung diseases such as chronic obstructive pulmonary disease, bronchiectasis, acute lung injury, acute respiratory distress syndrome, and cystic fibrosis, excessive accumulation of NSPs causes an imbalance between available endogenous PIs and NSPs leading to a perpetuation of the inflammatory response. For example, in cystic fibrosis approximately 70% of the inflammatory cell population in the lung are PMNs as compared to only 1% in healthy patients.[65] Cystic fibrosis is a genetic disease with a prevalence in the United States of 1 in 3500 births.[66] A majority of the inflammatory lung disease listed above have a significant prevalence, however, COPD has the highest mortality and, according to the World Health Organization, is the fifth leading cause of death in the world with projections to reach 3rd place by 2030.[67]

The primary cause of COPD was established to be tobacco smoke, however, recent studies indicate that 25-45% of COPD cases can be attributed to other factors such as biomass smoke, occupational dusts and/or chemicals, and outdoor pollution.[68, 69] COPD progresses slowly and usually undetected until the disease reaches an advanced state. There is no cure for COPD, as well as most inflammatory lung diseases, and the available therapeutics such as bronchodilators only help control the symptoms.[70, 71] Hence, it is estimated that total deaths from COPD as well as other inflammatory lung diseases will increase at an alarming rate over the next years unless new therapeutics emerge.

Acute lung injury and acute respiratory distress syndrome have lower prevalence than COPD, 200,000 cases per year reported, however the mortality rate is estimated to be around 40%.[72, 73] Clinical factors that affect the incidence and severity of these diseases are sepsis caused by bacterial infections, trauma and exposure to various

toxicants. For this class of diseases a preventative type of therapy administered prior to exposure would be beneficial.

The hypothesis guiding the study presented here is that structurally unique *N*-arylacyl *O*-sulfonated aminoglycoside derivatives will selectively bind and modulate the function of NSPs both *in vitro* and *in vivo*, thus representing novel lead structures for future development of a new class of therapeutic agents capable of modulating excessive NSP activity in the lung. To this end, a comprehensive analysis was initiated to first identify inhibitors of the three NSPs, to characterize their type of inhibition, to evaluate their activity *in vitro* and *in vivo* and finally to design and synthesize a second generation of compounds.

2.1 Goals

The first goal of this study was to screen a panel of *N*-arylacyl *O*-sulfonated aminoglycosides for their ability to inhibit each of the NSPs in a dose-dependent manner, and to determine if one *N*-arylacyl *O*-sulfonated aminoglycoside could inhibit multiple NSPs. It was envisioned that the ideal outcome would be to identify a single lead structure that inhibits all three proteases in a dose dependent manner. Inhibition of HNE, CatG, and Pr3 by the *N*-arylacyl *O*-sulfonated aminoglycosides was measured using a chromogenic substrate hydrolysis assay. This initial study would also provide key insight into the structural requirements for NSP inhibition to be used for the development of a second generation of compounds.

The second goal of this study was to elucidate the mechanism of inhibition of one or more lead compounds. The mechanism of protease inhibition was determined using CatG as the representative NSP and two lead compounds identified in the first goal. The first compound selected was *O*-sulfonated *N*-carbobenzyloxy Kanamycin, an inhibitor of all three NSPs, and the second was *O*-sulfonated *N*-carbobenzyloxy Neomycin, the most potent inhibitor of CatG and HNE.

The third goal of this study was to determine if the protease inhibition demonstrated in the enzymatic assay was translatable to a more functional cell based assay that evaluated the ability of the *N*-arylacyl *O*-sulfonated aminoglycosides to inhibit the three NSPs from promoting detachment of A549 lung epithelial cells from the surface of a 96-well plate. As discussed in Chapter 1, NSPs are known to cleave cell-surface adhesion molecules causing destruction of the lung matrix. The assay employed in this study mimics the *in vivo* proteolytic activity of the NSPs and evaluates the ability of our compounds to block this detrimental NSP activity.

Owing to success in achieving the first three goals, the next goal was to evaluate the lead compound, *O*-sulfonated *N*-carbobenzyloxy Kanamycin, *in vivo.* This was accomplished in two parts. The first part was to demonstrate that this novel lead structure, specifically, and the structural type (chemical space) of *N*-arylacyl *O*-sulfonated aminoglycosides, in general, does not afford inherent toxicity when administered to the lung. The second part was to demonstrate that *O*-sulfonated *N*-carbobenzyloxy Kanamycin can indeed mitigate toxicant-induced inflammation of the lung.

Finally, the last goal of this study was to design and synthesize a next generation of compounds to improve potency towards the three NSPs. Guided by the structure activity relationships identified in the first goal presented above, along with molecular modeling and docking studies, a second generation of derivatives was envisioned to contain three aminoglycoside cores kanamycin, neomycin and tobramycin with three new *N*-arylacyl groups. These new derivatives feature longer linkers as well as fused aromatic rings to further promote cation-π interactions.

CHAPTER 3: EVALUATION OF INHIBITORY PROFILE OF *N*-

ARYLACYL *O*-SULFONATED AMINOGLYCOSIDES AGAINST

NEUTROPHIL SERINE PROTEASES

HNE, CatG, and Pr3 play a crucial antimicrobial role in the innate immune system.[74, 75] This is accomplished by cleaving bacterial outer membrane proteins and virulence factors.[76, 77, 78] Due to their proteolytic activity, NSPs are kept in check and regulated by endogenous PIs. However, in inflammatory lung diseases there are excessive levels of NSPs secreted and an imbalance is created. NSPs can also propagate inflammation via processing of chemokines to highly active forms and are implicated in the overall regulation of the inflammatory response.[6, 79, 80, 81] Development of a drug molecule that inhibits all three NSPs is believed to be a viable therapeutic approach to restore the protease-protease inhibitor balance and decrease the inflammatory response. A great deal of effort has been invested in the development of synthetic as well as natural NSP inhibitors to restore the protease-protease inhibitor imbalance in inflammatory lung diseases.[36, 40, 42, 45, 82, 83] Current synthetic, small molecule NSP inhibitors have had little success in clinical applications and this limited success has been attributed to the fact that they are generally designed to target one NSP, mainly HNE, with only a few reports of inhibitors capable of inhibiting two of the three proteases.[48, 82, 84, 85, 86, 87]

3.1 Goal of this study

The goal of this first study was to screen a panel of nine *N*-arylacyl *O*-sulfonated aminoglycosides (presented in Chapter 1, Figure 1.3) to characterize the ability of each *N*-arylacyl *O*-sulfonated aminoglycoside to inhibit each NSP, and more importantly to determine if this structural class of agents might yield a novel small molecule that inhibits all three of the NSPs. Protease inhibition was evaluated by employing a chromogenic substrate hydrolysis assay in which enzyme specific substrates are cleaved by uninhibited enzyme to release *p*-nitroaniline (Figure 3.1).[29] Each NSP was incubated with increasing

concentrations of inhibitor and absorbance of *p*-nitroaniline as a function of time was measured and normalized to enzyme only controls in order to determine percent enzyme activity. Dose response curves of percent enzyme activity versus compound concentration were constructed and half-maximal inhibitory concentrations (IC_{50}) values were determined (Section 3.6). Uninhibited enzyme control data points that represent 100% enzyme activity were included in the dose response curves as a point of reference.
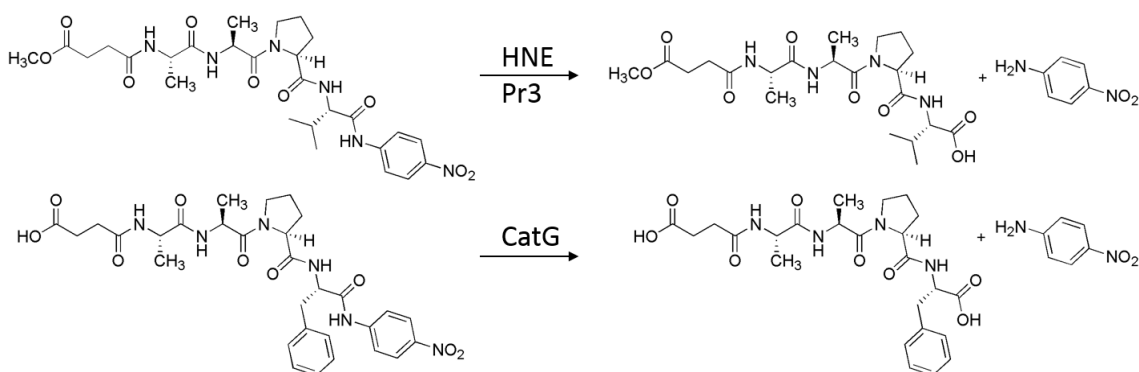
Figure 3.1: Cleavage of protease specific substrate resulting in release of *p*-nitroaniline. HNE and Pr3 specific substrate *N*-methoxysuccinyl-Ala-Ala-Pro-Val-*p*-nitroanilide is shown on top and CatG specific substrate *N*-succinyl-Ala-Ala-Pro-Phe-*p*-nitroanilide shown on bottom.

3.2 Inhibition of HNE by *N*-arylacyl *O*-sulfonated aminoglycosides

Each *N*-arylacyl *O*-sulfonated aminoglycoside was evaluated for its ability to inhibit HNE in a concentration dependent manner (Figure 3.2). Test compound concentrations varied from 0 to 350 µM. A wide range of inhibition was observed with some derivatives showing potent HNE inhibition while for others limited to no inhibition of the enzyme was observed. No evidence of hyperbolic inhibition of HNE was observed, as has been previously shown to occur with heparin (Figure 1.2, Chapter 1). None of the nine derivatives tested achieved complete inhibition of HNE (Figure 3.2, A-

C). The inability of test compounds to achieve 100% inhibition was not surprising, and

these results are consistent with the varied levels of fractional inhibition of serine

proteases observed for sulfated low molecular weight lignins as well as other polysulfated

polysaccharides.[28, 26]
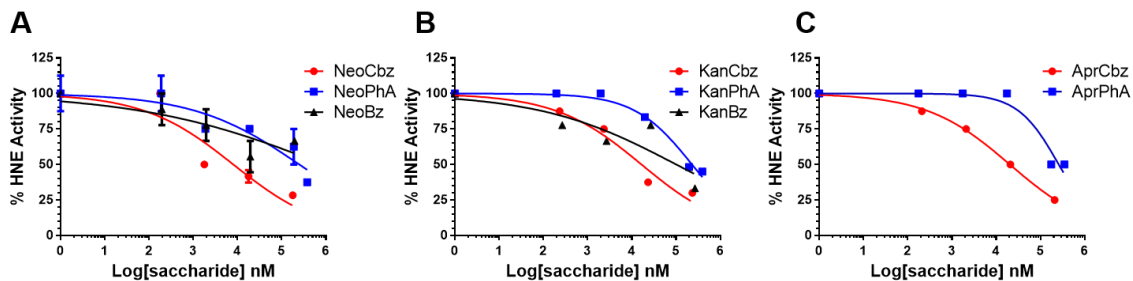
Figure 3.2: Inhibition of HNE. Dose-dependent inhibition of HNE by *N*-arylacyl *O*-
sulfonated neomycin (A), *N*-arylacyl *O*-sulfonated kanamycin (B) and *N*-
arylacyl *O*-sulfonated apramycin (C) derivatives. Absorbance as a function of
time, of *p*-nitroaniline released from HNE specific chromogenic substrate was
measured at 405 nm and normalized to enzyme only control. Nonlinear
regression curve fitting was performed to obtain IC_{50} values summarized in
Table 3.1. Data are presented as mean $\pm$ SEM (n = 3). Structures are shown
in Figure 1.3.

Of the nine compounds evaluated, **NeoCbz**, shown in red closed circles (Figure

3.2 A), was the most potent HNE inhibitor (IC_{50} = 8.1 µM, Table 3.1). As a general

trend, the carbobenzyloxy substituted derivatives were the most potent inhibitors of HNE.

When comparing each core with the carbobenzyloxy *N*-aryl function group, the neomycin

core derivative (**NeoCbz**) was the most potent followed by the kanamycin core derivative

(**KanCbz**), and the apramycin core derivative (**AprCbz**) was the least potent of the three.

The phenylacetyl substituted derivatives inhibited HNE only at high concentrations with

IC_{50} values in the 250 µM range (Table 3.1 or Figure 3.2 above). The benzoyl substituted

derivatives did not achieve 50% inhibition of HNE, regardless of the aminoglycoside

core, while **AprBz** had no inhibitory effect (Figure 3.2, A-C).

15

It is apparent that inhibition of HNE is strongly dependent on the *N*-aryl functional group and to a lesser extent on the aminoglycoside core. For the carbobenzyloxy substituted derivatives the phenyl moiety is positioned further away from the aminoglycoside core due to the carbamate linkage, and is thus likely able to not only reach and occupy a deeper binding pocket but also orient to make multiple binding contacts with cationic residues on the surface of HNE. As the distance between the phenyl moiety and the aminoglycoside core is decreased, the compounds lose their ability to bind and inhibit the enzyme, as was observed with the benzoyl substituted derivatives.

3.3 Inhibition of CatG by *N*-arylacyl *O*-sulfonated aminoglycosides

Each *N*-arylacyl *O*-sulfonated aminoglycoside was evaluated for its ability to inhibit CatG in a concentration dependent manner with concentration once again varying from 0 to 350 µM. All 9 derivatives tested inhibited CatG with more than half of the compounds screened having IC_{50} values in the single digit micromolar range. Once again, as seen with inhibition of HNE, the compounds inhibited CatG in a dose-dependent manner with no evidence of hyperbolic inhibition observed. The carbobenzyloxy substituted derivatives, shown in red closed circles (Figure 3.3 A-C) appear to completely inhibit CatG activity at the highest concentration tested.
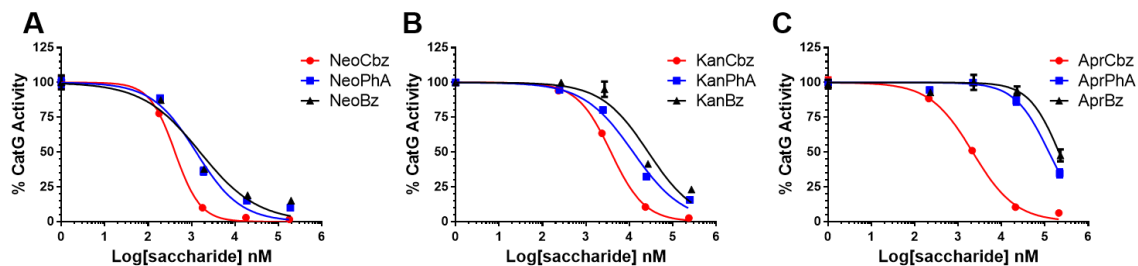
Figure 3.3: Inhibition of CatG. Dose-dependent inhibition of CatG by *N*-arylacyl *O*-sulfonated neomycin (A), *N*-arylacyl *O*-sulfonated kanamycin (B) and *N*-arylacyl *O*-sulfonated apramycin (C) derivatives. Absorbance as a function of time, of *p*-nitroaniline released from CatG specific chromogenic substrate was measured at 405 nm and normalized to enzyme only control. Nonlinear regression curve fitting was performed to obtain IC_{50} values summarized in Table 3.1. Data are presented as mean ± SEM (n = 3). Structures are shown in Figure 1.3.

The IC_{50} values ranged from 0.42 μM for **NeoCbz** to 209 μM for **AprBz** (Figure 3.3 A-C, Table 3.1). The concentration-dependent inhibitory profiles revealed that the neomycin core derivatives (Figure 3.3 A) were the most potent inhibitors of CatG, followed by the kanamycin core derivatives (Figure 3.3 B) with slightly higher IC_{50}s and apramycin derivatives with the lowest overall potency as a group (Figure 3.3 C). It appears that a larger and flexible aminoglycoside core is more favorable for inhibiting CatG. When comparing the *N*-aryl functional groups, the carbobenzyloxy substituted derivatives, shown in red, were the most potent inhibitors with all compounds having IC_{50} values in the single digit micromolar range. The phenylacetyl substituted derivatives had reduced potency when compared to their carbobenzyloxy analogs and a similar effect was observed with the benzoyl substituted derivatives. The trend in activity between the carbobenzyloxy, phenylacetyl and benzoyl substituted derivatives can be best observed for the aparmycin core series of derivatives, where the IC_{50} values increase from 2.14 μM for the carbobenzyloxy derivative to 123 μM for the phenylacetyl derivative, to 209 μM for the benzoyl derivative. Also, the **AprBz** derivative barely reaches more than 50% inhibition of CatG. These results suggest that a longer and more flexible core such as

neomycin and *N*-aryl derivative such as carbobenzyloxy are generally favored for CatG inhibition.

3.4 Inhibition of Pr3 by *N*-arylacyl *O*-sulfonated aminoglycosides

Each member of the panel of *N*-arylacyl *O*-sulfonated aminoglycosides was tested for its ability to inhibit Pr3 activity. As compared to results obtained for the ability of the nine derivatives to inhibit HNE and CatG, inhibition of Pr3 was moderate with only four *N*-arylacyl *O*-sulfonated aminoglycosides achieving more than 50% inhibition of the proteolytic activity of this protease. IC_{50} values ranged from about 17 μM to 165 μM. Once again, as was the case with HNE and CatG, no hyperbolic inhibition was observed in the presence of increasing concentration of these compounds. Due to the fact that the *N*-arylacyl *O*-sulfonated aminoglycosides were less active towards Pr3, a clear trend in the inhibitory profile necessary for Pr3 inhibition was not elucidated. However, for the kanamycin core derivatives as the distance between the aryl moiety and aminoglycoside core decreases there is a drastic loss in activity, consistent with the IC_{50} values obtained for inhibition of HNE. **AprCbz** also had similar IC_{50} values for inhibition of Pr3 and HNE, which follows the same trend that was seen for *N*-arylacyl *O*-sulfonated kanamycin derivatives (Table 3.1).
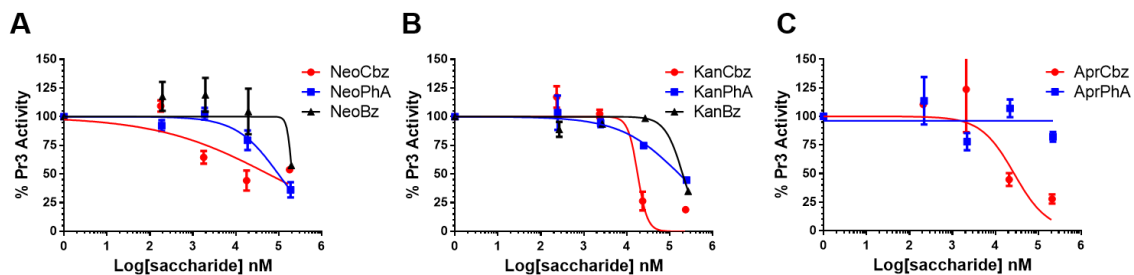
Figure 3.4: Inhibition of Pr3. Dose-dependent inhibition of Pr3 by *N*-arylacyl *O*-sulfonated neomycin (A), *N*-arylacyl *O*-sulfonated kanamycin (B) and *N*-arylacyl *O*-sulfonated apramycin (C) derivatives. Absorbance as a function of time, of *p*-nitroaniline released from Pr3 specific chromogenic substrate was measured at 405 nm and normalized to Pr3 only control. Nonlinear regression curve fitting was performed to obtain IC_{50} values summarized in Table 3.1. Data are presented as mean ± SEM (n = 3). Structures are shown in Figure 1.3.

N-arylacyl *O*-sulfonated neomycin derivatives did not follow this same trend. Interestingly, **NeoCbz**, the most potent inhibitor of HNE and CatG, did not achieve 50% inhibition of Pr3 (Figure 3.4 A). This was unexpected since most inhibitors that are active towards HNE tend to also inhibit Pr3. **NeoPhA** was a weak inhibitor of Pr3 and the benzoyl substituted neomycin derivative did not achieve 50% inhibition. A general trend consistent with the results obtained with HNE, was that *N*-phenylacetyl *O*-sulfonated aminoglycosides were weak inhibitors of Pr3, while the *N*-benzoyl *O*-sulfonated aminoglycosides derivatives showed an inhibitory effect only at high concentrations. **KanCbz** was a potent inhibitor of Pr3 and thus, the inhibition of CatG, HNE and Pr3 by our panel of *N*-arylacyl *O*-sulfonated aminoglycosides revealed *O*-sulfonated *N*-carbobenzyloxy Kanamycin as a novel inhibitor of all three NSPs, and *O*-sulfonated *N*-carbobenzyloxy Neomycin as a potent inhibitor of HNE and CatG.

3.5 Discussion and conclusions

In general, *N*-arylacyl *O*-sulfonated neomycin and kanamycin derivatives were more potent inhibitors of the three NSPs when compared to the corresponding *N*-arylacyl

O-sulfonated apramycin derivatives. As was mentioned above, these results indicate that a flexible core structure allows for more favorable binding to the proteases resulting in inhibition of their proteolytic activity. As can be seen from the 3D-molecular structure of the aminoglycoside cores featuring the benzoyl *N*-aryl moiety, neomycin core derivatives are generally more flexible (Figure 3.5). This increased flexibility is partly a result of having four glycosidic or glycoside-like bonds in the neomycin structure. Kanamycin and apramycin derivatives have only two glycosidic or glycoside-like bonds; however, apramycin derivatives also possess a centered fused-ring system making them more rigid and resulting in more linear type derivatives that lack the curvature characteristic of the kanamycin and neomycin core derivatives (Figure 3.5).
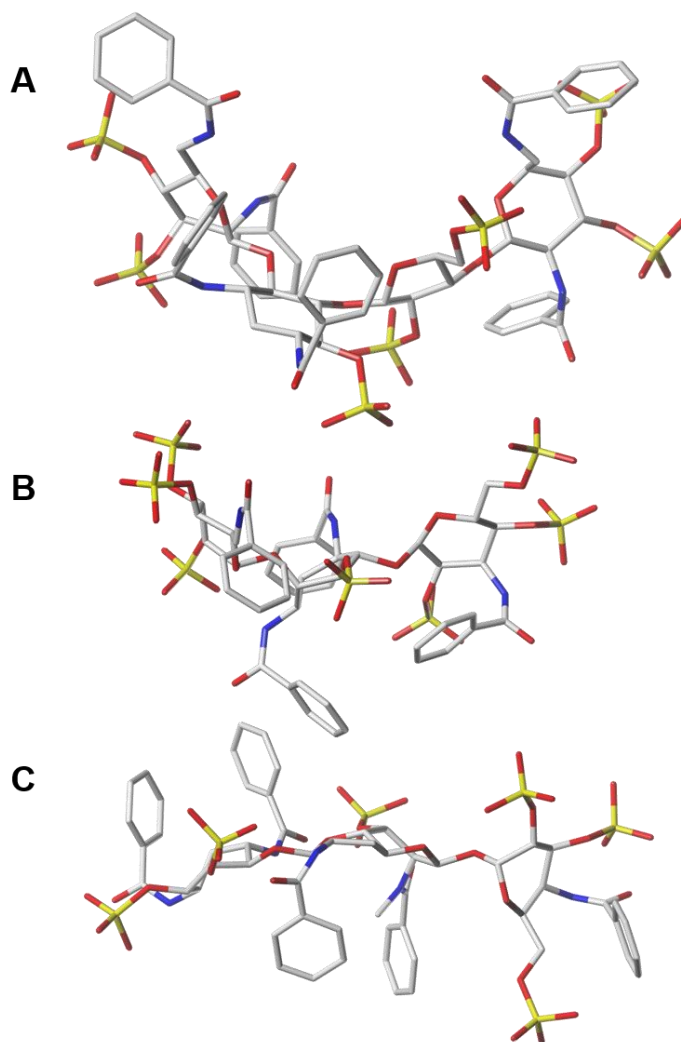
Figure 3.5: Spatial orientation of *N*-benzoyl *O*-sulfonated aminoglycosides. Energy minimized conformation of **NeoBz** (A) **KanBz** (B) and **AprBz** (C). Nitrogen atoms are shown in blue, sulfur atoms in yellow and oxygen atoms in red.

The apramycin derivatives had consistently higher IC_{50} values and lower protease inhibition activity (Table 3.1). It is expected that the binding sites for the *N*-arylacyl *O*-sulfonated aminoglycosides are most likely large and shallow, with pockets available for the *N*-aryl groups to potentially form hydrophobic binding contacts and cation-π interactions. Thus a flexible core accommodates structural changes for optimal

positioning to bind to one or multiple proteases. The length of the aminoglycoside cores also appears to play a role in the potency of the compounds. Neomycin is a tetrasaccharide and the **NeoCbz** derivative was the most potent inhibitor characterized. Although the smaller **KanCbz** derivative, possessing a tri-saccharide core, had lower optimal inhibition with any single NSP, it was overall the more potent inhibitor of all three NSPs, making it a novel non-peptide based small inhibitor of all three serine proteases.

Table 3.1: Half-maximal inhibitory concentration of *N*-arylacyl *O*-sulfonated aminoglycosides for inhibition of each NSP[64]

Compound	Human Neutrophil Elastase[a] IC_{50} (µM)			Cathepsin G[b] IC_{50} (µM)			Proteinase 3[a] IC_{50} (µM)		
NeoCbz	8.1	±	3.5	0.42	±	0.03		>300	
NeoPhA		>300		1.29	±	0.21	98	±	23
NeoBz		>300		1.55	±	0.36		>300	
KanCbz	17	±	8	3.72	±	0.17	17	±	5
KanPhA	230	±	60	12.3	±	1.4	166	±	59
KanBz		>300		26.9	±	5.6		>300	
AprCbz	20	±	12	2.14	±	0.2	27	±	18
AprPhA	260	±	30	123	±	11		NI	
AprBz		NI		209	±	25		ND	

NI: no inhibition; ND: not determined.
IC_{50} values derived from nonlinear regression curve fitting to log(inhibitor) vs normalized response. Data shown as mean ± SEM (n = 3).
[a]Substrates: *N*-methoxysuccinyl-Ala-Ala-Pro-Val-*p*-nitroanilide; [b]*N*-succinyl-Ala-Ala-Pro-Phe-*p*-nitroanilide.

The benzoyl substituted derivatives for each aminoglycoside core structure, were either weak or did not inhibit the NSPs, suggesting that a longer distance between the aryl sidechain functional group and the aminoglycoside core is necessary for making binding contacts on the surface of the NSPs. As this length is increased from the benzoyl to phenylacetyl to carbobenzyloxy substituted derivatives there is a consistent decrease in

IC_{50} values. This effect was observed in the case of all three NSPs. Interestingly, members of the panel of *N*-arylacyl *O*-sulfonated aminoglycosides preferentially bind and completely inhibit peptidolytic activity of CatG. Complete inhibition of HNE and Pr3 was not observed for any of the compounds tested, however, even moderate inhibition of all three serine proteases is most likely sufficient to modulate their activity restoring the protease-protease inhibitor imbalance and attenuating the inflammatory response. NSPs play an important role in protecting the host against invading pathogens and complete inhibition of these proteases with a potent compound could leave the patient vulnerable to opportunistic lung infections.

3.6 Methods

3.6.1 Materials

N-arylacyl *O*-sulfonated aminoglycosides were previously synthesized and characterized by Amanda Fenner in the Kerns lab.[62, 63, 64] Human neutrophil elastase (HNE, EC 3.4.21.37) was purchased from Calbiochem (EMD Chemicals, San Diego, CA), human proteinase 3 (Pr3, EC 3.4.21.76) and human Cathepsin G (CatG, EC 3.4.21.20) were purchased from Cell Sciences (Canton, MA). HNE and Pr3 specific substrate *N*-methoxysuccinyl-Ala-Ala-Pro-Val-*p*-nitroanilide and CatG specific substrate *N*-succinyl-Ala-Ala-Pro-Phe-*p*-nitroanilide were purchased from Sigma-Aldrich (St. Louis, MO). Heparin sodium salt was purchased from MP Biomedicals (Aurora, OH, USA). Molecular biology grade Tris (99.9% pure) was obtained from Research Products International Corporation (Mt. Prospect, IL, USA). Sodium chloride for molecular biology ($\geq$ 98% pure) was obtained from Sigma Aldrich (St. Louis, MO, USA). Biotechnology grade bovine serum albumin was obtained from Amresco (Solon, OH, USA). Filtered, deionized water used with all buffers was from a Barnstead Nanopure Diamond system, Thermo Fisher Scientific (Hampton, NH, USA). A Fisher Accumet AB15 pH meter (Thermo Fisher Scientific (Hampton, NH, USA)) was used for all pH

determinations. All absorbance measurements were performed using a BioTek Synergy 2 plate reader equipped with an external automated dispenser (Winooski, VT, USA).

3.6.2 Hyperbolic inhibition of HNE and GatG by heparin

Inhibition of HNE and CatG by heparin was assessed according to published procedures to validate the assay used for the evaluation of *N*-arylacyl *O*-sulfonated aminoglycosides.[29] Briefly, heparin at various concentrations 0 to 10 mg/mL (60 µL) was pre-incubated on ice with HNE (10 µL, 10.6 nM final concentration) and CatG (10 µL, 140 nM final concentration) for 30 min after which they were aliquoted in a 96-well plate. The plate was incubated in the plate reader for 10 min at 30 °C for HNE and 37°C for CatG with medium shake. Following incubation, 50 µL of 2 mM *N*-methoxysuccinyl-Ala-Ala-Pro-Val-*p*-nitroanilide (HNE specific substrate) or 1 mM *N*-succinyl-Ala-Ala-Pro-Phe-*p*-nitroanilide (CatG specific substrate) was dispensed using the automated dispense system to each well of the 96-well plate to reach a final volume of 160 µL. This was followed by a fast shake for 3 sec. Release of *p*-nitroaniline was monitored by measuring absorbance at 405 nm. Enzyme activity was determined by calculating the initial rate of each progress curve in the linear region and was expressed as a percentage of the initial rate of the uninhibited enzyme. The incubation medium used throughout the experiment was 50 mM Tris buffer, pH 7.4, containing 150 mM NaCl and 0.1 mg/mL bovine serum albumin.

3.6.3 Inhibition of HNE

Inhibition of HNE by each member of the panel of *N*-arylacyl *O*-sulfonated aminoglycosides was measured using a chromogenic substrate hydrolysis assay.[29] Compounds at various concentrations ranging from 0 to 350 µM were pre-incubated on ice with 10.6 nM HNE for 30 min after which they were aliquoted in a 96-well plate (10 µL HNE, 60 µL test compound and 40 µL buffer). The plate was incubated in the plate reader for 10 min at 30°C with medium shake. Following incubation, 50 µL of 2 mM *N*-

methoxysuccinyl-Ala-Ala-Pro-Val-*p*-nitroanilide was dispensed using the automated dispense system to each well of the 96-well plate to reach a final volume of 160 µL. This was followed by a fast shake for 3 sec. Release of *p*-nitroaniline was monitored by measuring absorbance at 405 nm. Enzyme activity was determined by calculating the initial rate of each progress curve in the linear region and was expressed as a percentage of the initial rate of the uninhibited enzyme. Data are analyzed in Prism^{TM} 6 (GraphPad Software, Inc., La Jolla, CA) using nonlinear regression curve fit to determine the half maximal inhibitory concentration (IC_{50}) values of each compound. The incubation medium used throughout the experiment was 50 mM Tris buffer, pH 7.4, containing 150 mM NaCl and 0.1 mg/mL bovine serum albumin.

3.6.4 Inhibition of CatG

Inhibition of CatG by *N*-arylacyl *O*-sulfonated aminoglycosides was determined similarly to HNE.[29] Compounds at various concentrations ranging from 0 to 350 µM were pre-incubated on ice with 140 nM CatG for 30 min after which they were aliquoted in a 96-well plate (10 µL CatG, 60 µL test compound and 40 µL buffer). The plate was incubated further for 10 min at 37°C with medium shake. Following incubation, 50 µL of 2 mM *N*-succinyl-Ala-Ala-Pro-Phe-*p*-nitroanilide was dispensed using the automated dispense system to each well of the 96-well plate to reach a final volume of 160 µL. This was followed by a fast shake for 3 sec. Release of *p*-nitroaniline was monitored by measuring absorbance at 405 nm. Enzyme activity was determined by calculating the initial rate of each progress curve in the linear region and was expressed as a percentage of the initial rate of the uninhibited enzyme. Data are analyzed in Prism^{TM} 6 using nonlinear regression curve fit to determine IC_{50} values of each compound. The incubation medium used throughout the experiment was 50 mM Tris buffer, pH 7.4, containing 150 mM NaCl and 0.1 mg/mL bovine serum albumin.

3.6.5 Inhibition of Pr3

Inhibition of Pr3 by *N*-arylacyl *O*-sulfonated aminoglycosides was measured using similar methodology to experiments with HNE and CatG.[29] Compounds at various concentrations ranging from 0 to 350 μM were pre-incubated with 150 nM Pr3 for 30 min on ice (10 μL HNE, 60 μL test compound and 40 μL buffer). Following pre-incubation the Pr3-compound mix was aliquoted in a 96-well plate and incubated for 10 min at 37°C with medium shake. Following incubation, 50 μL of 2 mM *N*-methoxysuccinyl-Ala-Ala-Pro-Val-p-nitroanilide was dispensed using the automated dispense system to each well of the 96-well plate to reach a final volume of 160 μL. This was followed by a fast shake for 3 sec. Release of *p*-nitroaniline was monitored by measuring absorbance at 405 nm. Enzyme activity was determined by calculating the initial rate of each progress curve in the linear region and was expressed as a percentage of the initial rate of the uninhibited enzyme. Data are analyzed in Prism™ 6 using nonlinear regression curve fit to determine IC_{50} values of each compound. The incubation medium used throughout the experiment was 50 mM Tris buffer, pH 7.4, containing 150 mM NaCl and 0.1 mg/mL bovine serum albumin.

CHAPTER 4: MODE OF PROTEASE INHIBITION BY *N*-ARYLACYL

O-SULFONATED AMINOGLYCOSIDES

HNE, CatG and Pr3 are sequentially homologous serine proteases belonging to the chymotrypsin family and are stored in the azurophilic granules of neutrophils.[39, 88, 89] They contain between 218 and 235 residues with multiple clusters of arginine or lysine residues on the surface. HNE contains 19 arginine residues, Pr3 13 arginine and 2 lysine residues, while CatG contains 34 arginine residues and 4 lysine residues thus making CatG the most basic (pI of ~12) of the serine proteases followed by HNE and Pr3 (pI of ~10.5 and 9.5 respectively).[90, 91, 92] HNE and Pr3 have 56% sequence identity and 35% sequence identity with CatG.[93, 94] From the crystal structure of the three NSPs it is observed that the proteases differ greatly in the surface distribution of the cationic amino acids (Figure 4.1).[93, 95, 96] CatG also has a cluster of positively charged residues as well as a larger hydrophobic pocket near the active site thus preferentially binding aromatic residues at this substrate binding pocket.
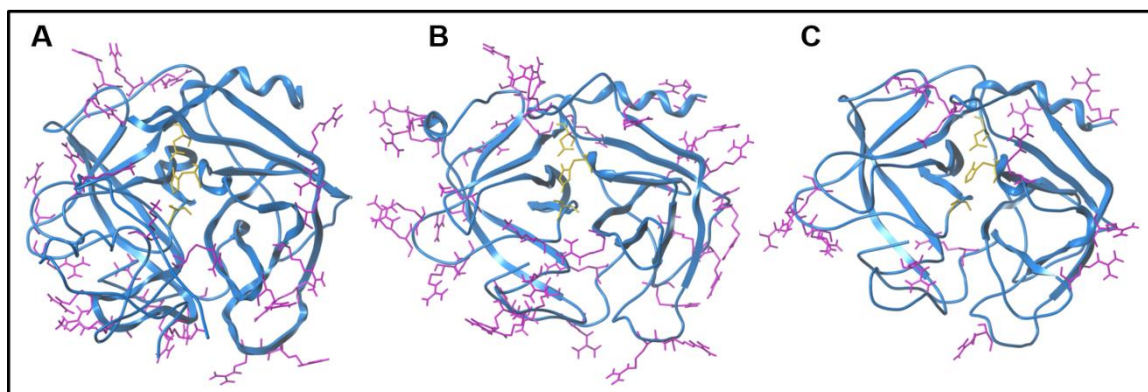
Figure 4.1: Comparison of crystal structures of the three NSPs. Ribbon representation of (A) HNE (PDB: 1PPF) (B) CatG (PDB: 1CGH) and (C) Pr3 (PDB: 1FUJ). Arginine and Lysine side chains are shown in magenta and catalytic triad residues (His57, Asp102, Ser195) in yellow.

Heparin has been shown to bind such clusters of positively charged amino acids, which act as a clamp, tightly binding the negatively charged heparin and stretching it across the active site, thus blocking substrate from binding.[30] A minimum length of 12-14 saccharide units has been shown to be necessary for heparin to inhibit HNE. Considering that the *N*-arylacyl *O*-sulfonated aminoglycosides contain only tri or tetra-saccharide cores, and could not reach across the active site of these NSPs, their mechanism of inhibition merited further study.

4.1 Goal of this study

HNE, Pr3 and CatG are homologous cationic proteases, and it is anticipated that each inhibitor will likely have the same general mechanism of inhibition for each protease and therefore for this study CatG was used as a model for all three NSPs. A majority of the protease inhibitors proposed as therapeutics for targeting NSPs target the active site. However, most proteases *in vivo* are in a substrate-saturated environment which hinders the ability of competitive inhibitors to bind the active site.[97] Based on studies with heparin and other polysulfated polysaccharides, it was anticipated that *N*-arylacyl *O*-sulfonated aminoglycosides are unlikely to directly compete with substrate for binding to the active site.[30, 98, 99, 100] In the study presented here, the mechanism of inhibition of *O*-sulfonated *N*-carbobenzyloxy Kanamycin and *O*-sulfonated *N*-carbobenzyloxy Neomycin with respect to CatG was explored to further understand the mechanism of protease inhibition for this unique class of potential therapeutics.

4.2 Initial velocity studies with CatG and two lead compounds

From the analysis of each test compound's ability to inhibit each NSP (Chapter 3), two compounds were chosen for further studies to determine their mechanism of inhibition. **NeoCbz** was chosen for its potent inhibition of HNE and CatG. **KanCbz** was selected for its ability to inhibit each of the three NSPs. Initial velocity studies were

carried out using CatG specific substrate *N*-succinyl-Ala-Ala-Pro-Phe-*p*-nitroanilide (0.315 to 2 mM), in the presence of **KanCbz** or **NeoCbz** (0, 0.5[IC_{50}], [IC_{50}] 2[IC_{50}] and 4[IC_{50}]). The enzyme inhibition data were fit, using the Enzyme Kinetics packet in SigmaPlot, to eight enzyme kinetics models: mixed partial and full, noncompetitive partial and full, uncompetitive partial and full, and competitive partial and full. All enzyme kinetics models were compared and ranked according to the goodness of fit of the data (R^2 values) and Michaelis-Menten and Lineweaver-Burk plots were generated in SigmaPlot as well (Figure 4.2). Both **KanCbz** and **NeoCbz** were found to be partial mixed inhibitors of CatG.
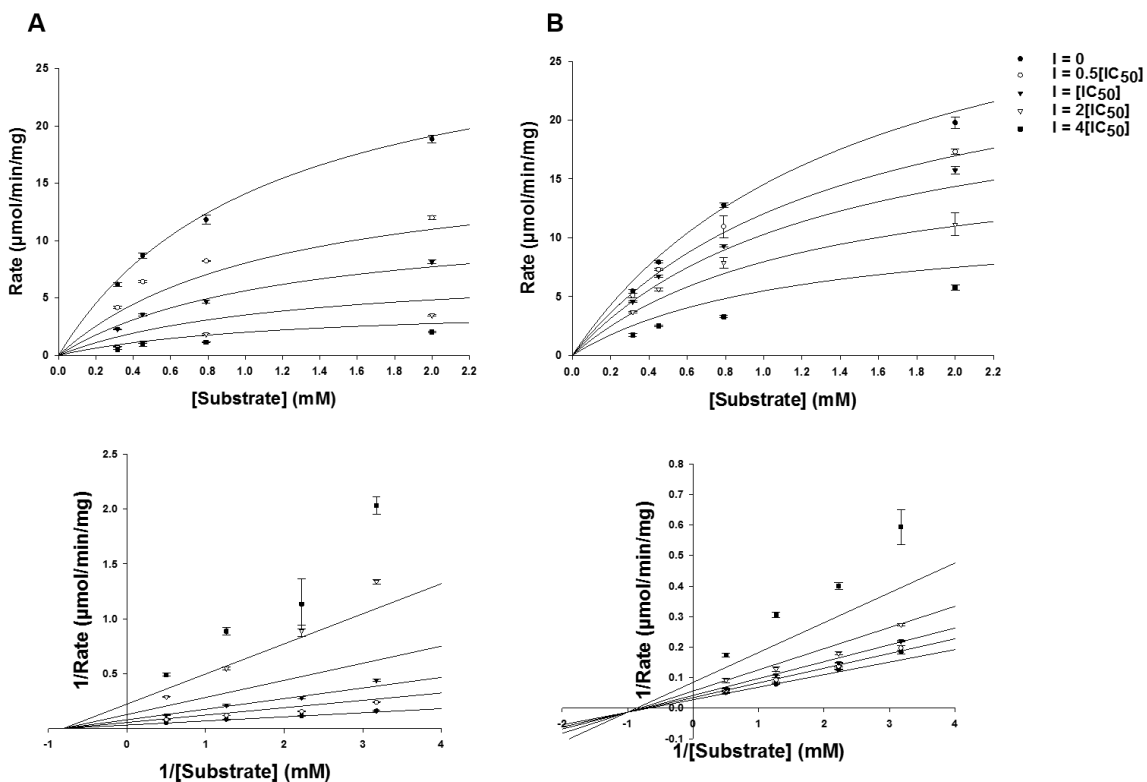
Figure 4.2: Mode of CatG inhibition. Michaelis-Menten plot (top) and Lineweaver-Burk Plot (bottom) of (A) **KanCbz** and (B) **NeoCbz** inhibition of CatG. The concentration of CatG chromogenic substrate was varied at four different inhibitor concentrations (0, 0.5[IC_{50}], [IC_{50}], 2[IC_{50}] and 4[IC_{50}]). Both compounds were partial mixed inhibitors of CatG. **KanCbz** Ki = 2.4, α = 1.1, β = 1.7 e-9; **NeoCbz** Ki = 1.2, α = 0.67, β = 3.87 e-17

Of note is the fact that at high concentrations of inhibitor there is a higher

inhibition of CatG than would be expected, as can be seen from the Michaelis-Menten

plots (Figure 4.2). Control studies were performed in order to ensure that these results

were not due to interference of the carbobenzyloxy functional groups with released *p*-

nitroaniline or that the *O*-sulfo groups were causing a decrease in enzyme activity. The

control studies included constructing a *p*-nitroaniline standard curve in the presence of

different concentrations of **KanCbz** and secondly, measuring the catalytic activity of CatG in the presence of increasing concentrations of sulfate salts. The absorbance of *p*-nitroaniline at 405 nm was unchanged upon addition of **KanCbz** and the catalylic activity of CatG was unchanged in the presence of increasing concentrations of sulfate salts.

4.3 Molecular modeling studies with CatG

In order to further corroborate the partial mixed mechanism of inhibition, docking studies with **KanCbz** and **NeoCbz** were performed to determine possible binding sites on the surface of CatG (Figure 4.3) as well as in the active site or close to the active site. Docking runs were performed by creating protomols (idealized binding pockets generated by the docking program) around exposed positively charged residues. Heparin was included in these studies as a control since it is known that a heparin hexamer will bind at clusters in close proximity to the active site.[30, 101, 102]
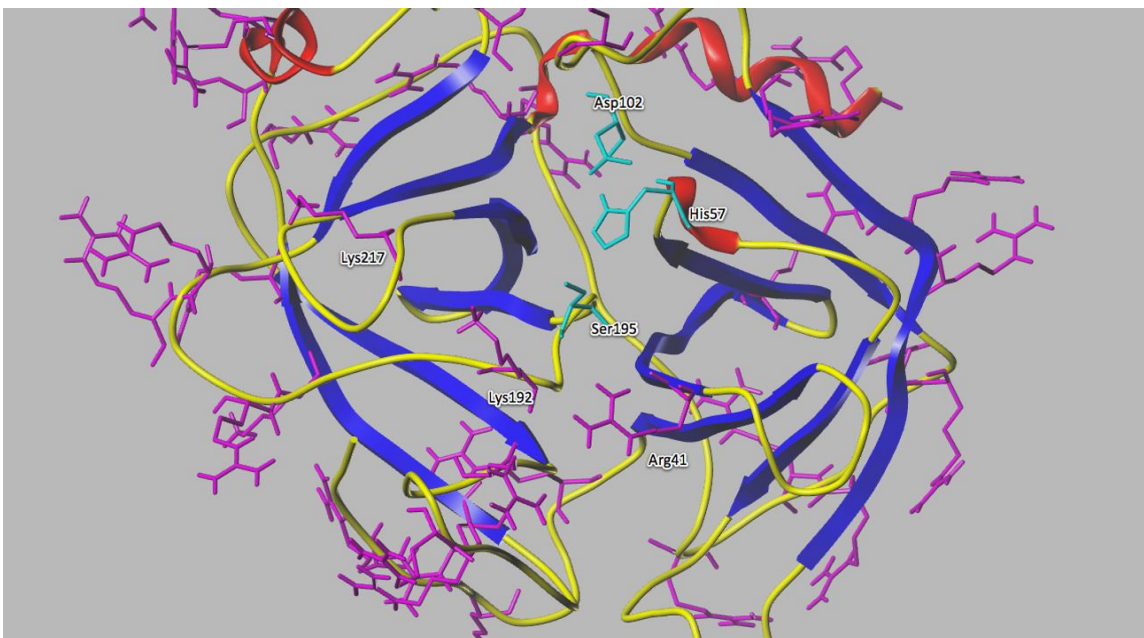
Figure 4.3: Crystal structure of CatG. Structure of CatG (PDB: 1CGH) showing catalytic triad residues His57, Asp102 and Ser195 in cyan and positively charged residues in magenta. Arg41, Lys192 and Lys 217 line the exterior of the active site pocket.

KanCbz binds in the active site with one of the carbobenzyloxy groups extending into the P1 pocket of the CatG (Figure 4.4). Aromatic moieties are preferred for binding at P1 pocket as is observed in the binding of the chromogenic CatG specific substrate *N*-succinyl-Ala-Ala-Pro-Phe-*p*-nitroanilide that contains a Phe capable of forming edge-to-edge electrostatic interactions with a Glu residue.[88, 96]
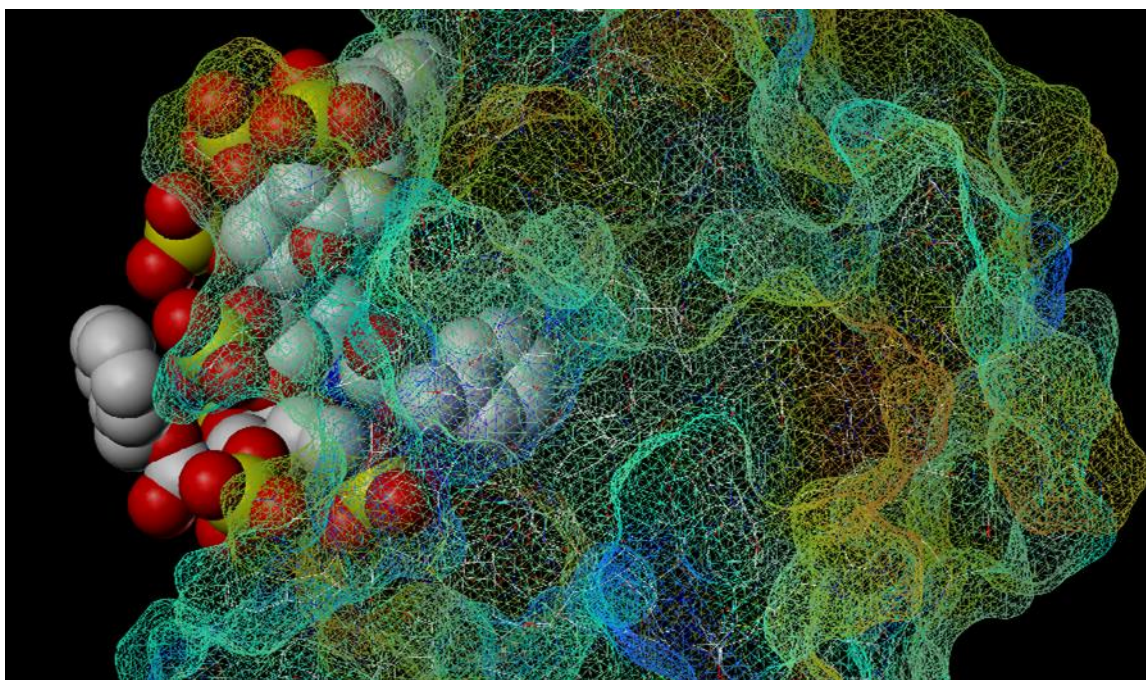
Figure 4.4: **KanCbz** docked in active site. **KanCbz** shown as a space filling model
extends into the active site of CatG rendered as an opaque molecular surface
colored based on relative electrostatic potential (blue = basic to red = acidic).

CatG also contains three positively charged residues Arg41, Lys192 and Lys 217

on the edge of the active site that might be involved in substrate selectivity. **KanCbz** can

form charge-charge binding contacts with Arg41 as well as cation-π interactions with

Lys192 (Figure 4.5). These interactions could inhibit substrate from binding to the active

site resulting in a competitive-like mode of inhibition. Other than binding in close

proximity to the active site or in the active site, **KanCbz** also binds clusters of positively

charged residues further away from the active site (Figure 4.6 and Figure 4.7). Binding at

these sites could cause a conformational change in CatG thus also resulting in inhibition

of substrate binding through a non-competitive-like mode of inhibition.
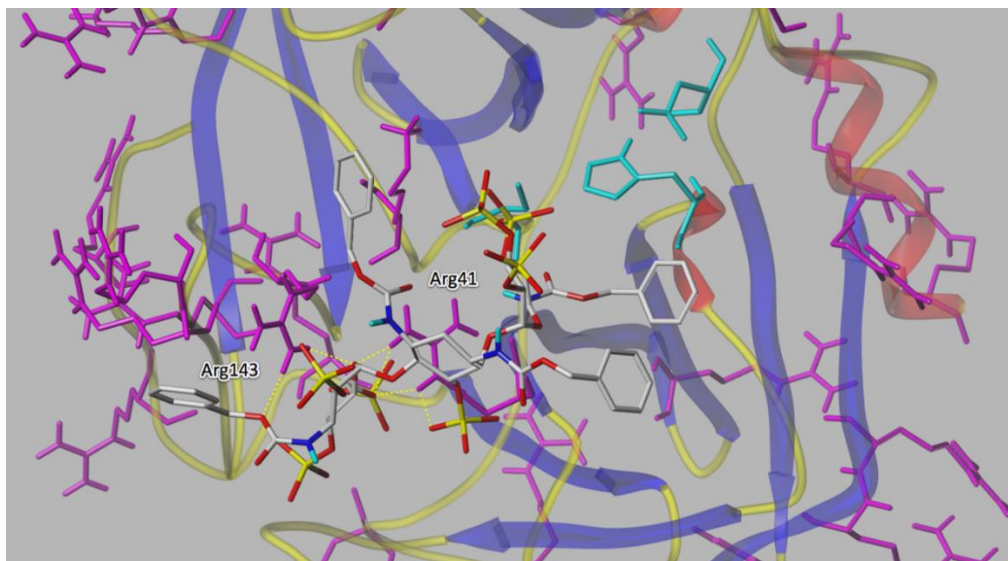
Figure 4.5: Docking to cationic cluster on edge of active site. **KanCbz** forms charge-charge binding contacts with Arg41 as well as cation-pi interactions with Lys192. Catalytic triad residues His57, Asp102 and Ser195 are shown in cyan and positively charged residues in magenta. **KanCbz** is portrayed as a stick model (carbon = white, nitrogen = blue, oxygen = red and sulfur = yellow).
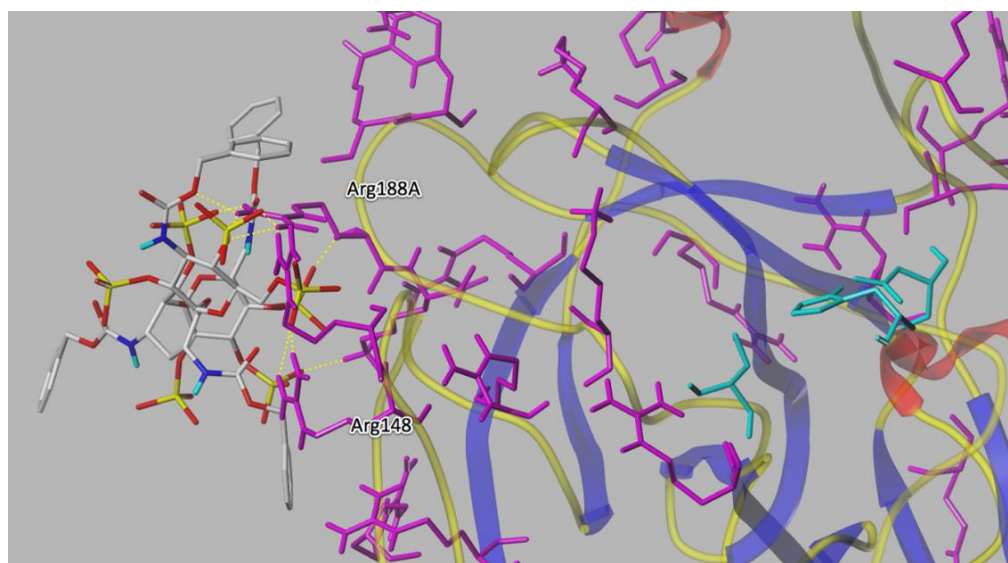
Figure 4.6: Docking to cationic cluster on surface of CatG. **KanCbz** forms charge-charge binding contacts with Arg188A and Arg148. Catalytic triad residues are shown in cyan and positively charged residues in magenta. **KanCbz** is portrayed as a stick model (carbon = white, nitrogen = blue, oxygen = red and sulfur = yellow).
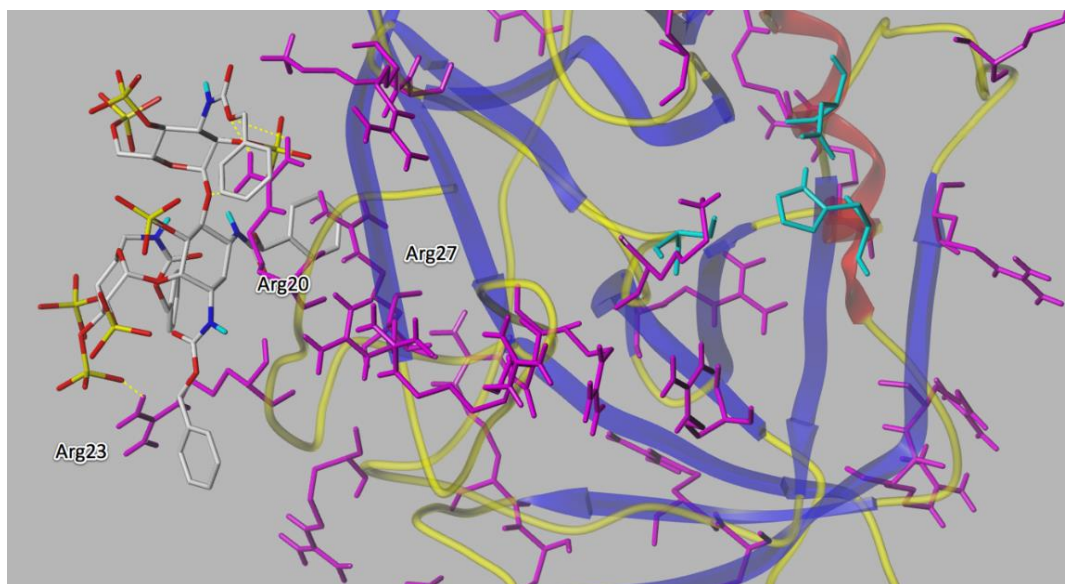
Figure 4.7: Docking of **KanCbz** on surface of CatG. **KanCbz** binds at various sites on the surface of CatG by forming cation-π interactions or charge-charge interactions with either Arg or Lys residues. Here **KanCbz** is shown forming binding contacts with Arg20 and Arg23. Catalytic triad residues are shown in cyan and positively charged residues in magenta. **KanCbz** is portrayed as a stick model (carbon = white, nitrogen = blue, oxygen = red and sulfur = yellow.

4.4 Discussion and conclusions

KanCbz and **NeoCbz** were identified as partial mixed inhibitors of CatG, having both competitive and non-competitive modes of enzyme inhibition. This mode of inhibition indicates that these compounds bind the serine proteases either at clusters of basic residues close to the catalytic site and/or further away from the active site on the surface of the protease, whether or not substrate is bound, and may act as allosteric inhibitors of protease activity. These results also explain why complete inhibition of HNE and Pr3 was not observed for many of the compounds tested, while complete or near complete inhibition of CatG was observed for most compounds; partial mixed inhibitors reduce the catalytic activity of the enzyme-substrate-inhibitor complex without completely inhibiting its function. Docking studies performed suggest the compounds

presented here can bind in different poses, and with different affinities, to the clusters of positively charged residues near the protease active sites, thus each individual compound can impede substrate binding and reduce protease activity to a different level of maximum inhibition. Also it was shown that **KanCbz** and **NeoCbz** can bind other sites on the surface of CatG. The docking results from this study are summarized in Table 4.1, where high docking scores indicate a favorable binding site while low docking scores indicate that binding at that site is not favorable. These results are also consistent with the varied levels of fractional inhibition of serine proteases observed for sulfated low molecular weight lignins.[26]

It is notable that protease inhibitors that do not directly compete with substrate for active site binding are favorable for modulating activity of lung proteases because the lung is saturated with protease substrates, which causes a loss of *in vivo* efficacy for competitive inhibitors.[97] Indeed, small molecule active site inhibitors have been optimized to be potent protease inhibitors having *in vitro* IC_{50} values in the mid nanomolar range, however, such compounds typically target only one of the three proteases, and require high doses *in vivo*.[13] Therapeutic reduction of protease activity in the lung will hopefully restore the protease-protease inhibitor balance without leaving patients susceptible to infections that trigger exacerbations.[103] Use of endogenous or recombinant NSP inhibitors such as elafin and SLPI has also been unsuccessful to date because they do not simultaneously inhibit all three NSPs and they are susceptible to proteolysis. Larger nonpeptidic sulfated macromolecules that target multiple mechanisms of inflammation, even though they are less potent *in vitro*, have been shown to retain their activity *in vivo*, and to attenuate elastase- and cigarette smoke extract-induced emphysema in rats.[28, 27] Furthermore, pro-inflammatory mediators such as IL-8 have been shown to bind heparan sulfate as well as other GAGs leading to activation and recruitment of neutrophils to the site of inflammation.[104, 105] It is anticipated that compounds screened in this study, will maintain their activity *in vivo* when dosed directly

to the lung, without a significant increase in IC_{50} values by allosterically modulating the function of the three NSPs, as well as potentially interacting with key proinflammatory mediators to block their ability to recruit neutrophils.

Table 4.1: Docking scores for **KanCbz**, **NeoCbz** and heparin at various sites on CatG

#	Residue	Docking Score		#	Residue	Docking Score	
1	R20	KanCbz	3.9	11	R125, 131	KanCbz	3.8
		NeoCbz	0.35			NeoCbz	-0.8
		Heparin	-2.6			Heparin	-2.2
2	R20, 23	NeoCbz	4.5	12	R143, 147, 148, 156	Heparin	5.3
		KanCbz	3.7			KanCbz	3.9
		Heparin	1.39			NeoCbz	0.6
3	R23, 27	NeoCbz	5.19	13	R161	KanCbz	4.98
		KanCbz	3.8			Heparin	3.54
		Heparin	-0.8			NeoCbz	-7.1
4	R41*	KanCbz	5.9	14	R164, 166, 170	KanCbz	5.2
		NeoCbz	5.62			NeoCbz	2.3
		Heparin	4.23			Heparin	2
5	R 48	Heparin	2.9	15	R178, 179	KanCbz	5.87
		KanCbz	1.79			Heparin	4.86
		NeoCbz	-0.9			NeoCbz	1.3
6	R75, 76	KanCbz	3.9	16	R185, 186	NeoCbz	4
		Heparin	2.3			KanCbz	2.1
		NeoCbz	1.7			Heparin	-2.5
7	R86, 87	KanCbz	2.28	17	R188A	KanCbz	7.07
		NeoCbz	-3.4		K188, 192	Heparin	6.6
		Heparin	-4.5			NeoCbz	3.6
8	R86, 87, 90	KanCbz	1	18	K217*	KanCbz	5.3
		Heparin	0.6			NeoCbz	4.4
		NeoCbz	-1.9			Heparin	2
9	R90, 97	KanCbz	4	19	R230	KanCbz	5.7
		Heparin	1			NeoCbz	2.6
		NeoCbz	-1			Heparin	N/A
10	R110, 111, 113,114, 116	NeoCbz	5.06	20	R239, 243	KanCbz	5.08
		KanCbz	3.3			NeoCbz	3.37
		Heparin	3.3			Heparin	1.15

4.5 Methods

4.5.1 Materials

Human Cathepsin G (CatG, EC 3.4.21.20) was purchased from Cell Sciences (Canton, MA). CatG specific substrate *N*-succinyl-Ala-Ala-Pro-Phe-*p*-nitroanilide was purchased from Sigma-Aldrich (St. Louis, MO). Molecular biology grade Tris (99.9% pure) was obtained from Research Products International Corporation (Mt. Prospect, IL, USA). Sodium Chloride for molecular biology ($\geq$ 98% pure) was obtained from Sigma Aldrich (St. Louis, MO, USA). Biotechnology grade bovine serum albumin was obtained from Amresco (Solon, OH, USA). Filtered, deionized water used with all buffers was from a Barnstead Nanopure Diamond system, Thermo Fisher Scientific (Hampton, NH, USA). A Fisher Accumet AB15 pH meter (Thermo Fisher Scientific (Hampton, NH, USA)) was used for all pH determinations. All absorbance measurements were performed using a BioTek Synergy 2 plate reader equipped with an external automated dispenser (Winooski, VT, USA).

All molecular structure files were obtained from the Protein Data Bank (PDB). The protein structure for HNE was taken from PDB file 1PPF, for CatG from 1CGH and for Pr3 from 1FUJ. Structure of heparin was taken from PDB file 1HPN.[101, 102] Energy minimization and molecular modeling studies were performed using SYBYL X from Tripos, Certara Company (St. Louis, MO, USA). *N*-arylacyl *O*-sulfonated aminoglycosides were drawn manually in ChemDraw and 3D structures were prepared as a mol2 file in ChemDraw Ultra, CambridgeSoft (Cambridge, MA, USA).

3.5.2 Enzyme kinetics study

Initial velocity studies were performed by maintaining the inhibitor concentration at 0, 0.5[IC_{50}], [IC_{50}], 2[IC_{50}] and 4[IC_{50}] and varying the CatG specific substrate concentration (0.315 to 2 mM *N*-succinyl-Ala-Ala-Pro-Phe-*p*-nitroanilide). Compounds were pre-incubated on ice with CatG for 30 min after which they were plated in a 96-well

plate (10 µL CatG, 60 µL test compound and 40 µL buffer). The inhibitors, at the various concentrations, were further incubated with CatG (140 nM final concentration) for 10 min at 37°C in assay buffer (50 mM Tris buffer, pH 7.4, containing 150 mM NaCl and 0.1 mg/mL bovine serum albumin) after which 50 µL substrate was rapidly dispensed to each well and the increase in absorbance was measured at 405 nm every 4 s for 1 min. The mechanism of inhibition was determined by fitting the initial velocity at each CatG substrate concentration to eight models mixed partial and full, noncompetitive partial and full, uncompetitive partial and full and competitive partial and full in SigmaPlot (Systat Software, San Jose, CA). Results obtained with each model were compared and ranked based on R^2 values, and it was determined that the partial mixed model had the best fit. Michaelis-Menten and Lineweaver-Burk plots were generated in SigmaPlot.

4.5.3 Molecular modeling and docking studies

CatG (PDB: 1CGH) crystal structure was downloaded from the RCSB protein databank and prepared in SYBYL X for docking studies by adding all hydrogens to the protein structure and charging the termini. CatG crystal structure was energy minimized using the Powell method with preset MMFF94s force field in a staged manner with 1000 steps and termination gradient of 0.5 kcal/(mol*Å). **KanCbz** and **NeoCbz** structures were first prepared in ChemDraw as mol2 structures and energy minimized in SYBYL X using MMFF94s force field with MMFF94 charges and were placed in a database used for later screening. Docking studies were performed using the Surflex-Dock Geom suite in SYBYL. The previously prepared minimized structure of CatG was opened in Surflex-Dock and the co-crystalized ligand was extracted or removed along with all water molecules. The protomol was generated (A) for the active site by extracting the co-crystalized ligand or (B) for alternative binding sites on surface of CatG by specifying residues or groups of residues in possible binding sites with a radius of 0.1 Å. Threshold

was kept at 0.5 (default) and bloat at 10. Ligands from database were uploaded into the Surflex-Docking Geom and docking screen was executed. Ligand poses were examined and docking scores reported.

CHAPTER 5: *N*-ARYLACYL *O*-SULFONATED AMINOGLYCOSIDE

INHIBITION OF SERINE PROTEASE MEDIATED CELL

DETACHMENT

Besides their antimicrobial properties, NSPs have been shown to contribute to the pathogenesis of lung injury via degradation of matrix macromolecules, plasma proteins, and they can also attack intact cells.[4, 106, 107, 108] Selectins initiate the tethering and rolling of PMNs along postcapillary venules towards the site of inflammation, where chemokines activate integrins causing the arrest from rolling and migration of PMNs into the alveolar space.[109] Once in the alveolar space PMNs release large amounts of the stored serine proteases, and their concentration in the lung correlates with the degree of progression and severity of inflammatory lung diseases. *In vitro* studies have shown that HNE, CatG and Pr3 can induce cell permeability as well as cause disruption of the epithelial cell monolayer, resulting in circular defects and loss of the monolayer.[110, 111, 112]

5.1 Goal of the study

It was shown in Chapter 3 that select *N*-arylacyl *O*-sulfonated aminoglycosides can inhibit each serine protease in a dose-dependent manner; however, the assays were performed using small chromogenic substrates. The goal of this study was to determine if *N*-arylacyl *O*-sulfonated aminoglycosides that directly inhibit the three NSPs would maintain their ability to inhibit the serine proteases in the extracellular milieu, and also to gain an initial assessment of their potential for inhibiting known detrimental proteolytic functions of NSPs such as the cleavage of epithelial cells and cell-surface adhesion molecules. This was accomplished by using a cell detachment assay where a monolayer of lung epithelial cells was exposed to HNE, CatG and Pr3 in the presence and absence of decreasing concentrations of *N*-arylacyl *O*-sulfonated aminoglycosides. Non-detached cells were imaged and quantified using the Operetta High Content Imaging System,

allowing for the cell-based evaluation of *N*-arylacyl *O*-sulfonated aminoglycosides'
ability to block biologically relevant proteolytic functions of the NSPs. The assay
employed is amenable to rapid quantification of results and was thus established to
evaluate the ability of each *N*-arylacyl *O*-sulfonated aminoglycoside to inhibit each NSP.

5.2 High throughput assay development

As an initial assessment of the potential for *N*-arylacyl *O*-sulfonated
aminoglycosides to protect lung epithelial cells from proteolytic cell detachment induced
by NSPs, a cell detachment assay was performed according to published procedures.[46, 84]
A549 lung epithelial cells were exposed to either CatG alone or CatG and **KanCbz** at
two concentrations. Detachment of cells in CatG only-treated wells and CatG in the
presence of 0.125 µM **KanCbz** was observed, while intact cell monolayer was still
present in control wells and CatG with 250 µM **KanCbz** (Figure 5.1). Removal of
remaining adherent cells for quantification via counting with a hemocytometer proved to
be problematic as cells exhibited a drastic change in morphology and loss of membrane
integrity, especially in CatG only wells. The inability to quantify **KanCbz**'s ability to
impede CatG-mediated detachment of lung epithelial cells prompted the development of
a quantitative high throughput assay.
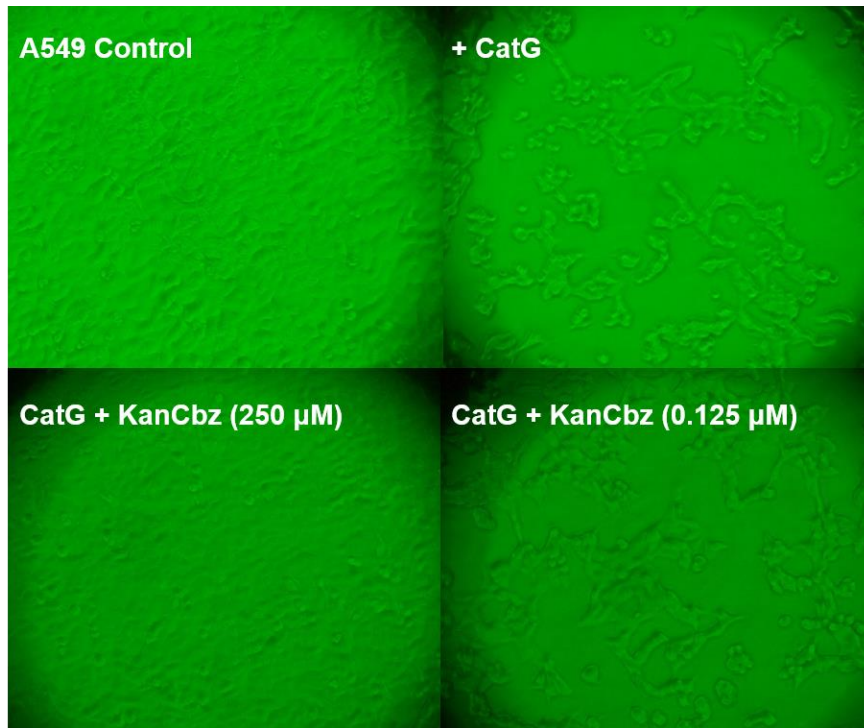
Figure 5.1: Protection of lung epithelial cells against CatG-mediated cell detachment. Photomicrographs of A549 lung epithelial cells exposed to CatG in presence or absence of **KanCbz**. CatG (150 nM) was pre-incubated with **KanCbz** (0.125 μM and 250 μM) for 30 min on ice before addition to confluent A549 cells. At 250 μM concentration **KanCbz** inhibits CatG induced cell detachment. At 0.125 μM concentration this protection is lost and CatG mediated cell detachment is once again observed.

The initial cell detachment assay was miniaturized from a 24-well plate to a 96-well plate and optimized for seeding density, incubation times, plating consistency and enzyme concentration that results in maximal cell detachment. In order to quantify the remaining adherent cells, Hoechst 33342 nuclear dye was used to stain the cell nuclei thus enabling them to be visualized and counted using the Operetta High Content Imaging System (Figure 5.2). The Operetta High Content Imaging System detects only the cells present in one plane, in this case attached cells on the bottom of each well, thus using an appropriate seeding density was crucial to obtain a consistent monolayer for accurate counting of the cells.

44
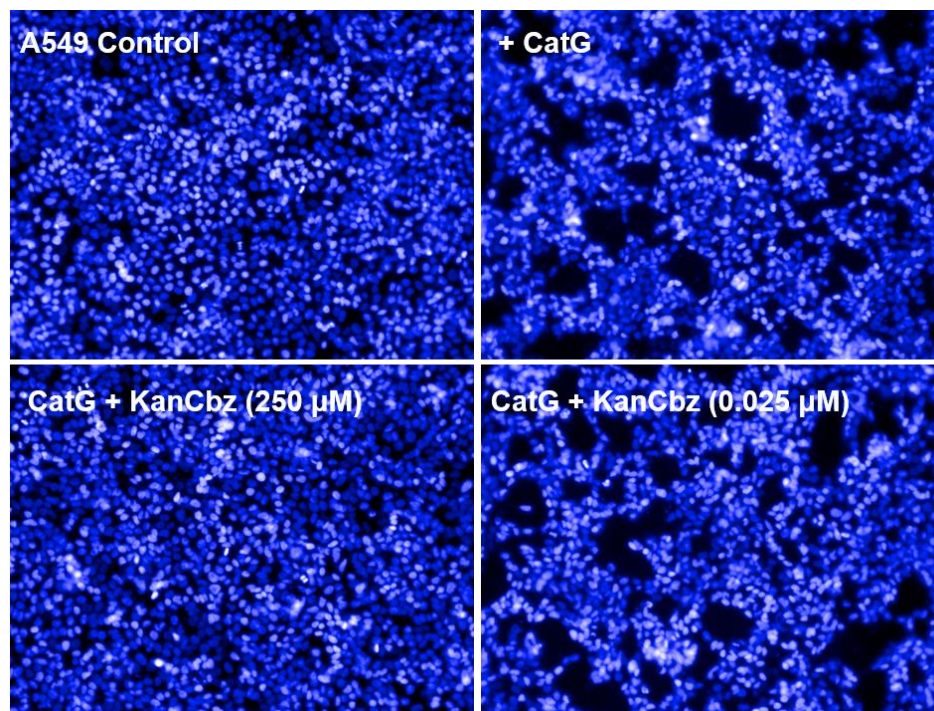
Figure 5.2: Optimization of cell detachment assay. CatG (250 nM) was pre-incubated with **KanCbz** (0.025 μM and 250 μM) for 30 min on ice before addition to confluent A549 cells. Cells were incubated for 24 h after which the media was aspirated and cells were stained with Hoechst 33342 nuclear dye for imaging and counting using the Operetta High Content Imaging System. At 250 μM concentration **KanCbz** inhibits CatG induced cell detachment, while at the lower concentration of 0.025 μM the ability of **KanCbz** to inhibit the proteolytic activity of CatG is diminished and cell detachment is observed.

5.3 Evaluation of *N*-arylacyl *O*-sulfonated aminoglycoside

inhibition of HNE-mediated cell detachment

A549 lung epithelial cell monolayers were incubated in the presence of HNE and decreasing concentrations of each *N*-arylacyl *O*-sulfonated aminoglycoside. After 24 h cells were imaged and the monolayer was analyzed for circular defects and morphological changes in the cells, indicative of HNE proteolytic damage (Figure 5.3). Incubation of cells with 50 nM HNE caused a complete loss of the cell monolayer and very few adherent cells were detected. The remaining adherent cells appeared rounded and their structural integrity seemed to be compromised due to the proteolytic activity of

HNE. At the highest dose of test compound explored, more adherent cells were detected on the surface of each well as compared to HNE only controls, however the cell morphology was rounded and membrane integrity was damaged resulting in leakage of the nuclear dye and indicating that **KanCbz** only partially decreases the ability of HNE to cleave the lung epithelial cells (Figure 5.3).
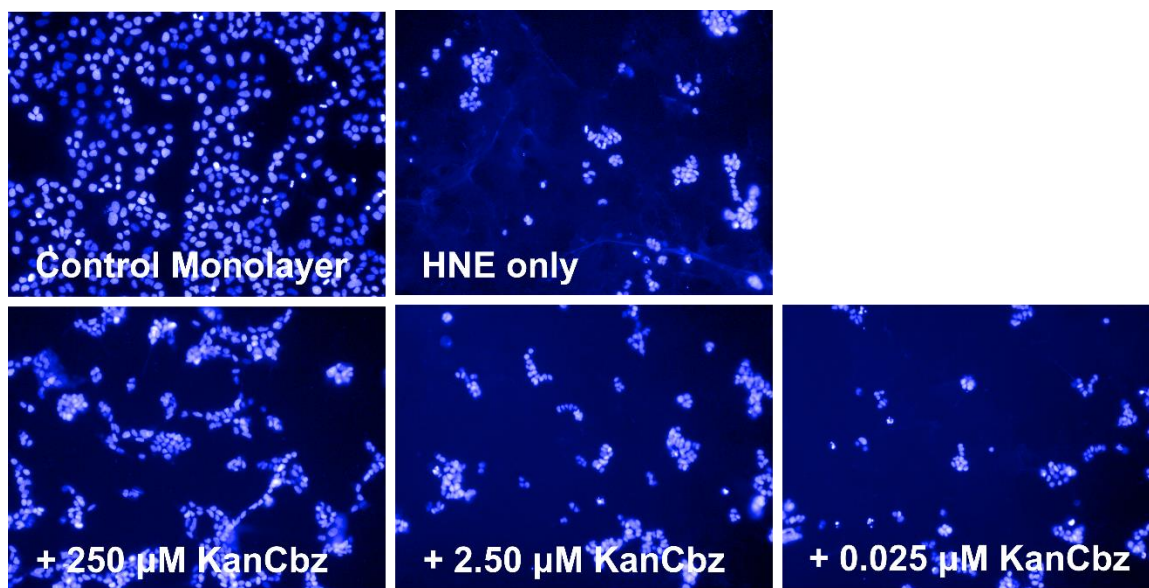
Figure 5.3: **KanCbz** inhibition of HNE-mediated cell detachment. A549 lung epithelial cells were exposed to HNE (50 nM) in the presence or absence of decreasing concentrations of **KanCbz**. HNE was pre-incubated with **KanCbz** (250 μM, 2.50 μM and 0.025 μM) for 30 min on ice before addition to confluent A549 cells. After 24 h lung epithelial cell nuclei were stained with Hoechst 33342 and cells were imaged using Operetta High Content Imaging System. Only one representative field for each experiment is shown for clarity. At 250 μM **KanCbz** inhibits HNE induced cell detachment. As the concentration of **KanCbz** is decreased, the ability to hinder the proteolytic activity of HNE is lost and **KanCbz** is no longer able to protect the cells thus detachment is once again observed.

Adherent cells remaining on the surface of the 96-well plates were quantified using the Harmony Analysis Software for each *N*-arylacyl *O*-sulfonated aminoglycoside (Figure 5.4). **NeoCbz** and **KanCbz** showed significant protection against HNE-mediated

cell detachment at the highest concentration used. These results are consistent with data obtained in the enzyme inhibition assay (Chapter 3), where each compound was identified as a potent inhibitor of HNE. When comparing the IC_{50} values of each *N*-arylacyl *O*-sulfonated aminoglycoside, it is not surprising that the apramycin core derivatives along with phenylacetyl and benzoyl substituted derivatives were unable to block HNE-mediated cleavage of adhesion proteins and subsequent detachment of cells.
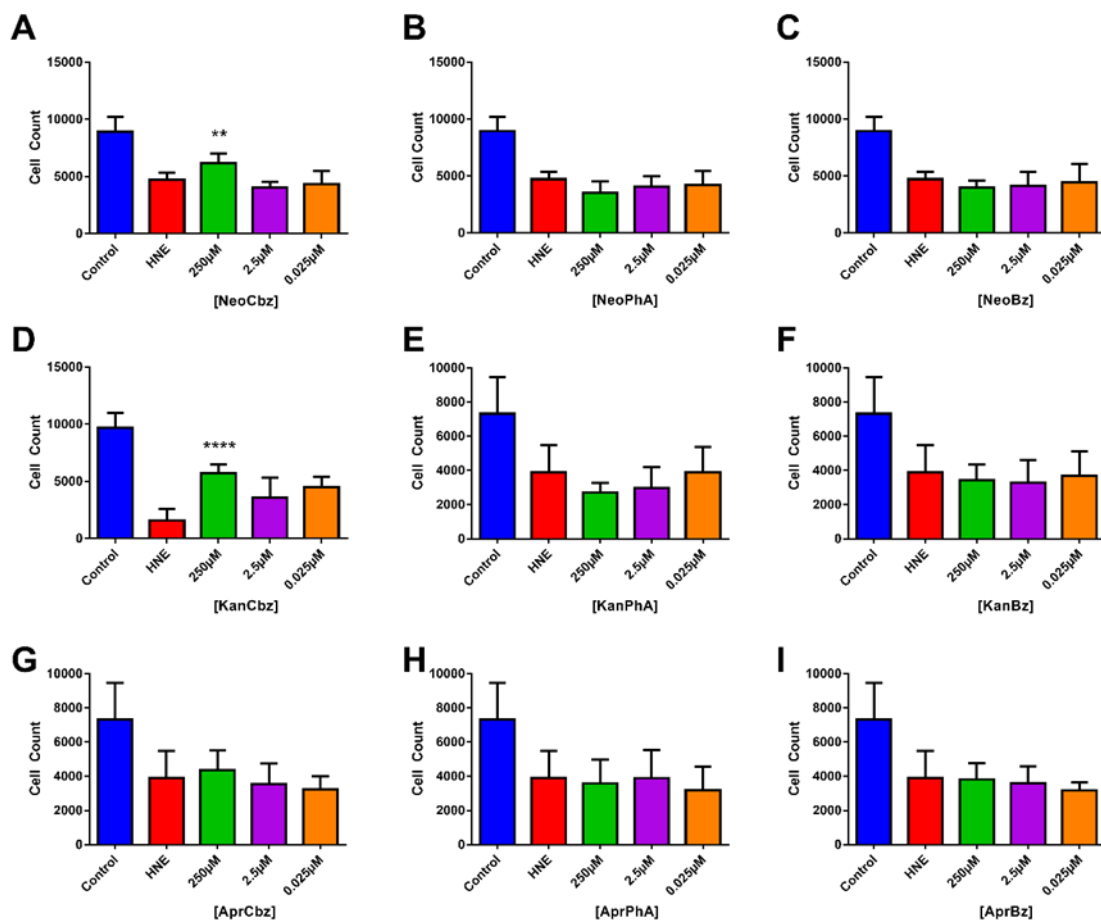
Figure 5.4: Quantification of HNE-mediated cell detachment in the presence of *N*-arylacyl *O*-sulfonated aminoglycosides. A549 lung epithelial cells were exposed to 50 nM HNE in the presence of decreasing concentrations of **NeoCbz** (A), **NeoPhA** (B), **NeoBz** (C), **KanCbz** (D), **KanPhA** (E), **KanBz** (F), **AprCbz** (G), **AprPhA** (H) and **AprBz** (I) (structures shown in Figure 1.3). After 24 h cell media was aspirated off and lung epithelial cell nuclei were stained with Hoechst 33342. Cells were imaged and adherent cells were quantified using the Operetta High Content Imaging System and Harmony Analysis Software respectively. At the highest concentration explored (250 µM) both **NeoCbz** and **KanCbz** protected cells against HNE-mediated cell detachment. Data are presented as mean +SE, **$p < 0.01$, ***$p < 0.001$ ****$p < 0.0001$ as compared to protease treated cells (n = 3 from 3 independent experiments each done in triplicate).[64]

5.4 Evaluation of *N*-arylacyl *O*-sulfonated aminoglycoside

inhibition of CatG-mediated cell detachment

A549 lung epithelial cell monolayers were incubated in the presence of CatG and decreasing concentrations of each *N*-arylacyl *O*-sulfonated aminoglycoside in a similar manner to experiments performed in the presence of HNE. Following incubation in the presence of CatG and each *N*-arylacyl *O*-sulfonated aminoglycoside, cell monolayers were imaged (Figure 5.5). Examining the cell monolayer for cells treated with CatG and **KanCbz** at 250 µM indicates that **KanCbz** fully protects the cells from CatG proteolytic cleavage. The monolayer appears intact with no visible circular defects and cell morphology is similar to that of control cells. At the 2.5 µM concentration of **KanCbz**, although more adherent cells were detectable than in CatG only control, cells appeared rounded and monolayer was lost.
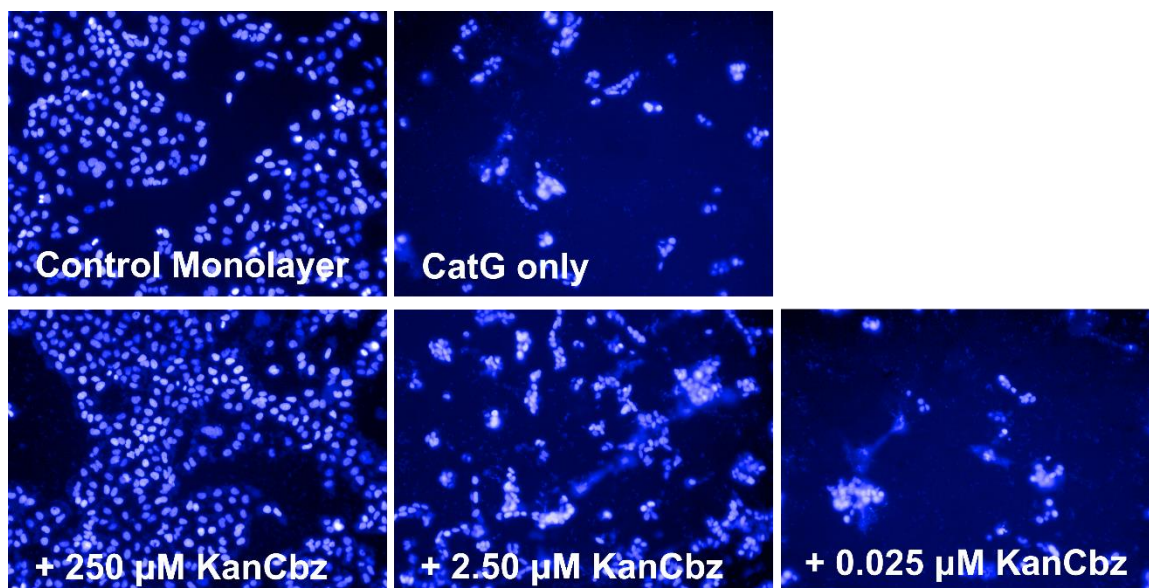
Figure 5.5 **KanCbz** inhibition of CatG-mediated cell detachment. A549 lung epithelial
cells were exposed to CatG (250 nM) in the presence or absence of decreasing
concentrations of **KanCbz**. CatG was pre-incubated with **KanCbz** (250 μM,
2.50 μM and 0.025 μM) for 30 min on ice before addition to confluent A549
cells. After 24 h the cell media was removed and the lung epithelial cell
nuclei were stained with Hoechst 33342. Cells were imaged using Operetta
High Content Imaging System and only one representative field for each
experiment is shown for clarity. **KanCbz** inhibits CatG induced cell
detachment at 250 μM and to a lesser extent at 2.5 μM. At the lowest
concentration tested **KanCbz** loses its ability to inhibit CatG and cell
detachment caused by CatG cleavage of adhesion molecules is observed.

Adherent cells remaining on the surface of the 96-well plates after incubation in

the presence of CatG and each *N*-arylacyl *O*-sulfonated aminoglycoside at three

concentrations were quantified and the data are presented in Figure 5.6. As seen with

HNE, results obtained for inhibiting the functional activity of the proteases are consistent

with the IC_{50} data obtained for each member of *N*-arylacyl *O*-sulfonated aminoglycoside

(Chapter 3). The neomycin core derivatives that were established to be the most potent

inhibitors of CatG significantly protected cells against CatG-mediated detachment at both

250 μM and 2.5 μM concentrations, thus reconfirming the structure activity relationships

proposed. The kanamycin core derivatives, which are still fairly potent inhibitors of

CatG with single to double digit μM IC_{50} values for CatG inhibition, provided a significant protective effect against CatG-mediated cell detachment only at the highest concentration tested. Finally, in the case of the apramycin core derivatives, only the carbobenzyloxy substituted apramycin derivative was able to inhibit CatG proteolytic cleavage of adhesion molecules, affording protection of the lung epithelial monolayer. The phenylacetyl and benzoyl substituted apramycin derivatives that had the highest IC_{50} values for inhibition of CatG, also had no activity in the cell-based model. Taken as a whole, from the information acquired from the chromogenic peptidolytic assay described in Chapter 3 and the data presented in the cell-based model for *in vivo* protease mediated extracellular matrix destruction, it is reaffirmed that a larger flexible core and longer *N*-aryl substituent are preferred for inhibition of CatG.
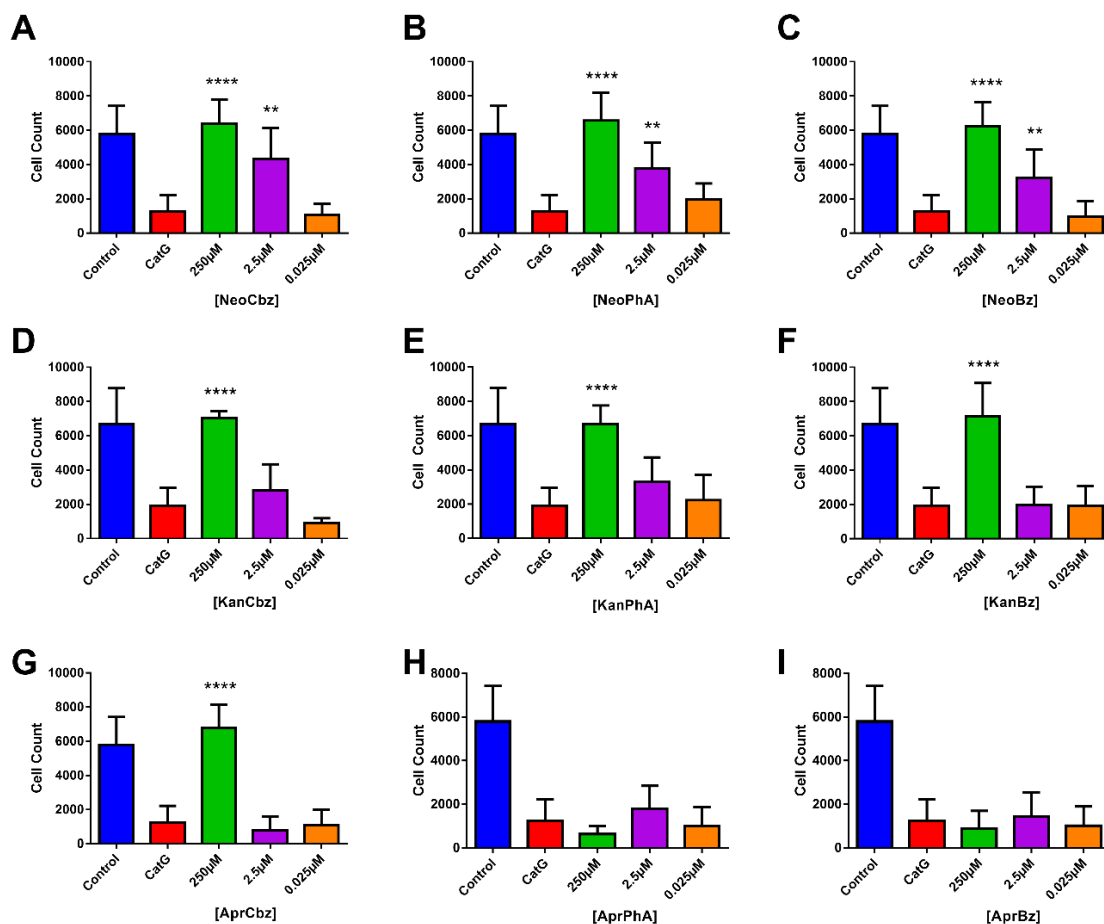
Figure 5.6: Quantification of CatG mediated cell detachment in the presence of *N*-arylacyl *O*-sulfonated aminoglycosides. A549 lung epithelial cells were exposed to 250 nM CatG in the presence of decreasing concentrations of **NeoCbz** (A), **NeoPhA** (B), **NeoBz** (C), **KanCbz** (D), **KanPhA** (E), **KanBz** (F), **AprCbz** (G), **AprPhA** (H) and **AprBz** (I) (structures shown in Figure 1.3). After 24 h the media was removed and lung epithelial cell nuclei were stained with Hoechst 33342. Cells were imaged and remaining adherent cells were quantified using the Operetta High Content Imaging System and Harmony Analysis Software respectively. Significantly less cells were cleaved by CatG in the presence of both 250 μM and 2.5 μM concentrations of the neomycin core derivatives. Kanamycin derivatives were also able to inhibit CatG-mediated cell detachment, however only at the 250 μM concentration. Apramycin core derivatives in general showed the least inhibition of CatG activity and only **AprCbz** showed significant protection of the cell monolayer at the highest concentration tested. Data are presented as mean +SE, **$p < 0.01$, ***$p < 0.001$ ****$p < 0.0001$ as compared to protease treated cells (n = 3 from 3 independent experiments each done in triplicate).[64]

52

5.5 Evaluation of *N*-arylacyl *O*-sulfonated aminoglycosides

inhibition of Pr3-mediated cell detachment

A549 lung epithelial cell monolayers were incubated in presence of Pr3 and decreasing concentrations of each *N*-arylacy *O*-sulfonated aminoglycoside similarly to the studies performed with HNE and CatG. Examining the cell monolayer (Figure 5.7), in the presence of 250 µM **KanCbz** small circular defects can be observed, however, the cell morphology is intact. As the concentration of **KanCbz** is decreased all protective effects to maintain the cell monolayer are lost, and uninhibited Pr3 is able to degrade structural proteins causing cell detachment.
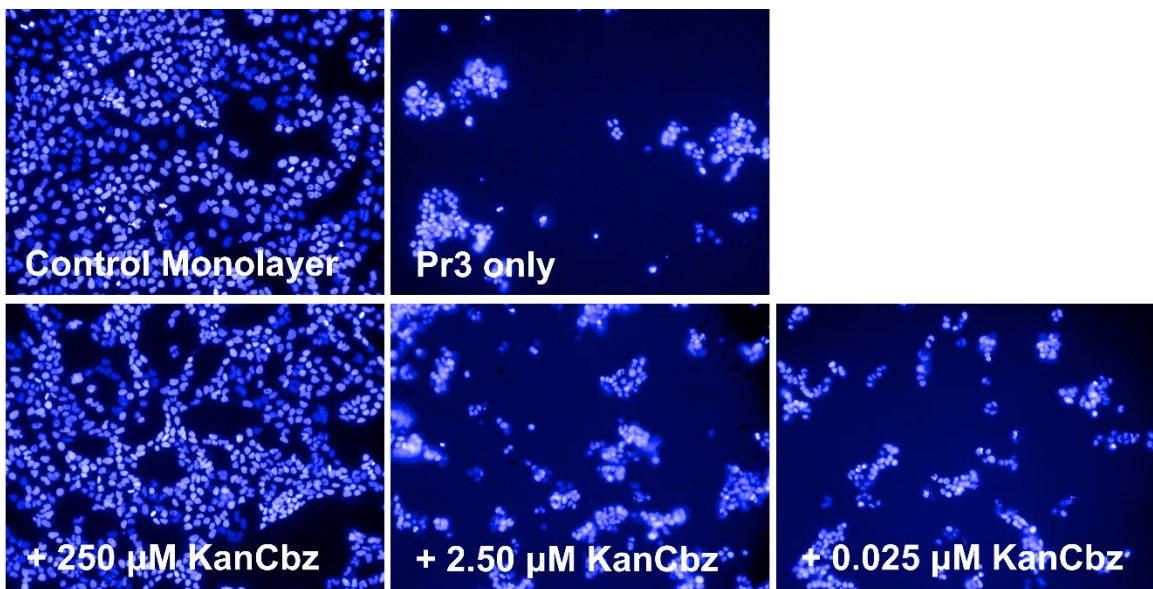
Figure 5.7: **KanCbz** inhibition of Pr3-mediated cell detachment. A549 lung epithelial cells were exposed to Pr3 (50 nM) in the presence or absence of decreasing concentrations of **KanCbz**. Pr3 was pre-incubated with **KanCbz** (250 µM, 2.50 µM and 0.025 µM) for 30 min on ice before addition to confluent A549 cells. After 24 h lung epithelial cell nuclei were stained with Hoechst 33342 and cells were imaged using Operetta High Content Imaging System. Only one representative field for each experiment is shown for clarity. At 250 µM **KanCbz** inhibits Pr3 induced cell detachment.

Remaining adherent cells on the surface of 96-well plates after exposure to Pr3 and decreasing concentrations of each member of the panel of *N*-arylacyl *O*-sulfonated aminoglycoside were quantified using a similar protocol to that presented for HNE and CatG and data as shown in Figure 5.8. The carbobenzyloxy substituted derivatives significantly protected cells against Pr3-mediated cell detachment. Interestingly, when examining the result for the phenylacetyl substituted derivatives, only **AprPhA** had a significant protective effect for inhibiting Pr3-mediated cell detachment. In the enzyme assay for inhibition of Pr3 using a chromogenic substrate, the apramycin core derivatives were overall weaker inhibitors and had higher IC_{50} values as compared to the neomycin or kanamycin core analogs (Chapter 3). Also of note, **AprPhA** showed no inhibition of Pr3 in the chromogenic peptidolytic assay. While there is no current explanation for this discrepancy, it could suggest that **AprPhA** interacts with Pr3 at a site distant from the active site so as to not interfere with peptide substrate binding, but close enough to interfere with binding of larger protein substrates. Indeed, it is well-known that different peptide substrates can afford different, contradictory results in evaluation of small molecule NSP inhibitors.
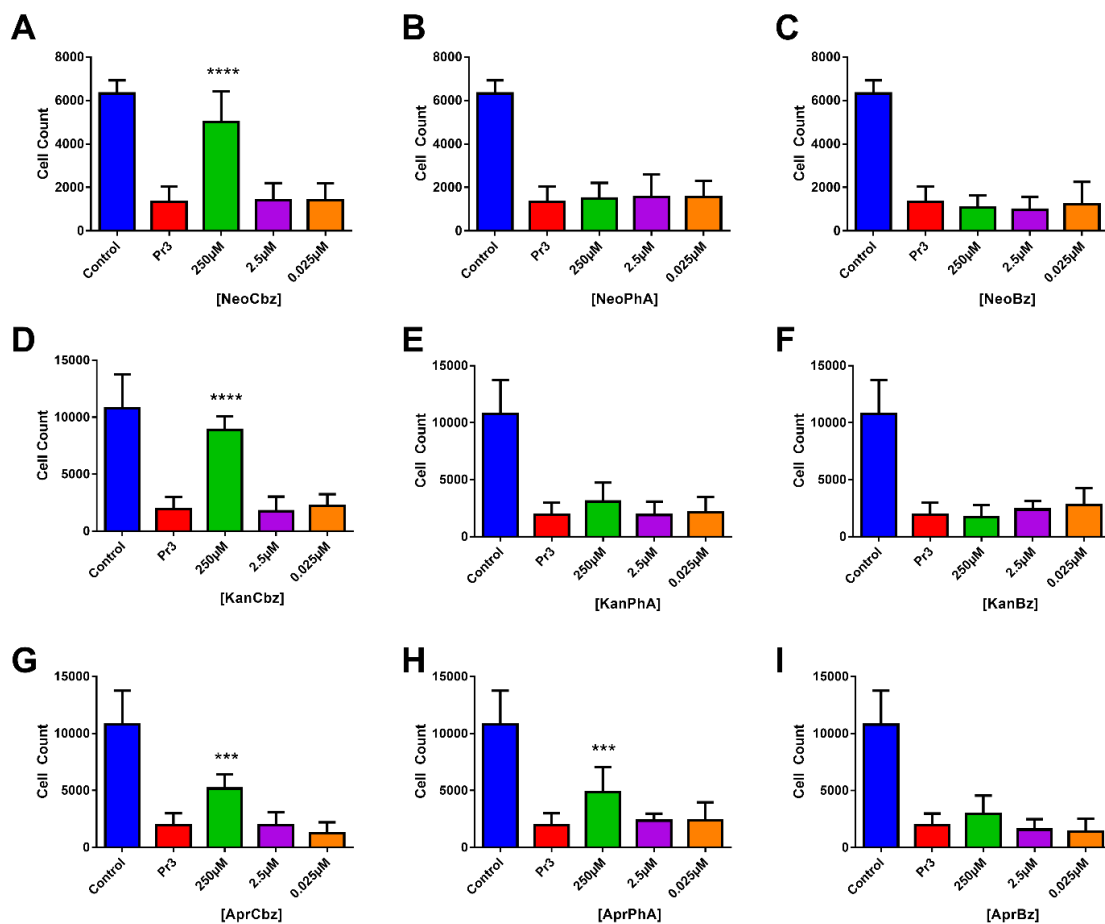
Figure 5.8: Quantification of Pr3-mediated cell detachment in the presence of *N*-arylacyl *O*-sulfonated aminoglycosides. A549 lung epithelial cells were exposed to 50 nM Pr3 in the presence of decreasing concentrations of **NeoCbz** (A), **NeoPhA** (B), **NeoBz** (C), **KanCbz** (D), **KanPhA** (E), **KanBz** (F), **AprCbz** (G), **AprPhA** (H) and **AprBz** (I) (structures shown in Figure 1.3). After 24 h cell media was removed and lung epithelial cell nuclei were stained with Hoechst 33342. Cells were imaged and remaining adherent cells were quantified using the Operetta High Content Imaging System and Harmony Analysis Software respectively. **AprPhA** and carbobenzyloxy substituted derivatives protected cells against Pr3-mediated cell detachment at the highest concentration tested. All other derivatives did not show an effect. Data are presented as mean +SE, **p < 0.01, ***p < 0.001 ****p < 0.0001 as compared to protease treated cells (n = 3 from 3 independent experiments each done in triplicate).[64]

5.6 Discussion and conclusions

In Chapter 3 it was demonstrated that select *N*-arylacyl *O*-sulfonated aminoglycosides inhibit NSPs. To further characterize the inhibitory effect of *N*-arylacyl *O*-sulfonated aminoglycosides with each NSP, a cell detachment assay that explores the functional inhibition of NSP-mediated cleavage of cell surface adhesion molecules was employed. Using a high throughput assay, the ability of each *N*-arylacyl *O*-sulfonated aminoglycoside to inhibit HNE, CatG and Pr3 induced detachment of lung epithelial cells was evaluated. HNE, as well as CatG and Pr3 are known to cleave components of the extracellular matrix, thus causing degradation of the lung matrix.[6, 113] A549 lung epithelial cells form a uniform monolayer covering the bottom of control wells on the surface of an uncoated 96-well plate. When each NSP is added, detachment of cells can be observed. Also, the cell morphology drastically changes, cells are rounded and a majority of them have lost their membrane integrity resulting in nuclear dye leakage, while circular defects are observed. At high concentrations **KanCbz** and **NeoCbz** significantly protected the cells from detachment induced by HNE, CatG as well as Pr3, and the cell morphology resembled that of the control cells (Figure 5.9). At low concentrations of inhibitor this protective effect was no longer observed and once again the monolayer was lost, cells were detached and their membrane integrity suffered similarly to that of protease only treated wells. *N*-arylacyl *O*-sulfonated aminoglycosides that were identified in Chapter 3 as potent inhibitors of substrate binding to NSPs, were also functionally able to block the proteolytic function of the NSP in a cell system. **KanCbz** and **NeoCbz** were identified as novel inhibitors that target the proteolytic function of all three NSPs blocking their ability to cleave cells and destroy the lung matrix.
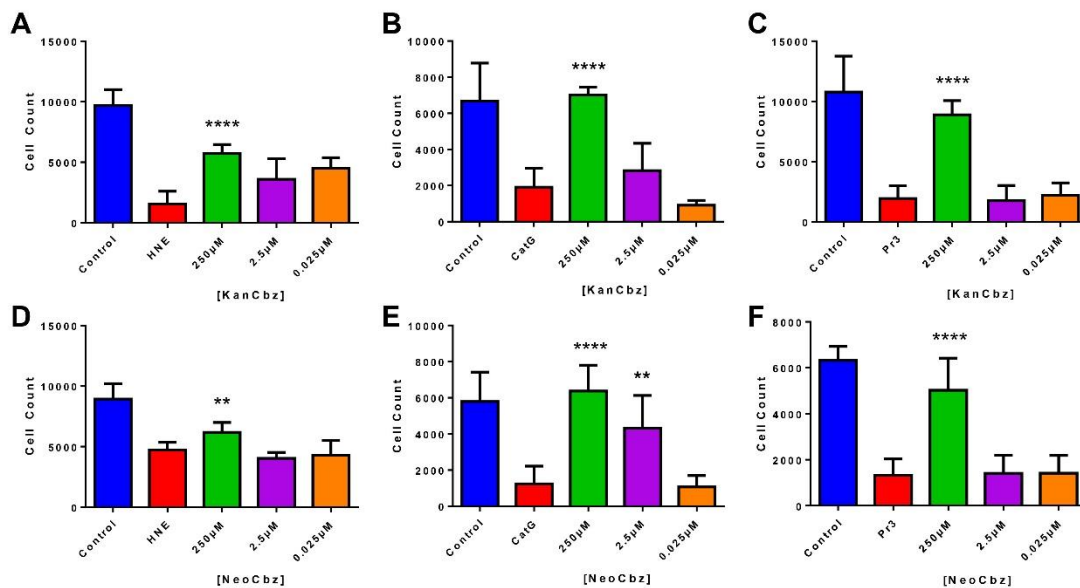
Figure 5.9: Summary of NSP-mediated cell detachment in the presence of **KanCbz** and
NeoCbz. A549 lung epithelial cells were exposed to each NSP (50 nM HNE,
250 nM CatG or 50 nM Pr3) in the presence of decreasing concentrations of
KanCbz (A-C) or **NeoCbz** (D-E). After 24 h lung epithelial cell nuclei were
stained with Hoechst 33342 and cells were imaged and remaining adherent
cells were quantified using an Operetta High Content Imaging System and
Harmony Analysis Software, respectively. At the highest concentration, both
KanCbz and **NeoCbz** inhibited NSP-mediated cell detachment. Data are
presented as mean +SE, **p < 0.01, ***p < 0.001 ****p < 0.0001 as
compared to protease treated cells (n = 3 from 3 independent experiments
each done in triplicate).[64]

5.7 Methods

5.7.1 Materials and cell culture

Human neutrophil elastase (HNE, EC 3.4.21.37) was purchased from Enzo Life

Sciences (Farmingdale, NY) as a lyophilized powder and was taken up in buffer

consisting of 50 mM sodium acetate and 150 mM NaCl, pH 5.5. Human proteinase 3

(Pr3, EC 3.4.21.76) and human Cathepsin G (CatG, EC 3.4.21.20) were purchased from

Cell Sciences (Canton, MA). A549 lung epithelial cells were obtained from ATCC

(CCL-185). Cells were grown in RPMI-1640 medium supplemented with 10% fetal

bovine serum (FBS), 0.1% penicillin-streptomycin and 2 mM GlutamaxTM at 37°C and 5% CO_2 atmosphere.

5.7.2 Initial study of **KanCbz** inhibition of CatG-mediated cell detachment assay

For this initial assay, protease induced cell detachment was determined according to published procedures with minor modifications.[46] Briefly A549 cells were seeded at 1 x 10^5 cells per well in uncoated, tissue culture treated 24-well plates and grown to confluence in complete growth medium (1 mL, RPMI-1640 medium supplemented with 10% FBS, 0.1% penicillin-streptomycin and 2mM GlutamaxTM). Cells were then washed with phosphate buffered saline (PBS) and cultured for 24 h in serum-free medium (500 µL, RPMI-1640 medium supplemented with 0.1% penicillin-streptomycin). CatG (150 nM) was incubated with **KanCbz** at various concentrations (0.125 µM and 250 µM) for 30 min on ice before addition of the compound-enzyme mixture to the cells (20 µL CatG, 100 µL **KanCbz** and 380 µL serum-free medium). Loss of the A549 cell monolayer induced by CatG was examined by phase contrast light microscopy.

5.7.3 High throughput cell detachment assay

A549 cells (passage number 86) were seeded at 2 x 10^4 cells per well in uncoated tissue culture treated 96-well black plates with clear bottom and grown for 18 h in complete growth medium (200 µL, RPMI-1640 medium supplemented with 10% FBS, 0.1% penicillin-streptomycin and 2mM GlutamaxTM). The growth medium was then removed via aspiration and cells were cultured for 24 h in serum-free medium (200 µL, RPMI-1640 medium supplemented with 0.1% penicillin-streptomycin). *N*-arylacyl *O*-sulfonated aminoglycosides at three concentrations (250, 2.5 and 0.025 µM) were incubated on ice for 30 min with enzyme (50 nM HNE, 250 nM CatG or 50 nM Pr3) before addition to cells. The 0.025 µM concentration of compound is sub stoichiometric however it was included to determine if at this concentration the compounds might affect

the NSPs' ability to bind larger substrates. Serum-free medium was removed via aspiration and cells were incubated in presence of compound and enzyme for 24 h (10 µL enzyme, 40 µL test compound and 50 µL serum-free medium). After 24 h, the serum free medium containing enzyme and test compound was aspirated off and cells were stained with Hoechst 33342 nuclear dye. Cells in each well (15 fields selected per well) were imaged and remaining adherent cells were quantified using the Operetta High Content Imaging System and Harmony Analysis Software (PerkinElmer Inc.).

5.7.4 Statistical analysis

Nonparametric data were analyzed by the Mann-Whitney U test using GraphPad Prism 6 (GraphPad Software, La Jolla, USA). A p value of 0.05 or less was considered to be significant. Error bars in all figures indicate means ± SE.

CHAPTER 6: EVALUATION OF TOXICITY AND MITIGATION OF

INFLAMMATORY RESPONSE BY *N*-ARYLACYL *O*-SULFONATED

AMINOGLYCOSIDES *IN VIVO*

Since the 1950's a great deal of effort has been invested in designing drugs that inhibit protease activity, with some examples of success seen in the case of angiotensin-converting enzyme (ACE) inhibitors, some examples of failure such as with designing matrix metalloproteinase (MMP) inhibitors, and many more inhibitors advancing through clinical trials.[114, 115, 116] Two typical reasons for failure of drug candidates in the field of protease inhibition are severe side effects and/or no therapeutic effect *in vivo*. The side effects are mainly attributed to two problems 1) designing substrate mimics that are not selective for a specific protease; 2) use of covalent irreversible inhibitors that are highly reactive and could potentially exhibit severe off-target effects.[114, 117] In order to validate *N*-arylacyl *O*-sulfonated aminoglycosides as novel protease inhibitors that are potential therapeutic lead structures, their potential for inherent toxicity must be evaluated and their ability to inhibit the three NSPs must be studied in a disease model that encompasses the complexity of biological pathways that the proteases influence. The *in vivo* study presented here was designed to specifically answer the two most important questions when proposing a new class of molecules, and more specifically a new type of protease inhibitors: do they have overt severe side effects and do they have a therapeutic effect *in vivo*.

6.1 Goal of the study

KanCbz was identified as a novel inhibitor of all three NSPs (Chapter 3). The inhibition of the NSPs also translated into the functional inhibition of their proteolytic activity in cell culture, thus protecting A549 lung epithelial cells from detachment mediated by the proteases (data summarized in Figure 6.1). These *in vitro* experiments mimic a simplified function of NSPs that emphasizes their ability to cleave a specific

substrate but does not take into account the plethora of networks by which NSPs propagate inflammation. One key aspect that is ignored in these in vitro experiments is that NSPs can attach to negatively charged proteoglycans on the surface of PMNs thus maintaining their activity while increasing their resistance to inactivation by endogenous PIs.[118, 1] **KanCbz** as well as other *N*-arylacyl *O*-sulfonated aminoglycosides could, due to the fact that they bind on the surface of the NSPs, inhibit the NSPs from attaching to the surface of PMNs thus increasing the amount of soluble enzyme that can be inactivated by endogenous PIs. Secondly, chemokines and cytokines play a central role in the regulation and propagation of the inflammatory response and have been shown to bind heparan sulfate and other glycosaminoglycans.[105, 119, 120] Inhibition of proinflammatory mediators likely represents another pathway by which *N*-arylacyl *O*-sulfonated aminoglycosides decrease inflammation. The goal of this study was to examine the effect of **KanCbz** *in vivo* in order to determine if and to what extent pulmonary toxicity occurs after exposing mice to the compound. Also, using a mouse model for acute pulmonary toxicity and inflammation, evaluation of **KanCbz**'s ability to decrease inflammation under *in vivo* conditions was investigated.
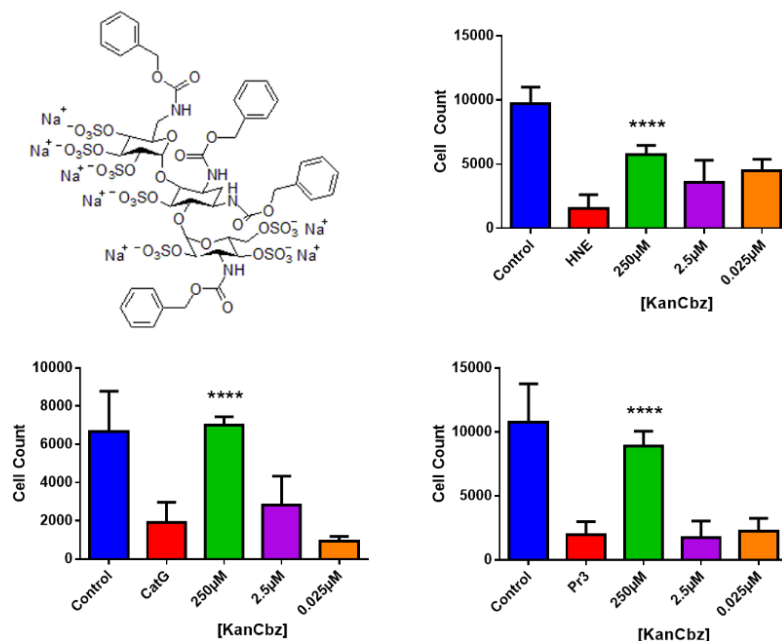
Figure 6.1: **KanCbz** protects A549 lung epithelial cells against HNE-, CatG- and Pr3-mediated cell detachment. **KanCbz** lead structure identified in *in vitro* studies presented in Chapter 3 and Chapter 5.

6.2 Dose escalation study to determine potential overt

toxicity of **KanCbz**

Initially the upper limit of **KanCbz** that produces a measurable toxic response was explored. Mice were exposed via nasal instillation to increasing doses of **KanCbz** selected based on concentrations used in the cell based assay (0.25, 2.5 and 5 mg/mouse) and euthanized 24 h after exposure. Weight and characteristics of the mice are described in experimental section. The bronchoalveolar lavage (BAL) fluid was collected and total cells counts were obtained using a hemocytometer. The cells were then fixed on microslides and differential cell counts of macrophages, PMNs, lymphocytes and eosinophils were determined and expressed as a percent of total cells per mouse (Figure 6.2, Table 6.1). Under normal, non-inflammatory conditions, there is a low total cell count and majority of the cells present in the BLA fluid are macrophages. If there is an

inflammatory response, PMNs are the first inflammatory cells that migrate to the site of

inflammation and thus higher numbers of PMNs will be present in the BAL fluid.

Lymphocyte and eosinophil BAL fluid counts are generally low, even in inflammatory

lung diseases, as compared to macrophages and PMNs which make up the bulk of

inflammatory cells present in the lung.[121]

No significant increase in total cell counts or total neutrophils was observed for

the 0.25 and 2.5 mg/mouse dose, as compared to control, however, there was an increase

in both total cell count and percent neutrophils at the highest dose of **KanCbz** (5

mg/mouse). Solubility of the 5 mg dose does become problematic and the observed

viscosity of the samples increased with increasing concentration, possibly causing the

inflammatory response at this high dose.
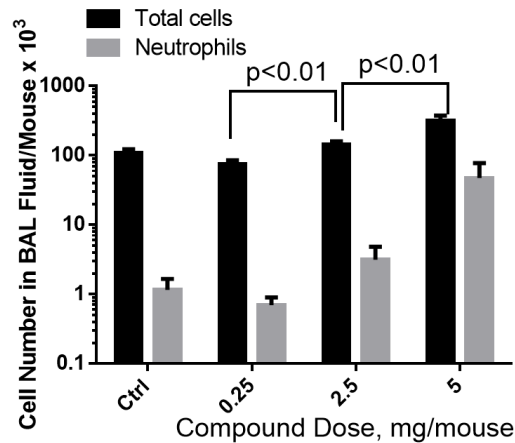
Figure 6.2: Total cell and neutrophil counts to determine pulmonary inflammation of
KanCbz. Cell counts in BAL fluid for mice exposed to 0.25, 2.5 and 5
mg/mouse of compound. There was no significant increase in total cell count
at the two low doses explored in comparison to controls. An increase in total
neutrophils in BAL fluid was observed at the 5 mg/mouse dose. Data shown
as mean ± SE (n = 5).

Table 6.1: Dose escalation of **KanCbz** to determine upper limit that produced measurable
pulmonary inflammation

Expt. Group	Body Weight change #	Cell numbers in bronchoalveolar lavage (BAL) fluid, Mean ± SE				
		Total Cells/ Mouse x 10^3	Macrophages /Mouse x 10^3 (%)*	PMNs/ Mouse x 10^3 (%)*	Lymph./ Mouse x 10^3 (%)*	Eosin./ Mouse x 10^3 (%)*
Control (Saline)	+ 0.15 g	107.9 ± 15.3	106.1 ± 15.0 (98.37%)	1.16 ± 0.5 (1.03%)	0.43 ± 0.23 (0.40%)	0 ± 0 (0%)
Compound **0.25** mg/mouse	-0.15 g	75.00 ± 10.40	73.03 ± 10.45 (97.3%)	0.70 ± 0.20 (1.1%)	0.97 ± 0.29 (1.4%)	0.16 ± 0.13 (0.2%)
Compound **2.5** mg/mouse	-0.37 g	145.4 ± 15.0	140.26 ± 14.64 (96.5%)	3.15 ± 1.68 (2.1%)	1.90 ± 0.21 (1.3%)	0.08 ± 0.08 (0.1%)
Compound **5** mg/mouse	-0.77 g	321.1 ± 53.8	269.34 ± 26.64 (87.0%)	47.25 ± 30.53 (11.6%)	4.10 ± 0.65 (1.4%)	0.0 ± 0.0 (0%)

after treatment, * proportion of each cell type in BAL

From this initial analysis it was determined that **KanCbz** shows no overt
inflammation to the lung at concentrations suitable for further study. The 2.5 mg dose
per mouse was selected for further studies to demonstrate **KanCbz's** ability to decrease
the inflammatory response in vivo.

6.3 **KanCbz** protection against LPS-induced inflammation

A mouse model for acute pulmonary toxicity and inflammation was used for
evaluating the potential of **KanCbz** to decrease lipopolysaccharide (LPS) induced
inflammation. This model has been successfully used in multiple studies conducted by
collaborators at the Pulmonary Toxicology Facility and their established protocols were
employed in the studies presented here.[122] There are multiple mouse models for each
inflammatory lung disease that encompass the hallmark features of the disease, for
example for COPD cigarette smoke-induced inflammation mouse models are more
appropriate.[123, 124] However, many of these mouse models have long time-frames until

the onset of the disease is established. As an initial proof-of-principle study the LPS-induced acute lung injury model was deemed appropriate.[125]

Pulmonary inflammation was induced by exposure to 6,000 EU/mouse/50 µL LPS, 2 h after initial exposure 2.5 mg/mouse/50 µL **KanCbz** was administered and mice were necropsied 8 h from the initial LPS exposure. The LPS only (positive control) group received only LPS at the same dose and were necropsied 8 h later. The BAL fluid was collected and total cells counts along with differential cell counts were determined (Figure 6.3, Table 6.2). A significant decrease in total neutrophils and total cells present in the BAL fluid was observed for LPS + **KanCbz** group as compared to LPS only group of mice. An inflammatory response is still observed in the compound treated group as compared to saline only control, however these results are encouraging in the fact that they indicate that **KanCbz** is able to decrease the LPS-induced acute inflammatory response *in vivo*.
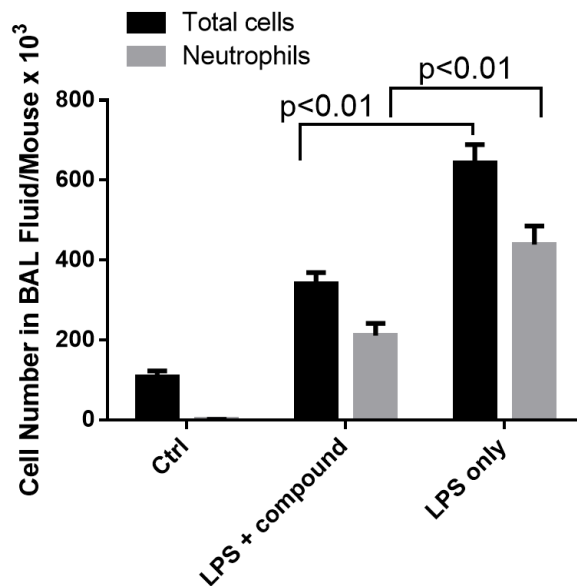
Figure 6.3: Lung inflammation inhibition by **KanCbz**. Total cell and neutrophil counts in BAL fluid for mice exposed LPS + **KanCbz** (2.5 mg/mouse/50 µL) or LPS only control group. A significant decrease in total cell count as well as neutrophils present with respect to LPS only group were observed. Saline control group data, previously determined in dose escalation study, was included for comparison. Data shown as mean ± SE (n = 4).

Table 6.2: Inhibition of LPS induced acute inflammation by **KanCbz**.

Expt. Group	Body Weight change #	Cell numbers in bronchoalveolar lavage (BAL) fluid, Mean ± SE				
		Total Cells/ Mouse x 10^3	Macrophages /Mouse x 10^3 (%)	PMNs/ Mouse x 10^3 (%)	Lymph./ Mouse x 10^3 (%)	Eosin./ Mouse x 10^3 (%)
Control (Saline)	+ 0.15 g	107.9 ± 15.3	106.1 ± 15.0 (98.37%)	1.16 ± 0.5 (1.03%)	0.43 ± 0.23 (0.40%)	0 ± 0 (0%)
LPS + compound	-1.24 g	341.50 ± 27.56 **	127.31 ± 10.25 (38.3%)	210.95 ± 30.75 ** (60.8%)	3.00 ± 1.08 (0.9%)	0 ± 0 (0%)
LPS only	-0.51 g	642.00 ± 47.15	197.29 ± 34.03 (30.8%)	438.68 ± 47.04 (68.3%)	5.29 ± 1.81 (0.9%)	0 ± 0 (0%)

after treatment, (%) proportion of each cell type in BAL fluid
** $p < 0.01$ significantly lower from LPS only control
Data for control group are from dose escalation study for comparison

6.4 Preventive effects of **KanCbz** on acute inflammation

In the previous study (section 6.3) it was shown that **KanCbz** was able to decrease inflammation in the acute toxicity and inflammation mouse model using LPS. To further investigate the *in vivo* effects of **KanCbz**, prophylactic attenuation of acute inflammation was explored. **KanCbz** was dosed via nasal instillation 1 h prior to LPS exposure (6,000 EU/mouse/50 µL) and necropsy was performed 16 h from the initial treatment. BAL fluid was collected and total cell counts along with differential cell counts were performed to assess the inflammatory response (Figure 6.4 and Table 6.3). **KanCbz** showed no preventive effect, and even more, there appears to be an increase in magnitude of the inflammatory response as compared to the LPS only treated group. Furthermore red blood cells were visible in both compound treated and LPS only treated groups, thus indicating possible hemorrhage and protein leak might have occurred.
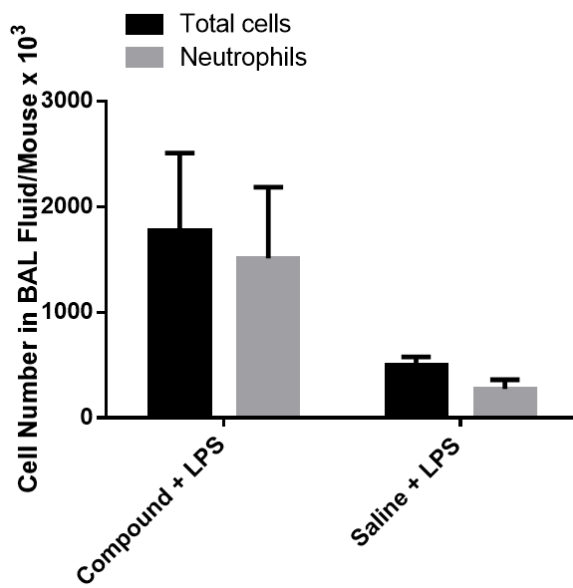
Figure 6.4: Assessment of prophylactic reduction in LPS induced acute inflammation mouse model. **KanCbz** was dosed 1 h prior to LPS exposure and total cell and neutrophil counts were assessed in the BAL fluid. An increase in both total cell counts and neutrophils present in the BAL fluid was observed. Data are mean ± SE (n = 5).

Table 6.3: Study of **KanCbz** preventative effects on acute lung inflammation

Expt. Group	Body Weight change #	Cell numbers in bronchoalveolar lavage (BAL) fluid, Mean ± SE				
		Total Cells/ Mouse x 10^3	Macrophages /Mouse x 10^3 (%)	PMNs/ Mouse x 10^3 (%)	Lymph./ Mouse x 10^3 (%)	Eosin./ Mouse x 10^3 (%)
Compound + LPS	- 1.14 g	1,773.6 ± 735.0	233.8 ± 44.3 (19.4%)	1,511.7 ± 674.7 (79.3%)	32.8 ± 16.8 (1.3%)	0 ± 0 (0%)
Saline + LPS	- 0.15 g	495.8 ± 80.6	219.1 ± 19.9 (47.5%)	274.5 ± 85.5 (52.0%)	2.2 ± 0.4 (0.5%)	0 ± 0 (0%)

after treatment, (%)proportion of each cell type in BAL fluid

6.5 Discussion and conclusions

It was demonstrated in this study that mice exposed to **KanCbz** exhibited no

pulmonary inflammatory effects. A measurable inflammatory response, denoted by an

increase in PMNs recruited to the lungs compared to controls ($p < 0.01$), was however present at a concentration of 5 mg/mouse/50 µL. At a concentration of 2.5 mg/mouse/50 µL, after 24 h, there was a slight increase in total cells present in the BAL fluid and a 1% increase in the percent of PMNs present (no statistically significant increase). The increase in total cells and PMNs present in the BAL fluid at 2.5 mg/mouse/50 µL was not considered to be biologically significant and therefore this dose was selected for further evaluation of the ability **KanCbz** to decrease toxicant induced inflammation in the lung.

Using the model of LPS-induced acute pulmonary toxicity and inflammation in C57Bl/6 mice, it was demonstrated that **KanCbz** treated mice had lower total levels of cells present in the BAL fluid and thus lower overall recruitment of PMNs to the lungs, as compared to LPS-only treated mice. Additionally, **KanCbz** treated mice had fewer visible red blood cells present in the BAL fluid further demonstrating that **KanCbz** attenuated the LPS-induced inflammatory response resulting in a decrease in NSP secreting inflammatory cells present in the lungs and less hemorrhaging. Based on this decrease in total cell counts, the previous *in vitro* studies (Chapter 3 and 5) are confirmed and show that **KanCbz** can indeed decrease the inflammatory response *in vivo* by inhibiting the three NSPs which translates to a reduction in the inflammatory response.

The prophylaxis study presented in section 6.4 highlights some of the limitations encountered in the evaluation of **KanCbz** *in vivo*. Due to limited availability of test compound in this proof of principle study, nasal instillation was used for delivering *N*-arylacyl *O*-sulfonated aminoglycosides to the lung. Treatment at such high doses of 2.5 or 5 mg/mouse via nasal instillation could result in an initial inflammatory response, as was seen for the prophylaxis study. However, in this experiment **KanCbz** was administered only 1 h prior to LPS instillation, thus reducing the recovery time available between exposures when compared to primary experiments that evaluated the ability of **KanCbz** to diminish LPS-induced acute inflammation. Lower doses should be explored

as well as a time course study should be performed to determine more appropriate doses that are still efficacious.

Following these *in vivo* proof of principle studies, a few key aspects need to be examined further. One is the need for better formulation, and a delivery system for inhalation-based administration to the lung of **KanCbz**. This is an ongoing challenge in the field of inflammatory lung diseases such as COPD, cystic fibrosis, acute lung injury and emphysema, where local pulmonary delivery systems are needed to uniformly distribute the drug to the lung reaching as much of its surface as possible.[126, 127] By improving the formulation and delivery system of **KanCbz**, one could use lower and/or consecutive doses. Another key aspect that merits further examination is the effect of **KanCbz** on inflammatory cytokines and chemokines. BAL fluid and whole lung samples were preserved throughout the study for such further analyses to determine if **KanCbz** was able to not only decrease the propagation and inflammatory response by inhibiting the proteolytic activity of NSPs, but also by binding key proinflammatory mediators.

The results obtained in the *in vivo* studies are encouraging considering that **KanCbz** was identified using *in vitro* screens as a modest inhibitor of the three NSPs and was not further optimized prior to the *in vivo* studies, yet it was able to decrease LPS-induced acute pulmonary toxicity and inflammation. This successfully demonstrates that *N*-arylacyl *O*-sulfonated aminoglycosides, as novel unique molecules, merit further exploration as potential lead therapeutics for the treatment of inflammatory lung diseases.

6.6 Methods

6.6.1 Animals

All animal studies were conducted under protocols reviewed and approved by the University of Iowa IACUC, and all methods have been previously used and reported.[122, 128] Male C57BL/6J (4-6 weeks old) mice were purchased from The Jackson Laboratories

(Bar Harbor, ME) and acclimatized 7 days in the animal vivarium at the Institute of Rural and Environmental Health (IREH). The mice were housed in an AAALAC-accredited vivarium in polypropylene, fiber-covered cages in HEPA-filtered Thoren caging units supplied with HEPA-filtered air and operated under positive pressure to the hallway. They were supplied with food (sterile Teklad 5% stock diet, Harlan, Madison, WI) and water *ad libitum* and maintained on a 12 h light-dark cycle.

6.6.2 BAL fluid collection of total and differential cell count

After euthanasia (overdose of isoflurane), BAL fluid was obtained by flushing the lungs with three 1-mL aliquots of 0.9% sterile saline. The recovered fluid was immediately centrifuged and the pellet resuspended in cold RPMI media and aliquots were used to assess total cell counts by hemotocytometer. The rest of the cells were fixed on microslides using Cytospin, stained by Protocol® HEMA 3 stain set (Fisher Diagnostics, Pittsburgh, PA) and differential cell counts (monocytes, neutrophils, lymphocytes and eosinophils) were determined. A total of 200 cells were counted and along with the total cell count, the percent of each cell type in the BAL fluid was determined. The lavage supernatants were split into 3 aliquots and frozen at -80°C for possible later cytokine and total protein analysis. Also lungs of mice were preserved in 10% formaldehyde-PBS for later histopathology studies.

6.6.3 Dose escalation study

All experiments were performed according to protocols established by collaborators at the Pulmonary Toxicology Facility.[122, 128] Briefly, test solutions of **KanCbz** were prepared fresh in saline at 3 separate concentrations (0.25 mg/50 µL, 2.5 mg/50 µL and 5 mg/50 µL). Male C57Bl/6 mice (5 per group) were exposed by a nasal instillation under isoflurane anesthesia with a total of 50 µL (25 µL per each nostril) of saline alone or **KanCbz**. Mice were sacrificed at selected time points post exposure in

each experiment and BAL fluid for total and differential cell counts was collected as described in section 6.6.2. Mouse weights (A) 0.25 mg dose group: 24.14 g, 24.8 g, 25.32 g, 24.46 g, 23.82 g; (B) 2.5 mg dose group: 25.66 g, 25.26 g, 25.26 g, 26.22 g, 25.01 g; (C) 5 mg dose group: 24.82 g, 25.44 g, 27.4 g, 25.54 g, 25 g; (D) saline control group: 27.32 g, 23.58 g, 26.57 g, 23.55 g, 24.5 g.

6.6.4 Protection against LPS-induced inflammation study

Test solution of **KanCbz** was prepared fresh in saline at a concentration of 2.5 mg/50 µL). Acute pulmonary inflammation was induced by exposing mice to 6,000 EU of LPS (time = 0 h). 2 h after LPS instillation one group of mice (n = 5) was treated with **KanCbz**. Both LPS only control mice and LPS + **KanCbz** treated mice were sacrificed 8 h from initial exposure. BAL fluid for total and differential cell counts was collected as described in section 6.6.2 to assess the ability of **KanCbz** to decrease the inflammatory response. Mouse weights (A) saline control group: 27.32 g, 23.58 g, 26.57 g, 23.55 g, 24.5 g, (B) LPS only group: 23.9 g, 24.01 g, 24.16 g, 23.16 g; (C) LPS + **KanCbz** group 26.06 g, 25.44 g, 25.11 g, 23.22 g.

6.6.5 Prevention against LPS-induced inflammation study

Test solution of **KanCbz** was prepared fresh in saline at a concentration of 2.5 mg/50 µL). One group of mice was pretreated with **KanCbz** at time = 0 h while a second control group was pretreated with saline (n = 5). 1 h post pretreatment both groups of mice were exposed to 6,000 EU LPS. Mice were sacrificed 16 h from initial exposure to **KanCbz** or saline control. BAL fluid for total and differential cell counts was collected as described in section 6.6.2 to assess the ability of **KanCbz** to prevent LPS induced inflammatory response. Mouse weights (A) LPS+ **KanCbz** group: 23.54 g, 23.4 g, 24.48 g, 25.16 g, 25.94 g; (B) LPS only group: 23.22 g, 22.84 g, 25.13 g, 25.53 g, 24.11 g.

CHAPTER 7: EXPLORATION OF STRUCTURE-ACTIVITY BASED

SYNTHESIS OF NOVEL DERIVATIVES

Previously in the Kerns laboratory, studies with heparin demonstrated that replacement of *N*-sulfo groups on heparin with *N*-arylacyl groups resulted in heparin derivatives that maintained activity while exhibiting higher selectivity than heparin.[59, 60, 61] The increased selectivity of these heparin derivatives is believed to be a direct result of incorporating aromatic rings that impart selectivity by forming cation-π interactions with positively charged residues on the surface of cationic proteins or enzymes. The selectivity imparted by cation-π interactions is due to the fact that these types of interactions also require an optimal geometry in order for high affinity binding to occur, and for this reason cation-π interactions play an important role in a variety of biological processes such as molecular recognition between receptors and ligands, or drugs and receptors.[129, 130, 131] Further applying this idea that replacing charge-charge interactions with cation-π interactions would increase selectivity of modified heparins for binding to heparin-binding proteins, a panel of *N*-arylacyl *O*-sulfonated aminoglycosides was synthesized and shown to be the smallest known selective heparin mimics that still maintain heparin-like activity.[62, 63] This panel of *N*-arylacyl *O*-sulfonated aminoglycosides was employed in Chapter 3-6 studies as a new therapeutic approach to treat inflammatory lung diseases.

7.1 Goals of this study

Analysis of the inhibitory profile of the nine *N*-arylacyl *O*-sulfonated aminoglycosides with respect to each of the NSPs (Chapter 3) revealed that a flexible core such as the neomycin and kanamycin cores afforded *N*-arylacyl *O*-sulfonated derivatives that were better suited for binding and inhibiting the NSPs. The apramycin core derivatives, which are more rigid due to the center-fused ring, were overall the weakest inhibitors of the NSPs and were likely unable to accommodate binding to the

large, shallow cationic pockets on the surface of the proteases. When examining the effect of the three *N*-aryl moieties on the ability of *N*-arylacyl *O*-sulfonated aminoglycosides to bind and inhibit the three NSPs, the carbobenzyloxy substituted derivatives afforded the most potent compounds as compared to the phenylacetyl or benzoyl substituted derivatives. This suggests that a longer spacer between the phenyl ring and aminoglycoside core is more favorable for binding. Guided by the structure activity relationships established in the *in vitro* studies (Chapters 3-5), the goal of the study presented in this chapter was to design and synthesize a panel of second generation *N*-arylacyl *O*-sulfonated aminoglycosides optimized for binding to the three NSPs. A new aminoglycoside core, tobramycin, was incorporated as a replacement for the apramycin core and three new *N*-arylacyl groups were proposed (Figure 7.1). Tobramycin is an aminoglycoside similar in structure to kanamycin, possessing a 3-deoxy-2,6-diamino-D-glucopyranose instead of the 6-amino-D-glucopyranose ring. This results in tobramycin having a total of 5 hydroxyls and 5 amines as compared to kanamycin which contains a total of 4 amines and 7 hydroxyls. Using tobramycin as a new aminoglycoside scaffold will result in novel derivatives with reduced overall charge (5 total sulfates vs 7 total sulfates for kanamycin) and one extra *N*-aryl moieties thus increasing the potential of cation-π interactions as opposed to charge-charge interactions. Moreover, the 2,6-diamino-D-glucopyranose ring of tobramycin is also found in neomycin (Figure 7.1).

Naphthylacetyl (Naph) derivatives were envisioned to have increased cation-π interactions and a longer spacer from the aminoglycoside core. The phenylpropionyl (PhP) derivatives were designed as more *in vivo* stable derivatives of the carbobenzyloxy derivatives that maintain a similar length spacer between the phenyl moiety and aminoglycoside core. The phenylcyclopropionyl (PhcP) derivatives were included to examine the effect of a rigid *N*-aryl group on selectivity and/or potency.
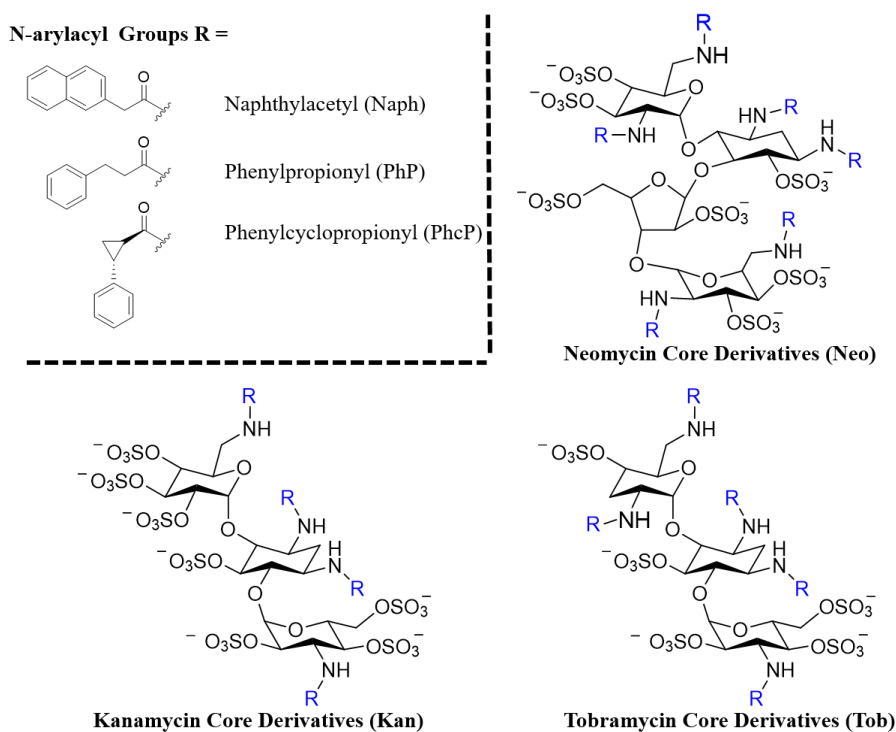
Figure 7.1: Proposed second generation *N*-arylacyl *O*-sulfonated aminoglycosides. Second generation of compounds will feature three aminoglycoside cores neomycin (Neo), kanamycin (Kan) and tobramycin (Tob) and three *N*-arylacyl groups naphthylacetyl (Naph), phenylpropionyl (PhP) and phenylcyclopropionyl (PhcP) thus resulting in a panel of nine novel compounds.

In addition to the synthesis of the nine novel derivatives, large scale synthesis of the lead compound **KanCbz** was accomplished for two purposes. The first purpose was to explore a new chemical approach where once per-*O*-sulfated *N*-carbobenzyloxy kanamycin is obtained, one could remove the carbobenzyloxy moieties by catalytic dehydrogenation to obtain an advanced intermediate onto which various *N*-arylacyl moieties could be installed. Secondly, large amounts of **KanCbz** were required for further exploration of possible intrinsic toxicity and ability to decrease LPS-induced inflammation *in vivo* (Chapter 6).

7.2 Results

Synthesis of second generation *N*-arylacyl *O*-sulfonated aminoglycosides was carried out in a similar manner to the synthesis of the first generation of compounds.[62, 63, 64] The first step involves acylation of the amine groups on the aminoglycoside core, followed by sulfation of the hydroxyl groups (Scheme 7.1). Initial efforts were focused on obtaining *N*-naphthylacetyl and *N*-phenylpropionyl derivatives of all three aminoglycosides by reacting the free amines with NHS-activated esters.[59, 61] Purification using cation exchange chromatography, to remove under-acylated side products, to obtain per-*N*-arylacyl aminoglycoside intermediates proved to be cumbersome especially in the case of the naphthylacetyl derivatives. Once the naphthylacetyl moieties are introduced the compounds become insoluble in most solvents as well as solvent combinations resulting in precipitation on the cation exchange column. After various unsuccessful purification attempts the target products *N*-naphthylacetyl neomycin, *N*-naphthylacetyl kanamycin, *N*-naphthylacetyl tobramycin, *N*-phenylpropionyl neomycin, and *N*-phenylpropionyl kanamycin were purified by semi-preparative HPLC.
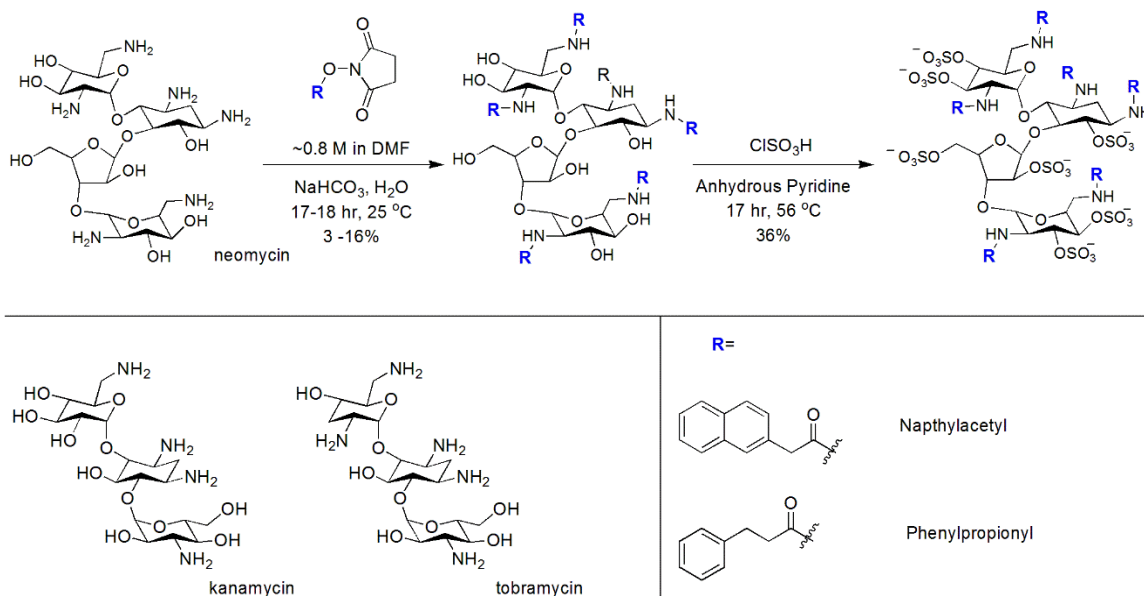
Scheme 7.1: Proposed synthesis of second generation *N*-arylacyl *O*-sulfonated aminoglycosides. Neomycin is shown as an example. Per *N*-acylation was accomplished by coupling the aminoglycoside core with the NHS-ester of 2-naphthylacetic acid and 3-phenylpropanoic acid. Subsequent *O*-sulfonation using ClSO₃H gave *N*-naphthylacetyl *O*-sulfonated neomycin, *N*-naphthylacetyl *O*-sulfonated kanamycin and *N*-phenylpropionyl *O*-sulfonated neomycin.

Chlorosulfonic acid was used to sulfonate the *N*-arylacyl neomycin, kanamycin and tobramycin derivatives according to methodology established for the synthesis of the first generation of compounds.[62, 63, 64] These reactions did not proceed to completion and product purification was attempted using a benchtop C18 column equilibrated in reversed-phase ion pairing (RPIP) buffers.[62] The aqueous reaction mixture was loaded onto the column and non-volatile salts were first eluted with an ammonium acetate buffer containing 0% acetonitrile (ACN) (10 mM ammonium acetate adjusted to pH 8.3 with triethylamine (TEA)). The ACN concentration was then increased stepwise to 10%, 20%, 30% and finally 50%. Eluent was collected in 1 mL fractions and analyzed at 258 nm to detect elution of the *N*-arylacyl *O*-sulfonated aminoglycosides and at 210 nm to detect the elution of the non-volatile salts. Only per-*O*-sulfonated desired final products

with a purity of ≥ 95% were analyzed via electrospray ionization mass spectrometry (ESI-MS). *O*-sulfonated *N*-naphthylacetyl neomycin, *O*-sulfonated *N*-naphthylacetyl kanamycin and *O*-sulfonated *N*-phenylpropionyl neomycin were successfully synthesized. After synthesizing *O*-sulfonated *N*-naphthylacetyl neomycin and kanamycin, the naphthylacetyl derivatives were abandoned due to their extreme detergent properties, a property also likely incompatible to the lung.

Large scale synthesis of **KanCbz** started with *N*-acylation of the kanamycin core (1 mmol per reaction) with *N*-(benzyloxycarbonyloxy) succinamide, was performed in three separate reactions, yield 13 - 49%. Each product mixture was diluted in 4:1 ACN:water and separated using cation exchange chromatography in small batches of ~ 25 mg per load, due to solubility concerns. Eluent was collected in fractions and pooled together to obtain a total of 914.8 mg of per-*N*-carbobenzyloxy kanamycin. Next, sulfonation of per-*N*-carbobenzyloxy kanamycin on large scale was assessed by performing multiple reactions ranging from 25 - 80 mg scale. While at the 50 mg reaction scale per-*O*-sulfonated product was obtained, these reactions typically did not reach completion and the final product could not be purified. It was determined that reactions performed on a 30 mg scale consistently reach completion, and therefore multiple ~ 30 mg scale reactions were performed (yield 16 - 57%, 171.7 mg). Due to purification using benchtop RPIP C18 column equilibrated in ammonium acetate buffers, the final per-*O*-sulfonated product is in the ammonium salt form. For *in vivo* testing there was a concern that high concentrations of ammonium salts could have deleterious effects. The ammonium salt form of *N*-carbobenzyloxy *O*-sulfonated kanamycin was exchanged for the sodium salt form using cation exchange chromatography where the column resin was regenerated with NaOH in order to contain the sodium counterion.

7.3 Discussion

Synthesis and purification of *N*-arylacyl *O*-sulfonated aminoglycosides is quite problematic and traditional synthesis and purification methods used for sulfated oligosaccharides fail in the case of these amphiphilic molecules. Introducing the hydrophobic *N*-arylacyl moieties causes compounds to become amphiphilic and thus display mild surfactant properties. Endogenous surfactant proteins have been shown to play a critical role in protecting the host against invading pathogens and modulate the inflammatory response.[132, 133, 134, 135] Deficiencies in endogenous surfactants have been associated with multiple inflammatory lung diseases; for example in acute respiratory distress syndrome decrease in surfactant proteins leads to increased surface tension of the lung and a decrease in gas exchange capabilities.[136] Surfactant replacement therapy has been shown to be effective in increasing the gas exchange capabilities of the lung, significantly improving patient outcome.[137, 138, 139] Mild detergent-like properties of *N*-arylacyl *O*-sulfonated aminoglycosides could potentially be beneficial for protection against invading pathogens and in breaking up mucus buildup, however strong detergents may also promote degradation of endogenous surfactant proteins causing further lung collapse, thus diminishing the oxygenation capability of the lung. It was observed that *N*-naphthylacetyl derivatives do possess strong detergent-like properties which may, in fact, result in highly toxic compounds that would not be appropriate for the treatment of inflammatory lung disease. For this reason preparation of the naphthylacetyl derivatives was abandoned.

Further studies and new methodology for separating mixtures of under-sulfated and per-sulfated products need to be developed and implemented for the efficient synthesis of second generation *N*-arylacyl *O*-sulfonated aminoglycosides. A viable possibility would be to explore other RPIP buffer systems. Tetraalkylammonium salts including tetraethyl- or tetrabutyl- salts could improve RPIP benchtop separation of reaction mixtures containing various levels of sulfated product. Tetrabutylammonium

salts have been previously used for the separation of complex mixture of heparin-derived oligosaccharides and thus could prove useful for separating *N*-arylacyl *O*-sulfonated aminoglycosides.[140]

7.4 Methods

7.4.1 Materials

Neomycin sulfate was from Sigma Aldrich (St. Louis, MO, USA); kanamycin sulfate was from Bristol Laboratories Inc. (Syracuse, NY, USA); tobramycin was purchased from TCI (Portland, OR, USA). $ClSO_3H$ acid was purchased from Acros Organics (Morris Plains, NJ, USA). 2-Naphthylacetic acid-NHS ester and 3-phenylpropanoic acid-NHS ester were synthesized as previously reported.[59] Cation exchange chromatography used Amberlite IR 120 resin, Sigma Aldrich. HPLC-grade ACN and TEA were from Fisher Scientific (Hampton, NH, USA). All other chemicals were purchased from Sigma. All water was filtered, deionized water from a Barnstead Nanopure Diamond system, Thermo Fisher Scientific (Hampton, NH, USA). A Fisher Accumet AB15 pH meter was used for all pH determinations. Analytical HPLC used a Phenomenex Luna C18 100Å LC column (4.6 mm × 250 mm) (Torrance, CA, USA) with a Shimadzu chromatography system consisting of an LC-10AT VP pump and a SPD-10A UV-VIS detector (Kyoto, Japan). Semi-preparative HPLC used a Phenomenex Luna 5 μm PFP(2) 100 Å LC Column (250 × 21.20 mm) with a Shimadzu HPLC system: dual LC-10AT VP pumps and SPD-M10A VP diode array detector. Centrifugation was done in a Fisher Marathon 21000R, Fisher Scientific. Benchtop C18 column chromatography used silica gel 60 RP C-18 resin, EMD Chemicals (Gibbstown, NJ, USA). Product collected from C18 column chromatography was identified by UV absorbance in 96-well plates using a BioTek Synergy 2 Multimode plate reader (Winooski, VT, USA).

7.4.2 General *N*-acylation methods

Each reaction was monitored using analytical HPLC: 20 μL of the reaction mixture was diluted in 80 μL ACN and 20 μL water; 40 μL of this solution was injected and eluted with a gradient of 10-95% ACN in water (0.1% trifluoroacetic acid (TFA)) over 40 min at 1 mL/min. After ~17-18 hours, the reaction was diluted with cold water (10 mL) to give additional white precipitate. The precipitate was collected by centrifugation (15 min, 4°C, 3500 rpm) and decanting followed by washing the solid with cold water (10 mL), centrifugation and decanting. This wash procedure was repeated ten times followed by lyophilization of a final suspension to give dry white solid. Under-reacted product was removed by dissolving the product in ACN:water (5:1) and passing the solution through a column of amberlite cation (H^+ form) exchange resin (23 mL bed volume). The partially purified material was eluted in ACN:water (5:1) (10 column volumes) and lyophilized. Dry white solid was then purified by semi-preparative HPLC. To this end, the product mixture was dissolved in ACN:water or *N, N*-dimethylformamide (DMF) followed by dilution in ACN:water and replicate aliquots injected and separated. The per-*N*-arylacyl product was collected around 15 to 20 minutes, depending on ACN elution gradient used. Purified product was rotary evaporated to remove organic solvent and the resulting aqueous suspension lyophilized to give a white solid.

7.4.2.1 *N*-naphthylacetyl neomycin

A solution of 2-naphthylacetic acid-NHS ester (1.6 g, 1.2 mol/mol NH_2) in DMF (9 mL) was added fraction-wise (0.3 mL/hr to 0.5 mL/hr) to neomycin (0.5 mmol) dissolved in aqueous $NaHCO_3$ (17 mL). The reaction was stirred at room temperature for 17 hours after which 5 mL aqueous $NaHCO_3$ was added. A white precipitate formed as the reaction proceeded. The precipitate was collected by centrifugation. The precipitate was repeatedly washed with cold water (10 × 10 mL) by repeated steps of centrifugation

and decanting. The precipitate was dissolved in 5:1 ACN:H_2O and separated on semi-preparative HPLC (40-80% ACN over 45 min, peak eluted at 29 min). Organic solvent was removed *en vacuo*. The remaining aqueous precipitate was lyophilized to dryness (2 days), 4 % yield. ESI-HRMS calcd for $C_{95}H_{94}N_6O_{19}$ $[M + H]^+$ m/z = 1624.798, found 1625.993.

7.4.2.2 *N*-naphthylacetyl kanamycin

A solution of 2-naphthylacetic acid-NHS ester (340 mg, 1.2 mol/mol NH_2) in DMF (2 mL) was added fraction-wise (0.15 mL/hr) to kanamycin (0.25 mmol) dissolved in aqueous $NaHCO_3$ (10 mL). The reaction was stirred at room temperature for 18 hours. A white precipitate formed as the reaction proceeded. The precipitate was collected by centrifugation. The precipitate was repeatedly washed with cold water (10×10 mL) by repeated steps of centrifugation and decanting. The precipitate was dissolved in 5:1 ACN:H_2O and loaded on a cation exchange column. Partially purified material was eluted with ACN:water (5:1) (10 column volumes) and lyophilized.   Dried powder was dissolved in 4 mL DMF and diluted in 4:1 ACN:water for separation on semi-preparative HPLC (50-70% ACN over 30 min, peak eluted at 18 min). Organic solvent was removed *en vacuo*. The remaining aqueous precipitate was lyophilized to dryness (2 days), 16 % yield. ESI-HRMS calcd for $C_{66}H_{68}N_4O_{15}$ $[M + Na]^+$ m/z = 1180.25, found 1180.103

7.4.2.3 *N*-naphthylacetyl tobramycin

A solution of 2-naphthylacetic acid-NHS ester (390 mg, 1.2 mol/mol NH_2) in DMF (2 mL) was added fraction-wise (0.25 mL/hr) to tobramycin (0.25 mmol) dissolved in aqueous $NaHCO_3$ (8 mL). The reaction was stirred at room temperature for 18 hours. A white precipitate formed as the reaction proceeded. The precipitate was collected by centrifugation and was repeatedly washed with cold water (10×10 mL) by repeated steps of centrifugation and decanting. The precipitate was dissolved in 5:1 ACN:H_2O and loaded on a cation exchange column. Partially purified material was eluted with

ACN:water (5:1) (10 column volumes) and lyophilized. Dried powder was dissolved in 4:1 ACN:water and separated on semi-preparative HPLC (50-70% ACN over 30 min, peak eluted at 25 min). Organic solvent was removed *en vacuo*. The remaining aqueous precipitate was lyophilized to dryness (2 days), 3 % yield. ESI-HRMS calcd for $C_{78}H_{77}N_5O_{14}$ $[M + Na]^+$ m/z = 1330.54 found 1330.260.

7.4.2.4 *N*-phenylpropionyl neomycin

A solution of 3-phenylpropanoic acid-NHS ester (1.5 g, 1.2 mol/mol NH_2) in DMF (9 mL) was added fraction-wise (0.3 mL/hr) to neomycin (0.5 mmol) dissolved in aqueous $NaHCO_3$ (17 mL). The reaction was stirred at room temperature. A white precipitate formed as the reaction proceeded. The precipitate was collected by centrifugation. The precipitate was repeatedly washed with cold water (10×10 mL) by repeated steps of centrifugation and decanting. The precipitate was dissolved in 5:1 $ACN:H_2O$ and separated on semi-preparative HPLC (45-60% ACN over 30 min, peak eluted at 15 min). Organic solvent was removed *en vacuo*. The remaining aqueous precipitate was lyophilized to dryness (2 days), 4 % yield. ESI-LRMS calcd for $C_{77}H_{94}N_6O_{19}$ $[M + Na]^+$ m/z = 1429.65, found 1430.07.

7.4.2.5 *N*-phenylpropionyl kanamycin

A solution of 3-phenylpropanoic acid-NHS ester (989 mg, 1.2 mol/mol NH_2) in DMF (5 mL) was added fraction-wise (0.35 mL/hr) to kanamycin (0.5 mmol) dissolved in aqueous $NaHCO_3$ (15 mL). The reaction was stirred at room temperature. A white precipitate formed as the reaction proceeded. The precipitate was collected by centrifugation. The precipitate was repeatedly washed with cold water (10×10 mL), by repeated steps of centrifugation and decanting. The precipitate was dissolved in 5:1 $ACN:H_2O$ and separated on semi-preparative HPLC (40-95% ACN over 40 min, peak eluted at 20 min). Organic solvent was removed *en vacuo*. The remaining aqueous

precipitate was lyophilized to dryness (2 days), 5 % yield. ESI-HRMS calcd for $C_{54}H_{68}N_4O_{15}$ [M + Na]$^+$ m/z = 1035.46, found 1035.394.

7.4.3 General *O*-sulfonation methods

All glassware was oven-dried; all reactions were performed under argon gas. *N*-arylacyl aminoglycoside (10-35 mg) was dissolved in anhydrous pyridine (2 mL) and evaporated for azeotropic removal of residual water 3 times and further dried under high-vacuum for 30 to 45 min. Separately ClSO$_3$H (8 equivalents per hydroxyl) was added drop-wise to anhydrous pyridine (2 mL) stirring at room temperature in a 50 mL 2-neck round bottom flask and the mixture then heated to 56 °C.[141, 142] The *N*-arylacyl aminoglycoside was dissolved in anhydrous pyridine (1 mL) and cannulated into the stirring ClSO$_3$H/pyridine solution. Heating was maintained at 56 °C and reaction progress monitored by analytical HPLC by extracting 10 μL of the reaction mixture and adding 40 μL aqueous NaHCO$_3$ and 60 μL H$_2$O. Pyridine was extracted from each aliquot using dichloromethane (DCM) prior to injection on HPLC. ACN (20 μL) was then added to each aliquot and 50 μL of the resulting solution was injected on HPLC and separated by gradient elution in RPIP buffers A and B: 0-100% buffer B over 20 min at 0.5 mL/min. Buffer A consisted of 9:1 water:ACN with 10 mm ammonium acetate and pH adjusted to 8.3 with TEA. Buffer B consisted of 7:3 water:ACN with 10 mm ammonium acetate and pH adjusted to 8.3 with TEA. For the phenylpropionyl and naphthyl substituted derivatives HPLC elution gradient of 10-95% ACN in water (0.1% TFA) over 40 min at 1 mL/min was used.

Upon reaction completion, ~ 9 hr, the mixture was cooled in an ice bath and adjusted to pH = 8 with addition of aqueous NaHCO$_3$. The resulting aqueous solution was transferred to a separatory funnel and extracted with DCM (10 × 15 mL) to remove pyridine. The water layer was then condensed on a rotary evaporator to remove residual organic solvent. Desalting and product purification was accomplished using a benchtop

C18 column. The aqueous mixture of sulfonation reaction product(s) was loaded onto a column packed with C18 silica resin (1×5.8 cm, 6.5 mL bed volume). Non-volatile salts were first eluted with the ammonium acetate buffer (10 mM ammonium acetate adjusted to pH = 8.3 with TEA) under gravity flow. Eluent was collected in fractions (1 mL) and analyzed at 210 and 258 nm to detect elution of sodium sulfate and aminoglycoside, respectively. Then, under-sulfated products followed by per-*O*-sulfonted product were eluted by addition of increasing concentrations of ACN (10%, 20%, 30% and 50%). As determined with 258 nm detection, fractions containing sulfated aminoglycoside were pooled, and ACN was removed *en vacuo*. The remaining water and volatile salts were removed by lyophilization to give product as a white solid.

7.4.3.1 *O*-sulfonated Hexa *N*-phenylpropionyl neomycin

$ClSO_3H$ (80 µL) was added drop-wise to anhydrous pyridine (2 mL) stirring at room temperature in a 2-neck round bottom flask and the mixture was then heated to 56 °C. *N*-phenylpropionyl neomycin (30 mg) was dissolved in anhydrous pyridine (2 mL) and was cannulated into the stirring $ClSO_3H$/pyridine solution. Heating was maintained at 56 °C and reaction progress monitored by analytical HPLC. Upon reaction completion, 9 hr, the mixture was cooled in an ice bath and adjusted to pH = 8 with addition of aqueous $NaHCO_3$ (10 mL). The resulting aqueous solution was transferred to a separatory funnel and extracted with DCM (7×25 mL) to remove pyridine. The water layer was then condensed on a rotary evaporator to remove residual organic solvent. Desalting and product purification were accomplished by loading the aqueous product on to a benchtop C18 column as described in section 7.4.3 general methodology. Final reaction products were analyzed on HPLC and MS (Appendix, Figure A.1 and A.2). Parent mass calcd. $[M+3H+Na]^{-3}$ m/z= 661.771, found 661.627. MS-induced loss of sulfate groups was also observed calcd. $[M-SO_3+2NH_4+TEA]^{-2}$ m/z = 504.383, found 504.052; calcd. $[M-2SO_3+2H+2Na]^{-3}$ m/z = 615.794, found 615.663; calcd. $[M-3SO_3+3H+Na]^{-3}$ m/z = 582.150 found 581.693; calcd. $[M-4SO_3+4H]^{-3}$ m/z = 547.835, found 547.720. Yield 36 %

7.4.3.2 O-sulfonated Hexa N-naphthylacetyl neomycin

$ClSO_3H$ (80 μL) was added drop-wise to anhydrous pyridine (2 mL) stirring at room temperature in a 2-neck round bottom flask and the mixture then heated to 56 °C. N-naphthylacetyl neomycin (32.88 mg) was dissolved in anhydrous pyridine (2 mL) and was cannulated into the stirring $ClSO_3H$/pyridine solution. Heating was maintained at 56 °C and reaction progress monitored by analytical HPLC. Upon reaction completion, 8 hr, the mixture was cooled in an ice bath and adjusted to pH = 8 with addition of aqueous $NaHCO_3$ (10 mL). The resulting aqueous solution was transferred to a separatory funnel and extracted with DCM (7×25 mL) to remove pyridine. The water layer was then condensed on a rotary evaporator to remove residual organic solvent. Desalting and product purification were accomplished by loading the aqueous product on to a benchtop C18 column as described in section 7.4.3 general methodology. Final reaction products were analyzed on HPLC and MS (Appendix, Figure A.3 and A.4). Parent mass calcd. $[M+3Na]^{-4}$ m/z = 561.067, found 561.06; calcd. $[M+5Na]^{-2}$ m/z = 1145.124, found 1145.59; calcd. $[M+3H+2Na]^{-2}$ m/z = 1112.152, found 1112.82. MS-induced loss of sulfate groups was also observed calcd. $[M-SO_3+H]^{-6}$ m/z = 349.392, found 349.49; calcd. $[M-SO_3+H+2Na]^{-4}$ m/z = 535.582, found 525.62; calcd. $[M-SO_3+2H+2Na]^{-3}$ m/z = 714.446, found 714.33; calcd. $[M-2SO_3+2H]^{-5}$ m/z = 403.480, found 403.49; calcd. $[M-2SO_3+2H+Na]^{-4}$ m/z = 510.098, found 510.04; calcd. $[M-6SO_3+3H]^{-3}$ m/z = 424.646 found 424.00; Yield 56 %

7.4.3.3 O-sulfonated Tetra N-naphthylacetyl kanamycin

$ClSO_3H$ (55 μL) was added drop-wise to anhydrous pyridine (2 mL) stirring at room temperature in a 2-neck round bottom flask and the mixture then heated to 56 °C. N-naphthylacetyl neomycin (16.64 mg) was dissolved in anhydrous pyridine (4 mL) and was cannulated into the stirring $ClSO_3H$/pyridine solution. Heating was maintained at 56 °C and reaction progress monitored by analytical HPLC. After 9 hr another equivalent of $ClSO_3H$ was added. After additional 9 hr reaction did not reach completion, the mixture was cooled in an ice bath and adjusted to pH = 8 with addition of aqueous $NaHCO_3$ (10 mL). The resulting aqueous solution was transferred to a separatory funnel and extracted with DCM (7×25 mL) to remove pyridine. The water layer was then condensed on a

rotary evaporator to remove residual organic solvent. Desalting and product purification were accomplished by loading the aqueous product onto a benchtop C18 column as described in section 7.4.3 general methodology. Final reaction products were analyzed by HPLC and MS (Appendix, Figure A.5 and A.6). Parent mass calcd. $[M]^{-7} = 244.158$, found 244.21; calcd. $[M+2Na]^{-5}$ m/z = 351.018, found 351.06; calcd. $[M+3Na]^{-4}$ m/z = 444.520, found 444.49; calcd. $[M+4Na]^{-3}$ m/z = 600.356, found 600.72. MS-induced loss of sulfate groups was also observed calcd. $[M-SO_3+H+2Na]^{-4}$ m/z = 419.035, found 419.12; calcd. $[M-SO_3+H+3Na]^{-3}$ m/z = 566.377, found 566.29; calcd. $[M-2SO_3+3H]^{-4}$ m/z = 388.055, found 388.80; calcd. $[M-2SO_3+2H+Na]^{-4}$ m/z = 393.550, found 393.43; calcd. $[M-2SO_3+2H+2Na]^{-4}$ m/z = 532.397, found 532.43. Yield 17 %

CHAPTER 8: FUTURE DIRECTIONS

In the studies presented here, **KanCbz** was identified as a novel inhibitor of HNE, CatG and Pr3, and **NeoCbz** was shown to be a potent dual inhibitor of HNE and CatG (Chapter 3). **KanCbz** and **NeoCbz** are partial mixed inhibitors of CatG and can bind and inhibit the protease even if substrate is bound, thus it is believed that they binds sites on the surface of each NSP resulting in inhibition of the proteases (Chapter 4). NSP-mediated proteolytic detachment of A549 lung epithelial cells was significantly inhibited by **KanCbz** and **NeoCbz** in the case of each protease (Chapter 5). Finally, the ability of **KanCbz** to inhibit the three NSPs and restore the protease-protease inhibitor imbalance was explored and confirmed using *in vivo* mouse model for acute lung toxicity and inflammation (Chapter 6). Guided by initial structure activity relationship models constructed from the screening of the library of compounds against each NSP, second generation *N*-arylacyl *O*-sulfonated aminoglycosides were proposed, and the synthesis of select compounds was accomplished (Chapter 7).

A logical extension of this study would be to characterize the interaction between the *N*-arylacyl *O*-sulfonated aminoglycosides and the endogenous PIs SLPI, a1PI and elafin. Heparin is known to bind these endogenous PIs and therefore it is possible that the *N*-arylacyl *O*-sulfonated aminoglycosides also bind the endogenous PIs. Binding to endogenous PIs could have multiple outcomes; one is that this could lead to inhibition of endogenous PIs which would be undesirable. Alternatively, *N*-arylacyl *O*-sulfonated aminoglycosides binding to the endogenous PIs could have a protective effect since endogenous PIs are cleaved by neutrophil serine proteases. Both effects at the same time would afford offsetting effects, where binding leads to a decrease in activity of the endogenous PIs, but increased protection from degradation by the proteases.[1, 143, 144]

Another direction would be to evaluate the panel of *N*-arylacyl *O*-sulfonated aminoglycosides for inhibition of MMPs as well as cytokines that play an important role

in propagating the inflammatory response.[145, 146] MMPs have been shown also degrade the extracellular matrix, inactivate endogenous PIs and propagate the inflammatory response via cytokine production or activation.[1] Heparin and other GAGs have been shown to interact with MMPs and modulate their activity and even though the role of MMPs in inflammatory lung diseases has not been thoroughly explored, it would be interesting to see if our compound also inhibit this class of proteases or if they are selective for NSPs only.[147, 148]

Apart from further characterizing the inhibitory profile of this specific panel of *N*-arylacyl *O*-sulfonated aminoglycosides with endogenous PIs, other classes of proteases, and mediators of inflammation, the synthesis of the second generation of compounds can be completed and these new compounds can be evaluated using the same *in vitro* assays described throughout this study. These compounds could have improved activity as well as stability and would add valuable information to our structure based activity model. From here, the next generation of compounds could be greatly improved and the overall charge and maybe even mass of the compounds could be reduced.

Most importantly, as these compounds advance through future studies one key problem needs to be solved, and that is a better formulation and direct delivery to the lung. The potency of these compounds, as well as other inhaled therapeutics for the treatment of inflammatory lung diseases, will always be limited by the available systems to formulate and deliver them to the lung. This proof-of-concept study demonstrates that *N*-arylacyl *O*-sulfonated aminoglycosides can be exploited as a promising new type of lead structure for further structural and functional optimization, however, formulation of these compounds needs to be tackled simultaneously.

REFERENCES

1.   Owen, C. A., Roles for proteinases in the pathogenesis of chronic obstructive pulmonary disease. *Int. J. Chron. Obstruct. Pulmon. Dis.* **2008,** *3* (2), 253-68.
2.   Hahn, I.; Klaus, A.; Janze, A. K.; Steinwede, K.; Ding, N.; Bohling, J.; Brumshagen, C.; Serrano, H.; Gauthier, F.; Paton, J. C.; Welte, T.; Maus, U. A., Cathepsin G and neutrophil elastase play critical and nonredundant roles in lung-protective immunity against Streptococcus pneumoniae in mice. *Infect. Immun.* **2011,** *79* (12), 4893-901.
3.   Owen, C. A.; Campbell, M. A.; Boukedes, S. S.; Stockley, R. A.; Campbell, E. J., A discrete subpopulation of human monocytes expresses a neutrophil-like proinflammatory (P) phenotype. *Am. J. Physiol.* **1994,** *267* (6 Pt 1), L775-85.
4.   Owen, C. A.; Campbell, E. J., The cell biology of leukocyte-mediated proteolysis. *J. Leukoc. Biol.* **1999,** *65* (2), 137-50.
5.   Guyot, N.; Wartelle, J.; Malleret, L.; Todorov, A. A.; Devouassoux, G.; Pacheco, Y.; Jenne, D. E.; Belaaouaj, A., Unopposed cathepsin G, neutrophil elastase, and proteinase 3 cause severe lung damage and emphysema. *Am. J. Pathol.* **2014,** *184* (8), 2197-210.
6.   Pham, C. T., Neutrophil serine proteases: specific regulators of inflammation. *Nat. Rev. Immunol.* **2006,** *6* (7), 541-50.
7.   Turino, G. M., The origins of a concept: the protease-antiprotease imbalance hypothesis. *Chest* **2002,** *122* (3), 1058-60.
8.   Lucas, S. D.; Costa, E.; Guedes, R. C.; Moreira, R., Targeting COPD: advances on low-molecular-weight inhibitors of human neutrophil elastase. *Med. Res. Rev.* **2013,** *33 Suppl 1* (S1), E73-101.
9.   Fregonese, L.; Stolk, J., Hereditary alpha-1-antitrypsin deficiency and its clinical consequences. *Orphanet J. Rare Dis.* **2008,** *3*, 16.
10.   Kessenbrock, K.; Dau, T.; Jenne, D. E., Tailor-made inflammation: how neutrophil serine proteases modulate the inflammatory response. *J. Mol. Med. (Berl.)* **2011,** *89* (1), 23-8.
11.   Dall'Acqua, W.; Halin, C.; Rodrigues, M. L.; Carter, P., Elastase substrate specificity tailored through substrate-assisted catalysis and phage display. *Protein Eng. Des. Sel.* **1999,** *12* (11), 981-987.
12.   Groutas, W. C.; Dou, D.; Alliston, K. R., Neutrophil elastase inhibitors. *Expert Opin. Ther. Pat.* **2011,** *21* (3), 339-54.
13.   Ohbayashi, H., Neutrophil elastase inhibitors as treatment for COPD. *Expert Opin Investig Drugs* **2002,** *11* (7), 965-80.
14.   Li, Y.; Dou, D.; He, G.; Lushington, G. H.; Groutas, W. C., Mechanism-based inhibitors of serine proteases with high selectivity through optimization of S' subsite binding. *Bioorg. Med. Chem.* **2009,** *17* (10), 3536-42.
15.   Hunkapiller, M. W.; Forgac, M. D.; Richards, J. H., Mechanism of action of serine proteases: tetrahedral intermediate and concerted proton transfer. *Biochemistry* **1976,** *15* (25), 5581-8.
16.   Lai, Z.; Gan, X.; Wei, L.; Alliston, K. R.; Yu, H.; Li, Y. H.; Groutas, W. C., Potent inhibition of human leukocyte elastase by 1,2,5-thiadiazolidin-3-one 1,1 dioxide-based sulfonamide derivatives. *Arch. Biochem. Biophys.* **2004,** *429* (2), 191-197.
17.   Wei, L.; Lai, Z.; Gan, X.; Alliston, K. R.; Zhong, J.; Epp, J. B.; Tu, J.; Perera, A. B.; Stipdonk, M. V.; Groutas, W. C., Mechanism-based inactivation of human leukocyte elastase via an enzyme-induced sulfonamide fragmentation process. *Arch. Biochem. Biophys.* **2004,** *429* (1), 60-70.
18.   Kuang, R.; Epp, J. B.; Ruan, S.; Chong, L. S.; Venkataraman, R.; Tu, J.; He, S.; Truong, T. M.; Groutas, W. C., Utilization of the 1,2,5-thiadiazolidin-3-one 1,1 dioxide scaffold in the design of potent inhibitors of serine proteases: SAR studies using carboxylates. *Bioorg. Med. Chem.* **2000,** *8* (5), 1005-1016.

19.   Groutas, W. C.; Kuang, R.; Ruan, S.; Epp, J. B.; Venkataraman, R.; Truong, T. M., Potent and specific inhibition of human leukocyte elastase, cathepsin G and proteinase 3 by sulfone derivatives employing the 1,2,5-thiadiazolidin-3-one 1,1 dioxide scaffold. *Bioorg. Med. Chem.* **1998,** *6* (6), 661-671.

20.   Kawabata, K.; Suzuki, M.; Sugitani, M.; Imaki, K.; Toda, M.; Miyamoto, T., ONO-5046, a novel inhibitor of human neutrophil elastase. *Biochem. Biophys. Res. Commun.* **1991,** *177* (2), 814-20.

21.   Ohmoto, K.; Yamamoto, T.; Okuma, M.; Horiuchi, T.; Imanishi, H.; Odagaki, Y.; Kawabata, K.; Sekioka, T.; Hirota, Y.; Matsuoka, S.; Nakai, H.; Toda, M.; Cheronis, J. C.; Spruce, L. W.; Gyorkos, A.; Wieczorek, M., Development of orally active nonpeptidic inhibitors of human neutrophil elastase. *J. Med. Chem.* **2001,** *44* (8), 1268-85.

22.   Oleksyszyn, J.; Powers, J. C., Irreversible inhibition of serine proteases by peptide derivatives of (alpha-aminoalkyl)phosphonate diphenyl esters. *Biochemistry* **1991,** *30* (2), 485-93.

23.   Sienczyk, M.; Lesner, A.; Wysocka, M.; Legowska, A.; Pietrusewicz, E.; Rolka, K.; Oleksyszyn, J., New potent cathepsin G phosphonate inhibitors. *Bioorg. Med. Chem.* **2008,** *16* (19), 8863-7.

24.   Korkmaz, B.; Kellenberger, C.; Viaud-Massuard, M.-C.; Gauthier, F., Selective Inhibitors of Human Neutrophil Proteinase 3. *Curr. Pharm. Des.* **2012,** *19* (6), 966-976.

25.   Epinette, C.; Croix, C.; Jaquillard, L.; Marchand-Adam, S.; Kellenberger, C.; Lalmanach, G.; Cadene, M.; Viaud-Massuard, M. C.; Gauthier, F.; Korkmaz, B., A selective reversible azapeptide inhibitor of human neutrophil proteinase 3 derived from a high affinity FRET substrate. *Biochem. Pharmacol.* **2012,** *83* (6), 788-96.

26.   Henry, B. L.; Thakkar, J. N.; Liang, A.; Desai, U. R., Sulfated, low molecular weight lignins inhibit a select group of heparin-binding serine proteases. *Biochem. Biophys. Res. Commun.* **2012,** *417* (1), 382-6.

27.   Saluja, B.; Li, H.; Desai, U. R.; Voelkel, N. F.; Sakagami, M., Sulfated caffeic acid dehydropolymer attenuates elastase and cigarette smoke extract-induced emphysema in rats: sustained activity and a need of pulmonary delivery. *Lung* **2014,** *192* (4), 481-92.

28.   Saluja, B.; Thakkar, J. N.; Li, H.; Desai, U. R.; Sakagami, M., Novel low molecular weight lignins as potential anti-emphysema agents: In vitro triple inhibitory activity against elastase, oxidation and inflammation. *Pulm. Pharmacol. Ther.* **2013,** *26* (2), 296-304.

29.   Fleddermann, J.; Pichert, A.; Arnhold, J., Interaction of serine proteases from polymorphonuclear leucocytes with the cell surface and heparin. *Inflammation* **2012,** *35* (1), 81-8.

30.   Spencer, J. L.; Stone, P. J.; Nugent, M. A., New insights into the inhibition of human neutrophil elastase by heparin. *Biochemistry* **2006,** *45* (30), 9104-20.

31.   Kennedy, T. P., Method and medicament for inhibiting neutrophil elastase and cathepsin g. Google Patents: 1994.

32.   Volpi, N., Inhibition of human leukocyte elastase activity by heparins: influence of charge density. *Biochim. Biophys. Acta* **1996,** *1290* (3), 299-307.

33.   Jegot, G.; Derache, C.; Castella, S.; Lahouassa, H.; Pitois, E.; Jourdan, M. L.; Remold-O'Donnell, E.; Kellenberger, C.; Gauthier, F.; Korkmaz, B., A substrate-based approach to convert SerpinB1 into a specific inhibitor of proteinase 3, the Wegener's granulomatosis autoantigen. *FASEB J.* **2011,** *25* (9), 3019-31.

34.   van der Geld, Y. M.; Limburg, P. C.; Kallenberg, C. G., Proteinase 3, Wegener's autoantigen: from gene to antigen. *J. Leukoc. Biol.* **2001,** *69* (2), 177-90.

35.   Sandhaus, R. A.; Turino, G., Neutrophil elastase-mediated lung disease. *COPD* **2013,** *10 Suppl 1* (S1), 60-3.

36.   McCarthy, C.; O'Dwyer, C. A.; Bergin, D. A.; McElvaney, N. G.; Reeves, E. P., Antiproteases as Therapeutics to Target Inflammation in Chronic Obstructive Pulmonary Disease. **2014**.

37.   Griese, M.; Latzin, P.; Kappler, M.; Weckerle, K.; Heinzlmaier, T.; Bernhardt, T.; Hartl, D., alpha1-Antitrypsin inhalation reduces airway inflammation in cystic fibrosis patients. *Eur. Respir. J.* **2007,** *29* (2), 240-50.

38.   Brennan, S., Revisiting α1-antitrypsin therapy in cystic fibrosis: can it still offer promise? *Eur. Respir. J.* **2007,** *29* (2), 229-230.

39.   Korkmaz, B.; Horwitz, M. S.; Jenne, D. E.; Gauthier, F., Neutrophil Elastase, Proteinase 3, and Cathepsin G as Therapeutic Targets in Human Diseases. *Pharmacol. Rev.* **2010,** *62* (4), 726-759.

40.   Barnes, P. J., Emerging pharmacotherapies for COPD. *Chest* **2008,** *134* (6), 1278-86.

41.   Vogelmeier, C.; Aquino, T. O.; O'Brien, C. D.; Perrett, J.; Gunawardena, K. A., A randomised, placebo-controlled, dose-finding study of AZD9668, an oral inhibitor of neutrophil elastase, in patients with chronic obstructive pulmonary disease treated with tiotropium. *COPD* **2012,** *9* (2), 111-20.

42.   Zani, M. L.; Baranger, K.; Guyot, N.; Dallet-Choisy, S.; Moreau, T., Protease inhibitors derived from elafin and SLPI and engineered to have enhanced specificity towards neutrophil serine proteases. *Protein Sci.* **2009,** *18* (3), 579-94.

43.   (a) Wiedow, O.; Luademann, J.; Utecht, B., Elafin is a potent inhibitor of proteinase 3. *Biochem. Biophys. Res. Commun.* **1991,** *174* (1), 6-10; (b) Wiedow, O.; Schroder, J. M.; Gregory, H.; Young, J. A.; Christophers, E., Elafin: an elastase-specific inhibitor of human skin. Purification, characterization, and complete amino acid sequence. *J. Biol. Chem.* **1990,** *265* (25), 14791-5.

44.   Guyot, N.; Zani, M. L.; Maurel, M. C.; Dallet-Choisy, S.; Moreau, T., Elafin and its precursor trappin-2 still inhibit neutrophil serine proteinases when they are covalently bound to extracellular matrix proteins by tissue transglutaminase. *Biochemistry* **2005,** *44* (47), 15610-8.

45.   Zani, M. L.; Tanga, A.; Saidi, A.; Serrano, H.; Dallet-Choisy, S.; Baranger, K.; Moreau, T., SLPI and trappin-2 as therapeutic agents to target airway serine proteases in inflammatory lung diseases: current and future directions. *Biochem. Soc. Trans.* **2011,** *39* (5), 1441-6.

46.   Tanga, A.; Saidi, A.; Jourdan, M. L.; Dallet-Choisy, S.; Zani, M. L.; Moreau, T., Protection of lung epithelial cells from protease-mediated injury by trappin-2 A62L, an engineered inhibitor of neutrophil serine proteases. *Biochem. Pharmacol.* **2012,** *83* (12), 1663-73.

47.   Qian, Y.; Xie, H.; Tian, R.; Yu, K.; Wang, R., Efficacy of low molecular weight heparin in patients with acute exacerbation of chronic obstructive pulmonary disease receiving ventilatory support. *COPD* **2014,** *11* (2), 171-6.

48.   Doherty, N. S.; Dinerstein, R. J.; Mehdi, S., Novel inhibitors of polymorphonuclear neutrophil (PMN) elastase and cathepsin G: Evaluation in vitro of their potential for the treatment of inflammatory connective tissue damage. *Int. J. Immunopharmacol.* **1990,** *12* (7), 787-795.

49.   Baici, A.; Salgam, P.; Fehr, K.; Böni, A., Inhibition of human elastase from polymorphonuclear leucocytes by a glycosaminoglycan polysulfate (Arteparon®). *Biochem. Pharmacol.* **1980,** *29* (12), 1723-1727.

50.   Redini, F.; Tixier, J. M.; Petitou, M.; Choay, J.; Robert, L.; Hornebeck, W., Inhibition of leucocyte elastase by heparin and its derivatives. *Biochem. J.* **1988,** *252* (2), 515-519.

51.   Sissi, C.; Lucatello, L.; Naggi, A.; Torri, G.; Palumbo, M., Interactions of low-molecular-weight semi-synthetic sulfated heparins with human leukocyte elastase and human Cathepsin G. *Biochem. Pharmacol.* **2006,** *71* (3), 287-93.

52.   Frommherz, K. J.; Faller, B.; Bieth, J. G., Heparin strongly decreases the rate of inhibition of neutrophil elastase by alpha 1-proteinase inhibitor. *J. Biol. Chem.* **1991,** *266* (23), 15356-62.

53.   Gupta, V. K.; Gowda, L. R., Alpha-1-proteinase inhibitor is a heparin binding serpin: molecular interactions with the Lys rich cluster of helix-F domain. *Biochimie* **2008,** *90* (5), 749-61.

54.   Ermolieff, J.; Boudier, C.; Laine, A.; Meyer, B.; Bieth, J. G., Heparin protects cathepsin G against inhibition by protein proteinase inhibitors. *J. Biol. Chem.* **1994,** *269* (47), 29502-29508.

55.   Ledoux, D.; Merciris, D.; Barritault, D.; Caruelle, J. P., Heparin-like dextran derivatives as well as glycosaminoglycans inhibit the enzymatic activity of human cathepsin G. *FEBS Lett.* **2003,** *537* (1-3), 23-29.

56.   Desai, U. R., The promise of sulfated synthetic small molecules as modulators of glycosaminoglycan function. *Future Med. Chem.* **2013,** *5* (12), 1363-1366.

57.   Volpi, N., Inhibition of human leukocyte elastase activity by chondroitin sulfates. *Chem.-Biol. Interact.* **1997,** *105* (3), 157-167.

58.   Lentini, A.; Ternai, B.; Ghosh, P., Synthetic inhibitors of human leukocyte elastase. Part 1 - Sulphated polysaccharides. *Biochem. Int.* **1985,** *10* (2), 221-232.

59.   Huang, L.; Kerns, R. J., Diversity-oriented chemical modification of heparin: Identification of charge-reduced N-acyl heparin derivatives having increased selectivity for heparin-binding proteins. *Bioorg. Med. Chem.* **2006,** *14* (7), 2300-13.

60.   Fernandez, C.; Hattan, C. M.; Kerns, R. J., Semi-synthetic heparin derivatives: chemical modifications of heparin beyond chain length, sulfate substitution pattern and N-sulfo/N-acetyl groups. *Carbohydr. Res.* **2006,** *341* (10), 1253-65.

61.   Huang, L.; Fernandez, C.; Kerns, R. J., Different protein-binding selectivities for N-acyl heparin derivatives having N-phenylacetyl and heterocycle analogs of N-phenylacetyl substituted in place of N-sulfo groups. *Bioorg. Med. Chem. Lett.* **2007,** *17* (2), 419-23.

62.   Fenner, A. M.; Kerns, R. J., Synthesis, separation, and characterization of amphiphilic sulfated oligosaccharides enabled by reversed-phase ion pairing LC and LC-MS methods. *Carbohydr. Res.* **2011,** *346* (17), 2792-800.

63.   Fenner, A. M.; Oppegard, L. M.; Hiasa, H.; Kerns, R. J., Selective inhibition of bacterial and human topoisomerases by arylacyl -sulfonated aminoglycoside derivatives. *ACS Med. Chem. Lett.* **2013,** *4* (5), 470-474.

64.   Craciun, I.; Fenner, A. M.; Kerns, R. J., N-Arylacyl O-sulfonated aminoglycosides as novel inhibitors of human neutrophil elastase, cathepsin G and proteinase 3. *Glycobiology* **2016**.

65.   Twigg, M. S.; Brockbank, S.; Lowry, P.; FitzGerald, S. P.; Taggart, C.; Weldon, S., The Role of Serine Proteases and Antiproteases in the Cystic Fibrosis Lung. *Mediators Inflamm.* **2015,** *2015*, 293053.

66.   Kosorok, M. R.; Wei, W. H.; Farrell, P. M., The incidence of cystic fibrosis. *Stat. Med.* **1996,** *15* (5), 449-62.

67.   Murray, C. J. L.; Lopez, A. D., Alternative projections of mortality and disability by cause 1990–2020: Global Burden of Disease Study. *The Lancet* **1997,** *349* (9064), 1498-1504.

68.   Salvi, S. S.; Barnes, P. J., Chronic obstructive pulmonary disease in non-smokers. *The Lancet 374* (9691), 733-743.

69.   Lamprecht, B.; McBurnie, M. A.; Vollmer, W. M.; Gudmundsson, G.; Welte, T.; Nizankowska-Mogilnicka, E.; Studnicka, M.; Bateman, E.; Anto, J. M.; Burney, P.; Mannino, D. M.; Buist, S. A., Copd in never smokers: Results from the population-based burden of obstructive lung disease study. *Chest* **2011,** *139* (4), 752-763.

70.   Ngkelo, A.; Adcock, I. M., New treatments for COPD. *Curr. Opin. Pharmacol.* **2013,** *13* (3), 362-9.

71.   Compton, C.; McBryan, D.; Bucchioni, E.; Patalano, F., The Novartis view on emerging drugs and novel targets for the treatment of chronic obstructive pulmonary disease. *Pulm. Pharmacol. Ther.* **2013,** *26* (5), 562-73.

72.   Johnson, E. R.; Matthay, M. A., Acute lung injury: epidemiology, pathogenesis, and treatment. *J. Aerosol Med. Pulm. Drug Deliv.* **2010,** *23* (4), 243-52.

73.   Ragaller, M.; Richter, T., Acute lung injury and acute respiratory distress syndrome. *J Emerg Trauma Shock* **2010,** *3* (1), 43-51.

74.   Segal, A. W., How neutrophils kill microbes. *Annu. Rev. Immunol.* **2005,** *23*, 197-223.

75.   Kobayashi, S. D.; Voyich, J. M.; Burlak, C.; DeLeo, F. R., Neutrophils in the innate immune response. *Arch. Immunol. Ther. Exp. (Warsz.)* **2005,** *53* (6), 505-17.

76.   Belaaouaj, A.; Kim, K. S.; Shapiro, S. D., Degradation of outer membrane protein A in Escherichia coli killing by neutrophil elastase. *Science* **2000,** *289* (5482), 1185-8.

77.   Weinrauch, Y.; Drujan, D.; Shapiro, S. D.; Weiss, J.; Zychlinsky, A., Neutrophil elastase targets virulence factors of enterobacteria. *Nature* **2002,** *417* (6884), 91-4.

78.   Lopez-Boado, Y. S.; Espinola, M.; Bahr, S.; Belaaouaj, A., Neutrophil serine proteinases cleave bacterial flagellin, abrogating its host response-inducing activity. *J. Immunol.* **2004,** *172* (1), 509-15.

79.   Padrines, M.; Wolf, M.; Walz, A.; Baggiolini, M., Interleukin-8 processing by neutrophil elastase, cathepsin G and proteinase-3. *FEBS Lett.* **1994,** *352* (2), 231-5.

80.   Nufer, O.; Corbett, M.; Walz, A., Amino-terminal processing of chemokine ENA-78 regulates biological activity. *Biochemistry* **1999,** *38* (2), 636-42.

81.   Coeshott, C.; Ohnemus, C.; Pilyavskaya, A.; Ross, S.; Wieczorek, M.; Kroona, H.; Leimer, A. H.; Cheronis, J., Converting enzyme-independent release of tumor necrosis factor alpha and IL-1beta from a stimulated human monocytic cell line in the presence of activated neutrophils or purified proteinase 3. *Proc. Natl. Acad. Sci. U. S. A.* **1999,** *96* (11), 6261-6.

82.   Madsen, J. L.; Andersen, T. L.; Santamaria, S.; Nagase, H.; Enghild, J. J.; Skrydstrup, T., Synthesis and evaluation of silanediols as highly selective uncompetitive inhibitors of human neutrophil elastase. *J. Med. Chem.* **2012,** *55* (17), 7900-8.

83.   Santana, A. B.; Lucas, S. D.; Goncalves, L. M.; Correia, H. F.; Cardote, T. A.; Guedes, R. C.; Iley, J.; Moreira, R., N-Acyl and N-sulfonyloxazolidine-2,4-diones are pseudo-irreversible inhibitors of serine proteases. *Bioorg. Med. Chem. Lett.* **2012,** *22* (12), 3993-7.

84.   Salvador, L. A.; Taori, K.; Biggs, J. S.; Jakoncic, J.; Ostrov, D. A.; Paul, V. J.; Luesch, H., Potent elastase inhibitors from cyanobacteria: structural basis and mechanisms mediating cytoprotective and anti-inflammatory effects in bronchial epithelial cells. *J. Med. Chem.* **2013,** *56* (3), 1276-90.

85.   Stevens, T.; Ekholm, K.; Granse, M.; Lindahl, M.; Kozma, V.; Jungar, C.; Ottosson, T.; Falk-Hakansson, H.; Churg, A.; Wright, J. L.; Lal, H.; Sanfridson, A., AZD9668: pharmacological characterization of a novel oral inhibitor of neutrophil elastase. *J. Pharmacol. Exp. Ther.* **2011,** *339* (1), 313-20.

86.   Feng, L.; Liu, X.; Zhu, W.; Guo, F.; Wu, Y.; Wang, R.; Chen, K.; Huang, C.; Li, Y., Inhibition of human neutrophil elastase by pentacyclic triterpenes. *PLoS One* **2013,** *8* (12), e82794.

87.   Hwang, T. L.; Wang, W. H.; Wang, T. Y.; Yu, H. P.; Hsieh, P. W., Synthesis and pharmacological characterization of 2-aminobenzaldehyde oxime analogs as dual inhibitors of neutrophil elastase and proteinase 3. *Bioorg. Med. Chem.* **2015,** *23* (5), 1123-34.

88.   Korkmaz, B.; Moreau, T.; Gauthier, F., Neutrophil elastase, proteinase 3 and cathepsin G: physicochemical properties, activity and physiopathological functions. *Biochimie* **2008,** *90* (2), 227-42.

89.   Hedstrom, L., Serine protease mechanism and specificity. *Chem. Rev.* **2002,** *102* (12), 4501-24.

90.   Korkmaz, B.; Hajjar, E.; Kalupov, T.; Reuter, N.; Brillard-Bourdet, M.; Moreau, T.; Juliano, L.; Gauthier, F., Influence of charge distribution at the active site surface on the substrate specificity of human neutrophil protease 3 and elastase. A kinetic and molecular modeling analysis. *J. Biol. Chem.* **2007,** *282* (3), 1989-97.

91.   Kao, R. C.; Wehner, N. G.; Skubitz, K. M.; Gray, B. H.; Hoidal, J. R., Proteinase 3. A distinct human polymorphonuclear leukocyte proteinase that produces emphysema in hamsters. *J. Clin. Invest.* **1988,** *82* (6), 1963-73.

92.   Shafer, W. M.; Onunka, V. C.; Martin, L. E., Antigonococcal activity of human neutrophil cathepsin G. *Infect. Immun.* **1986,** *54* (1), 184-8.

93.   Fujinaga, M.; Chernaia, M. M.; Halenbeck, R.; Koths, K.; James, M. N., The crystal structure of PR3, a neutrophil serine proteinase antigen of Wegener's granulomatosis antibodies. *J. Mol. Biol.* **1996,** *261* (2), 267-78.

94.   Hajjar, E.; Broemstrup, T.; Kantari, C.; Witko-Sarsat, V.; Reuter, N., Structures of human proteinase 3 and neutrophil elastase--so similar yet so different. *FEBS J.* **2010,** *277* (10), 2238-54.

95.   Bode, W.; Wei, A. Z.; Huber, R.; Meyer, E.; Travis, J.; Neumann, S., X-ray crystal structure of the complex of human leukocyte elastase (PMN elastase) and the third domain of the turkey ovomucoid inhibitor. *EMBO J.* **1986,** *5* (10), 2453-8.

96.   Hof, P.; Mayr, I.; Huber, R.; Korzus, E.; Potempa, J.; Travis, J.; Powers, J. C.; Bode, W., The 1.8 A crystal structure of human cathepsin G in complex with Suc-Val-Pro-PheP-(OPh)2: a Janus-faced proteinase with two opposite specificities. *EMBO J.* **1996,** *15* (20), 5481-91.

97.   Drag, M.; Salvesen, G. S., Emerging principles in protease-based drug discovery. *Nat. Rev. Drug Discov.* **2010,** *9* (9), 690-701.

98.   Kostoulas, G.; Horler, D.; Naggi, A.; Casu, B.; Baici, A., Electrostatic interactions between human leukocyte elastase and sulfated glycosaminoglycans: physiological implications. *Biol. Chem.* **1997,** *378* (12), 1481-9.

99.   Ermolieff, J.; Boudier, C.; Laine, A.; Meyer, B.; Bieth, J. G., Heparin protects cathepsin G against inhibition by protein proteinase inhibitors. *J. Biol. Chem.* **1994,** *269* (47), 29502-8.

100.   Peplow, P. V., Glycosaminoglycan: a candidate to stimulate the repair of chronic wounds. *Thromb. Haemost.* **2005,** *94* (1), 4-16.

101.   Ballut, L.; Sapay, N.; Chautard, E.; Imberty, A.; Ricard-Blum, S., Mapping of heparin/heparan sulfate binding sites on alphavbeta3 integrin by molecular docking. *J. Mol. Recognit.* **2013,** *26* (2), 76-85.

102.   Mulloy, B.; Forster, M. J.; Jones, C.; Davies, D. B., N.m.r. and molecular-modelling studies of the solution conformation of heparin. *Biochem. J.* **1993,** *293 (Pt 3)* (Pt 3), 849-58.

103.   Sethi, S., Infection as a comorbidity of COPD. *Eur. Respir. J.* **2010,** *35* (6), 1209-1215.

104.   Dias-Baruffi, M.; Pereira-da-Silva, G.; Jamur, M. C.; Roque-Barreira, M. C., Heparin potentiates in vivo neutrophil migration induced by IL-8. *Glycoconj. J.* **1998,** *15* (5), 523-6.

105.   Webb, L. M.; Ehrengruber, M. U.; Clark-Lewis, I.; Baggiolini, M.; Rot, A., Binding to heparan sulfate or heparin enhances neutrophil responses to interleukin 8. *Proc. Natl. Acad. Sci. U. S. A.* **1993,** *90* (15), 7158-62.

106.   Weiss, S. J., Tissue destruction by neutrophils. *N. Engl. J. Med.* **1989,** *320* (6), 365-76.

107.   Grommes, J.; Soehnlein, O., Contribution of neutrophils to acute lung injury. *Mol. Med.* **2011,** *17* (3-4), 293-307.

108.   Chua, F.; Laurent, G. J., Neutrophil elastase: mediator of extracellular matrix destruction and accumulation. *Proc. Am. Thorac. Soc.* **2006,** *3* (5), 424-7.

109.   McEver, R. P., Selectins: initiators of leucocyte adhesion and signalling at the vascular wall. *Cardiovasc. Res.* **2015,** *107* (3), 331-9.

110.   Carden, D.; Xiao, F.; Moak, C.; Willis, B. H.; Robinson-Jackson, S.; Alexander, S., Neutrophil elastase promotes lung microvascular injury and proteolysis of endothelial cadherins. *Am. J. Physiol.* **1998,** *275* (2 Pt 2), H385-92.

111.   Ginzberg, H. H.; Cherapanov, V.; Dong, Q.; Cantin, A.; McCulloch, C. A.; Shannon, P. T.; Downey, G. P., Neutrophil-mediated epithelial injury during transmigration: role of elastase. *Am. J. Physiol. Gastrointest. Liver Physiol.* **2001,** *281* (3), G705-17.

112.   Rochat, T.; Casale, J.; Hunninghake, G. W.; Peterson, M. W., Neutrophil cathepsin G increases permeability of cultured type II pneumocytes. *Am. J. Physiol.* **1988,** *255* (5 Pt 1), C603-11.

113.   Lu, P.; Takai, K.; Weaver, V. M.; Werb, Z., Extracellular matrix degradation and remodeling in development and disease. *Cold Spring Harb. Perspect. Biol.* **2011,** *3* (12), 10.1101/cshperspect.a005058 a005058.

114.   Turk, B., Targeting proteases: successes, failures and future prospects. *Nat. Rev. Drug Discov.* **2006,** *5* (9), 785-799.

115.   Cudic, M.; Fields, G. B., Extracellular Proteases as Targets for Drug Development. *Curr. Protein Peptide Sci.* **2009,** *10* (4), 297-307.

116.   Giovanni, A.; David, P. F., Protease Inhibitors in the Clinic. *Medicinal Chemistry* **2005,** *1* (1), 71-104.

117.   Scott, C. J.; Taggart, C. C., Biologic protease inhibitors as novel therapeutic agents. *Biochimie* **2010,** *92* (11), 1681-1688.

118.   Owen, C. A.; Campbell, M. A.; Sannes, P. L.; Boukedes, S. S.; Campbell, E. J., Cell surface-bound elastase and cathepsin G on human neutrophils: a novel, non-oxidative mechanism by which neutrophils focus and preserve catalytic activity of serine proteinases. *J. Cell Biol.* **1995,** *131* (3), 775-89.

119.   Bernfield, M.; Gotte, M.; Park, P. W.; Reizes, O.; Fitzgerald, M. L.; Lincecum, J.; Zako, M., Functions of cell surface heparan sulfate proteoglycans. *Annu. Rev. Biochem.* **1999,** *68* (1), 729-77.

120. Witt, D. P.; Lander, A. D., Differential binding of chemokines to glycosaminoglycan subpopulations. *Curr. Biol.* **1994,** *4* (5), 394-400.

121. Barnes, P. J., Mediators of chronic obstructive pulmonary disease. *Pharmacol. Rev.* **2004,** *56* (4), 515-48.

122. Thorne, P. S.; Adamcakova-Dodd, A.; Kelly, K. M.; O'Neill M, E.; Duchaine, C., Metalworking fluid with mycobacteria and endotoxin induces hypersensitivity pneumonitis in mice. *Am. J. Respir. Crit. Care Med.* **2006,** *173* (7), 759-68.

123. Beckett, E. L.; Stevens, R. L.; Jarnicki, A. G.; Kim, R. Y.; Hanish, I.; Hansbro, N. G.; Deane, A.; Keely, S.; Horvat, J. C.; Yang, M.; Oliver, B. G.; van Rooijen, N.; Inman, M. D.; Adachi, R.; Soberman, R. J.; Hamadi, S.; Wark, P. A.; Foster, P. S.; Hansbro, P. M., A new short-term mouse model of chronic obstructive pulmonary disease identifies a role for mast cell tryptase in pathogenesis. *J. Allergy Clin. Immunol.* **2013,** *131* (3), 752-62.

124. Barrios, R., Animal Models of Lung Disease. In *Molecular Pathology of Lung Diseases*, Zander, D. S.; Popper, H. H.; Jagirdar, J.; Haque, A. K.; Cagle, P. T.; Barrios, R., Eds. Springer New York: New York, NY, 2008; pp 144-149.

125. Mei, S. H.; McCarter, S. D.; Deng, Y.; Parker, C. H.; Liles, W. C.; Stewart, D. J., Prevention of LPS-induced acute lung injury in mice by mesenchymal stem cells overexpressing angiopoietin 1. *PLoS Med.* **2007,** *4* (9), e269.

126. Labiris, N. R.; Dolovich, M. B., Pulmonary drug delivery. Part I: Physiological factors affecting therapeutic effectiveness of aerosolized medications. *Br. J. Clin. Pharmacol.* **2003,** *56* (6), 588-599.

127. Labiris, N. R.; Dolovich, M. B., Pulmonary drug delivery. Part II: The role of inhalant delivery devices and drug formulations in therapeutic effectiveness of aerosolized medications. *Br. J. Clin. Pharmacol.* **2003,** *56* (6), 600-612.

128. Adamcakova-Dodd, A.; Stebounova, L. V.; Kim, J. S.; Vorrink, S. U.; Ault, A. P.; O'Shaughnessy, P. T.; Grassian, V. H.; Thorne, P. S., Toxicity assessment of zinc oxide nanoparticles using sub-acute and sub-chronic murine inhalation models. *Part. Fibre Toxicol.* **2014,** *11*, 15.

129. Ahern, C. A.; Eastwood, A. L.; Lester, H. A.; Dougherty, D. A.; Horn, R., A cation-pi interaction between extracellular TEA and an aromatic residue in potassium channels. *J. Gen. Physiol.* **2006,** *128* (6), 649-57.

130. Santarelli, V. P.; Eastwood, A. L.; Dougherty, D. A.; Horn, R.; Ahern, C. A., A cation-pi interaction discriminates among sodium channels that are either sensitive or resistant to tetrodotoxin block. *J. Biol. Chem.* **2007,** *282* (11), 8044-51.

131. Dougherty, D. A., The cation-pi interaction. *Acc. Chem. Res.* **2013,** *46* (4), 885-93.

132. Wright, J. R., Immunomodulatory functions of surfactant. *Physiol. Rev.* **1997,** *77* (4), 931-62.

133. Wright, J. R., Pulmonary surfactant: a front line of lung host defense. *J. Clin. Invest.* **2003,** *111* (10), 1453-5.

134. Lawson, P. R.; Reid, K. B., The roles of surfactant proteins A and D in innate immunity. *Immunol. Rev.* **2000,** *173*, 66-78.

135. Wu, H.; Kuzmenko, A.; Wan, S.; Schaffer, L.; Weiss, A.; Fisher, J. H.; Kim, K. S.; McCormack, F. X., Surfactant proteins A and D inhibit the growth of Gram-negative bacteria by increasing membrane permeability. *J. Clin. Invest.* **2003,** *111* (10), 1589-602.

136. Griese, M., Pulmonary surfactant in health and human lung diseases: state of the art. *Eur. Respir. J.* **1999,** *13* (6), 1455-76.

137. Jobe, A. H., Which surfactant for treatment of respiratory-distress syndrome. *Lancet* **2000,** *355* (9213), 1380-1.

138. Gunther, A.; Ruppert, C.; Schmidt, R.; Markart, P.; Grimminger, F.; Walmrath, D.; Seeger, W., Surfactant alteration and replacement in acute respiratory distress syndrome. *Respir. Res.* **2001,** *2* (6), 353-64.

139. Goerke, J., Pulmonary surfactant: functions and molecular composition. *Biochim. Biophys. Acta* **1998,** *1408* (2-3), 79-89.

140.   Thanawiroon, C.; Linhardt, R. J., Separation of a complex mixture of heparin-derived oligosaccharides using reversed-phase high-performance liquid chromatography. *J. Chromatogr. A* **2003,** *1014* (1-2), 215-23.

141.   Zhang, L.; Huang, W.; Tanimura, A.; Morita, T.; Harihar, S.; Dewald, D. B.; Prestwich, G. D., Synthesis and biological activity of metabolically stabilized cyclopentyl trisphosphate analogues of D-myo-Ins(1,4,5)P3. *ChemMedChem* **2007,** *2* (9), 1281-9.

142.   Wang, X.; Zhang, L., Physicochemical properties and antitumor activities for sulfated derivatives of lentinan. *Carbohydr. Res.* **2009,** *344* (16), 2209-16.

143.   Weldon, S.; McNally, P.; McElvaney, N. G.; Elborn, J. S.; McAuley, D. F.; Wartelle, J.; Belaaouaj, A.; Levine, R. L.; Taggart, C. C., Decreased levels of secretory leucoprotease inhibitor in the Pseudomonas-infected cystic fibrosis lung are due to neutrophil elastase degradation. *J. Immunol.* **2009,** *183* (12), 8148-56.

144.   Rao, N. V.; Marshall, B. C.; Gray, B. H.; Hoidal, J. R., Interaction of Secretory Leukocyte Protease Inhibitor with Proteinase-3. *Am. J. Respir. Cell Mol. Biol.* **1993,** *8* (6), 612-616.

145.   Lagente, V.; Manoury, B.; Nenan, S.; Le Quement, C.; Martin-Chouly, C.; Boichot, E., Role of matrix metalloproteinases in the development of airway inflammation and remodeling. *Braz. J. Med. Biol. Res.* **2005,** *38* (10), 1521-30.

146.   Navratilova, Z.; Kolek, V.; Petrek, M., Matrix Metalloproteinases and Their Inhibitors in Chronic Obstructive Pulmonary Disease. *Arch. Immunol. Ther. Exp. (Warsz.)* **2015**.

147.   Sasaki, M.; Kashima, M.; Ito, T.; Watanabe, A.; Sano, M.; Kagaya, M.; Shioya, T.; Miura, M., Effect of heparin and related glycosaminoglycan on PDGF-induced lung fibroblast proliferation, chemotactic response and matrix metalloproteinases activity. *Mediators Inflamm.* **2000,** *9* (2), 85-91.

148.   Roeb, E.; Schleinkofer, K.; Kernebeck, T.; Pötsch, S.; Jansen, B.; Behrmann, I.; Matern, S.; Grötzinger, J., The Matrix Metalloproteinase 9 (MMP-9) Hemopexin Domain Is a Novel Gelatin Binding Domain and Acts as an Antagonist. *J. Biol. Chem.* **2002,** *277* (52), 50326-50332.

APPENDIX: MS AND HPLC CHROMATOGRAMS USED TO CHARACTERIZE SYNTHESIZED DERIVATIVES

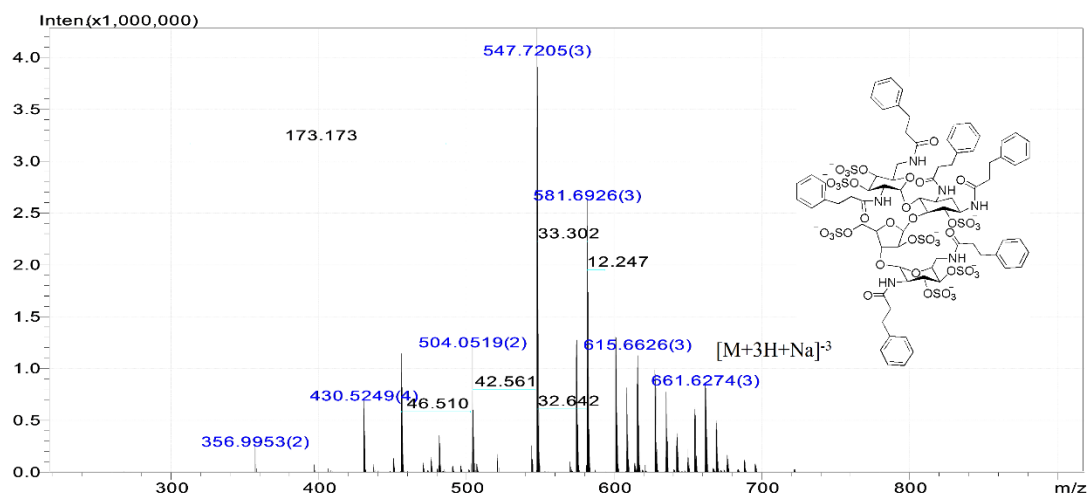Compounds were synthesized and purified as described in Chapter 7.

Figure A.1: ESI-MS chromatogram in negative ion mode for **NeoPhP** derivative.
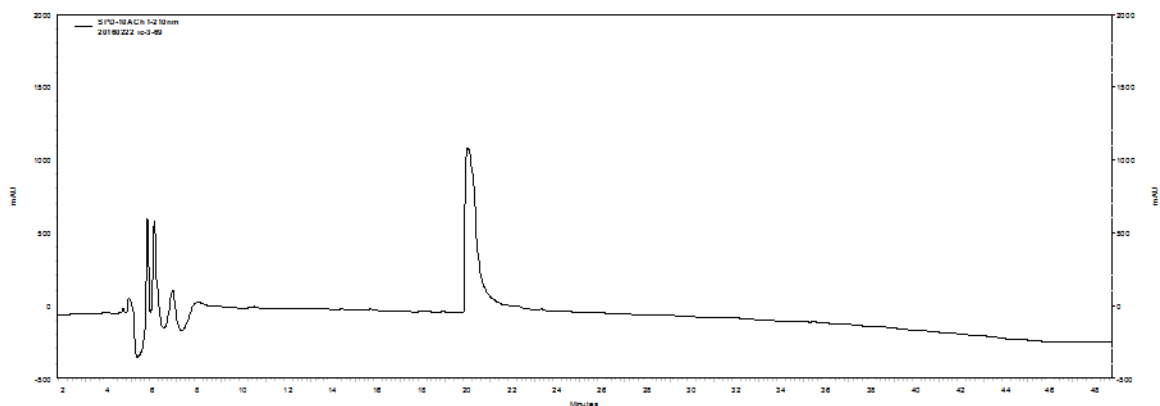

Figure A.2: Analytical HPLC trace of **NeoPhP**. HPLC elution gradient of 10-95% ACN in water (0.1% TFA) over 40 min at 1 mL/min was used.
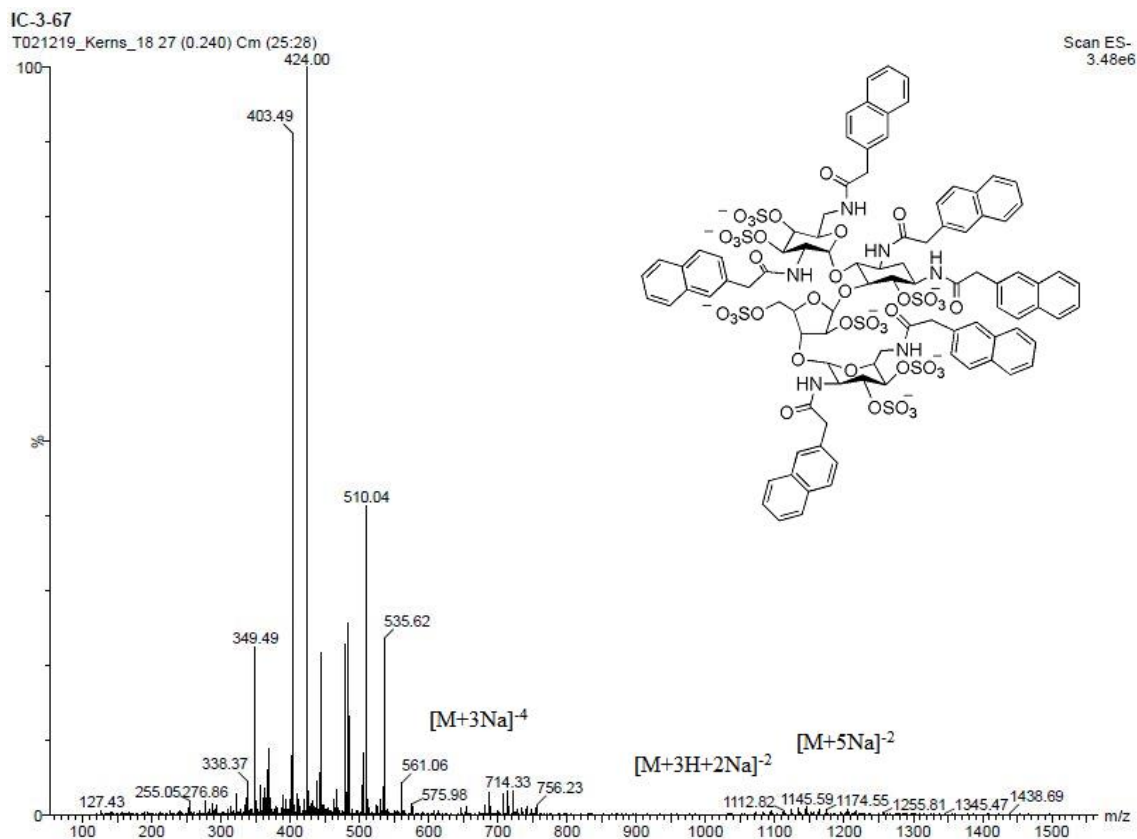
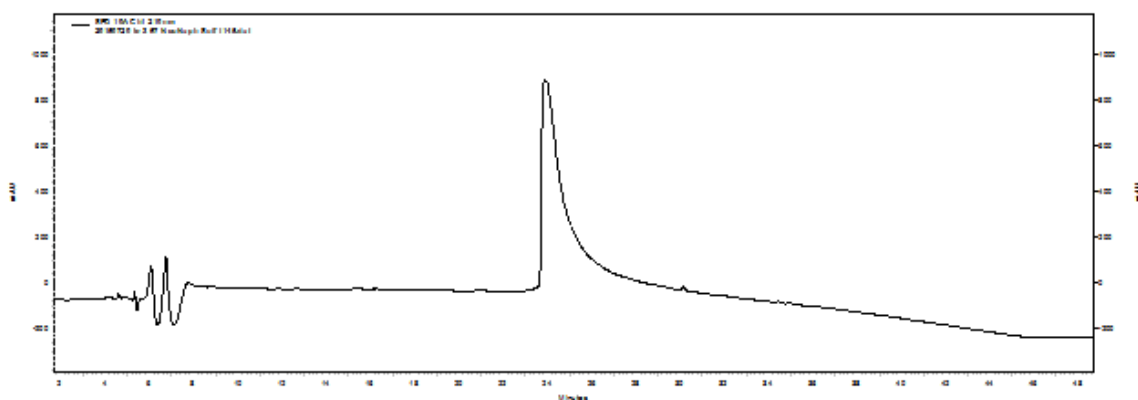Figure A.3: ESI-MS chromatogram in negative ion mode for **NeoNaph** derivative.

Figure A.4: Analytical HPLC trace of **NeoNaph**. HPLC elution gradient of 10-95% ACN in water (0.1% TFA) over 40 min at 1 mL/min was used.
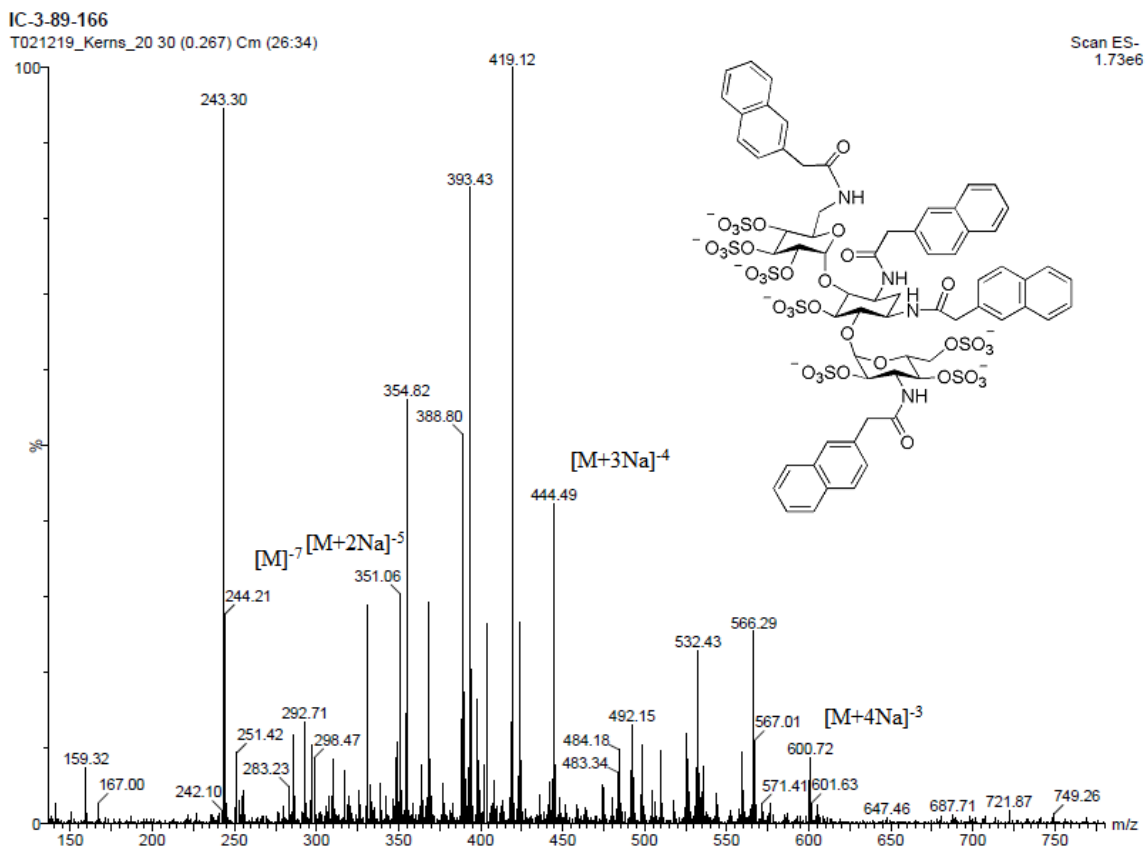
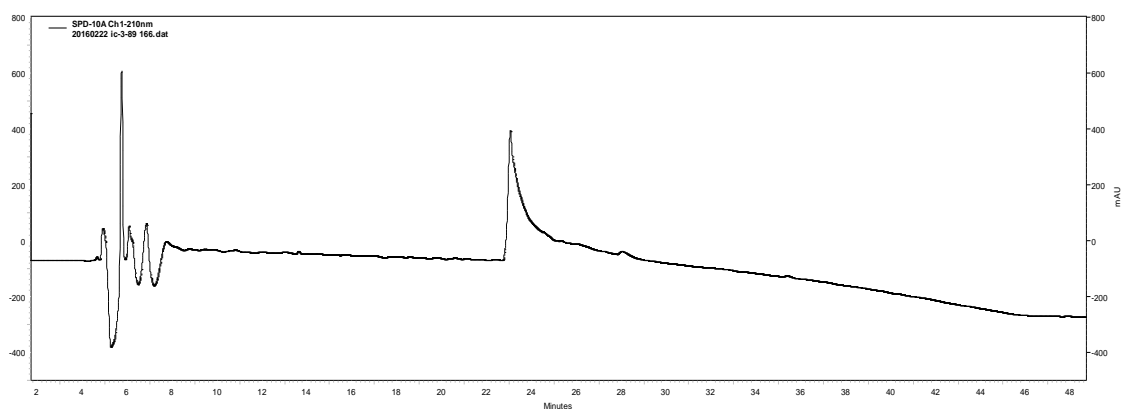Figure A.5: ESI-MS chromatogram in negative ion mode for **KanNaph** derivative.

Figure A.6: Analytical HPLC trace of **KanNaph**. HPLC elution gradient of 10-95% ACN in water (0.1% TFA) over 40 min at 1 mL/min was used.